Hong Kong Journal of Radiology

Vol. 26 No. 1, 2023 Pages 1-80

Hong Kong Journal of Radiology

HKJR

香港放射科醫學雜誌

VOLUME 26 • NUMBER 1 • 2023

ISSN 2223-6619

Highlights of this issue:

- Diagnostic Accuracy of ^{18}F-Fluorodeoxyglucose Positron Emission Tomography/Computed Tomography in Preoperative Mediastinal/ Extramediastinal Nodal Staging of Non–Small-Cell Lung Carcinoma
- Neoadjuvant Treatment of Locally Advanced Rectal Cancer in Elderly Patients: Real-World Experience at a Tertiary Institution
- Common Artifacts in Magnetic Resonance Imaging: A Pictorial Essay

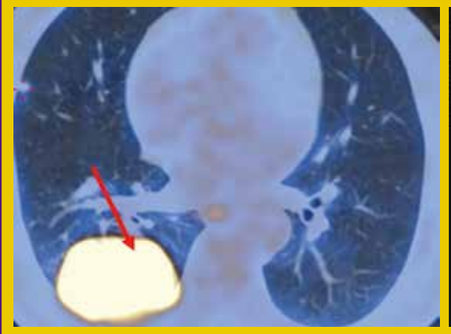

In the article “Diagnostic Accuracy of ^{18}F-Fluorodeoxyglucose Positron Emission Tomography/Computed Tomography in Preoperative Mediastinal/Extramediastinal Nodal Staging of Non-Small Cell Lung Carcinoma”. A large primary tumour can hinder the identification of an adjacent malignant intrapulmonary lymph node (arrow).

In the article “Contrast-Enhanced Ultrasonography and Its Application in Liver Interventions”. Contrast-enhanced ultrasound with SonoVue shows non-rim arterial phase hyperenhancement of the target lesion, which is typical of hepatocellular carcinoma.

Official Publication of
Hong Kong College of Radiologists

HKAM PRESS

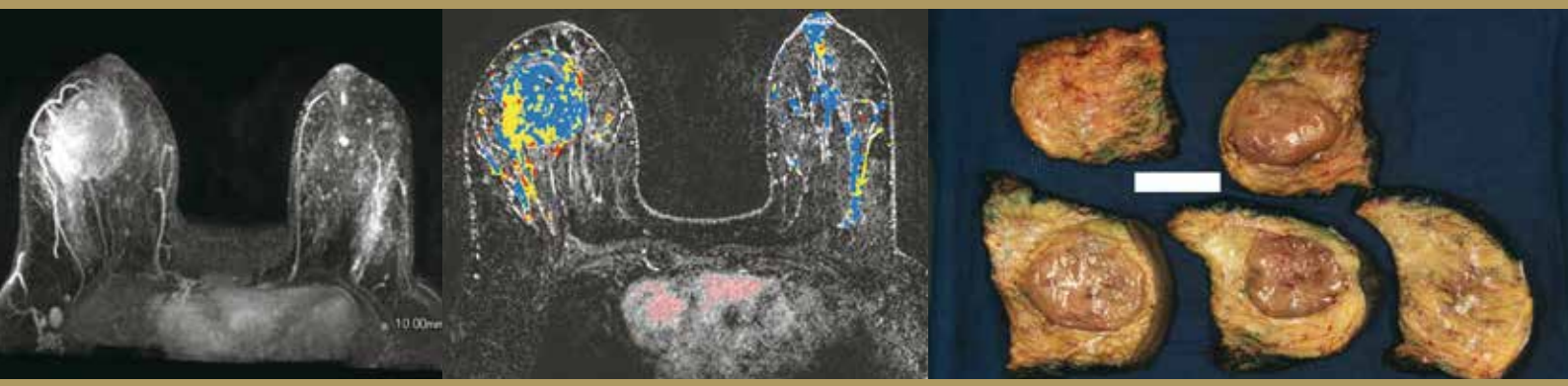

2023 AIRP Course in Hong Kong

26th - 28th May 2023

Hong Kong Academy of Medicine Jockey Club Building,

Hong Kong SAR, China

Subspecialty Focus:
Breast Imaging
Musculoskeletal Imaging
Pediatric Radiology

The renowned, unique training course for the pathophysiologic understanding of disease as the basis for radiologic interpretation

Stay tuned and learn more at airp.org and hkcr.org

AIRP
ACR INSTITUTE FOR RADIOLOGIC PATHOLOGY

HONG KONG COLLEGE OF RADIOLOGISTS

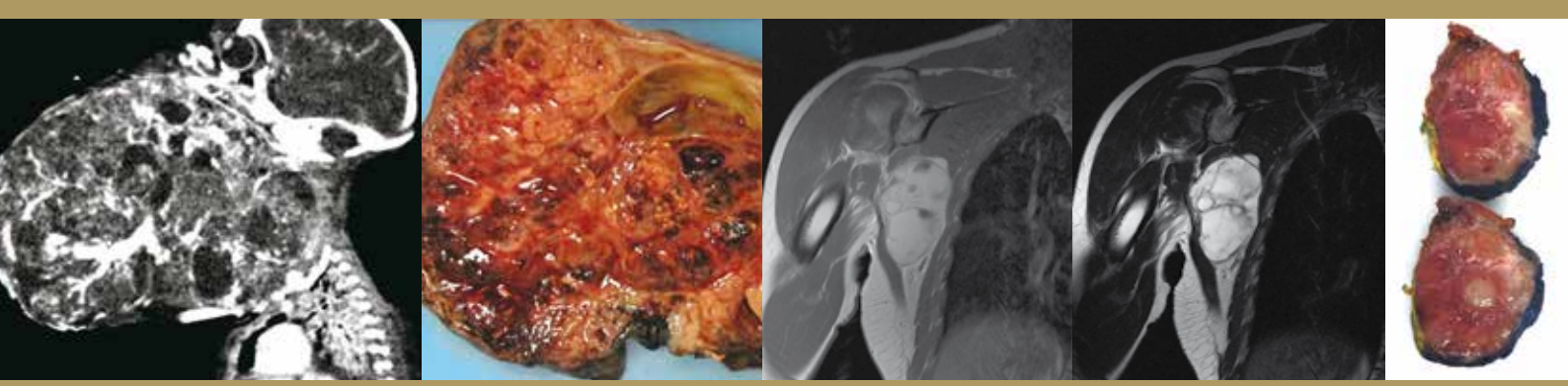

HKJR

COVER IMAGES

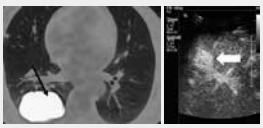

..... SEE PAGES 12 & 45

Hong Kong Journal of Radiology

Hong Kong Journal of Radiology is a continuation of the *Journal of the Hong Kong College of Radiologists*. This journal is dedicated to publish all aspects of clinical oncology, diagnostic radiology, and nuclear medicine.

VOLUME 26 • NUMBER 1 • MARCH 2023

Editorial

Original Articles

Perspective

Case Reports

Pictorial Essays

ePub-only Article

The following ePub-only article can be found on the HKJR website <http://www.hkjr.org>.

When citing this journal, abbreviate as ***Hong Kong J Radiol***.

INFORMATION FOR SUBSCRIBERS

Hong Kong Journal of Radiology (**香港放射科醫學雜誌**) is the official peer-reviewed publication of the Hong Kong College of Radiologists and is published by the Hong Kong Academy of Medicine Press.

Frequency
Quarterly, 1 volume a year.

Correspondence concerning subscriptions should be addressed to:

Executive Assistant
Hong Kong Journal of Radiology
Room 909, 9/F, Hong Kong Academy of Medicine Jockey Club Building
99 Wong Chuk Hang Road, Aberdeen, Hong Kong
Tel: (852) 2871 8788; Fax: (852) 2554 0739
Email: hkjr@hkcr.org

Annual subscription rate

Hong Kong delivery:	HK$400 per volume.
Overseas delivery (by airmail):	US$100* per volume.
	* Bank charges shall be borne by the subscriber.

- Rates are the same for individuals and institutions.
- Renewals should be promptly received to avoid a break in journal delivery. The Hong Kong College of Radiologists does not guarantee to supply back issues on late renewals.

Change of address
The College must be notified 60 days in advance. Journals undeliverable because of an incorrect address will be destroyed. Send address changes to:

Hong Kong Journal of Radiology
Room 909, 9/F, Hong Kong Academy of Medicine Jockey Club Building
99 Wong Chuk Hang Road, Aberdeen, Hong Kong

Please return your Subscription Order Form to:

Hong Kong Journal of Radiology
Room 909, 9/F, Hong Kong Academy of Medicine Jockey Club Building
99 Wong Chuk Hang Road, Aberdeen, Hong Kong

I enclose payment (US$/HK$) _____
Please make bank draft, cheque, or cashier's order payable to **"Hong Kong College of Radiologists"**

Name (in English): _____

Address: _____

_____

Tel: _____ Fax: _____ Email: _____

Please (✓) accordingly
I would like to subscribe to the *Hong Kong Journal of Radiology*

❒ Hong Kong delivery: HK$400/volume
❒ Overseas delivery: US$100/volume*
(Postage charge included)
*Bank charges shall be borne by the subscriber.

❒ 3 volumes ❒ 2 volumes ❒ 1 volume

Subscription period: From Volume _____ to Volume _____

Hong Kong Journal of Radiology

Aims and Editorial Policy

Hong Kong Journal of Radiology **香港放射科醫學雜誌** is the official peer-reviewed academic journal of Hong Kong College of Radiologists, a founder College of the Hong Kong Academy of Medicine. The Journal is published quarterly and is indexed in EMBASE/*Excerpta Medica*, SCOPUS, Emerging Sources Citation Index, and Index Copernicus. Papers are published on all aspects of diagnostic imaging, clinical oncology, and nuclear medicine, including original research, editorials, review articles, and case reports. Papers on radiological protection, quality assurance, audit in radiology, and matters related to radiological training or education are included.

All papers submitted are subject to peer review, and the Editorial Board reserves the right to edit papers in preparation for publication in the Journal. Authors are asked to refer to the *Information for Authors* published in each issue of the Journal, regarding the style and presentation of their articles. Failure to do so may result in rejection of their papers by the Editorial Board.

Manuscripts should be submitted online via the HKAMedTrack <www.hkamedtrack.org/hkjr>. Correspondence should be sent to:

Managing Editor, HKJR Editorial Office
c/o Hong Kong Academy of Medicine Press
10/F, Hong Kong Academy of Medicine Jockey Club Building
99 Wong Chuk Hang Road, Aberdeen, Hong Kong
Tel: (852) 2871 8809; Fax: (852) 2515 9061
Email: hkjr@hkam.org.hk

Advertisements

Correspondence concerning advertisements should be addressed to:

Executive Assistant
Hong Kong College of Radiologists
Room 909, 9/F Hong Kong Academy of Medicine Jockey Club Building
99 Wong Chuk Hang Road, Aberdeen, Hong Kong.
Tel: (852) 2871 8788; Fax: (852) 2554 0739
Email: hkjr@hkcr.org

Reprints

Reprints of individual articles are available to authors only. Reprints in large quantities (non-authors), for commercial or academic use, may be purchased from the publisher. For information and prices, please send an email to: hkjr@hkam.org.hk.

Copyright

On acceptance of an article by the Journal, the corresponding author will be asked to transfer copyright of the article to the College. The Copyright Transfer Assignment Form will be sent to the author at the time of acceptance.

Disclaimer

Hong Kong Journal of Radiology and the publisher do not guarantee, directly or indirectly, the quality or efficacy of any product or service described in the advertisements or other material which is commercial in nature in this issue. All articles published, including editorials and letters, represent the opinions of the authors and do not reflect the official policy of the Journal, Hong Kong College of Radiologists, the publisher, or the institution with which the author is affiliated, unless this is clearly specified.

Hong Kong Journal of Radiology
ISSN 2223-6619 (Print)
ISSN 2307-4620 (Online)

Hong Kong J Radiol. 2023;26:4-5 | https://doi.org/10.12809/hkjr23mared

EDITORIAL

Positron Emission Tomography/Computed Tomography Thoracic Nodal Staging of Non–Small-Cell Lung Cancer

WSK Cheung

Department of Nuclear Medicine, Hong Kong Sanatorium & Hospital, Hong Kong

Lung cancer is the leading cause of cancer-related death, with the highest incidence and mortality in Hong Kong.[1] Non–small-cell lung carcinoma (NSCLC) accounts for 94% of all lung cancers. For patients with NSCLC, accurate staging paves a determining role in treatment options and predicts survival. ^{18}F-fluorodeoxyglucose positron emission tomography–computed tomography (^{18}F-FDG PET/CT) has a well-established role in staging of NSCLC and is recommended in guidelines of the National Comprehensive Cancer Network,[2] the American College of Chest Physicians,[3] the American College of Radiology Appropriateness Criteria, and the Society of Nuclear Medicine and Molecular Imaging.[4]

The role of ^{18}F-FDG PET/CT in the TNM staging of NSCLC was reviewed for the eighth edition, and no changes were made to the N descriptors.[5] The N categories based on the location of the involved nodes can be used to consistently predict prognosis. For mediastinal nodal staging, ^{18}F-FDG PET/CT has higher accuracy than CT alone with nodes of >1 cm in the short axis, and it has a sensitivity of 58%-94% and a specificity of 76%-96%.[6] However, the sensitivity and specificity of FDG-PET vary among studies and centres owing to differences in the criteria for PET positivity and the performance metrics of PET/CT scanners.[7] Few studies have evaluated the accuracy of nodal staging in NSCLC when different diagnostic criteria are applied.

In this issue of the *Hong Kong Journal of Radiology*, Ng et al[8] conducted a retrospective study to evaluate the diagnostic accuracy of ^{18}F-FDG PET/CT for preoperative thoracic nodal staging of NSCLC. The authors compared ^{18}F-FDG PET/CT with a five-point visual score, the maximum standardised uptake value (SUV_{max}), and short-axis nodal diameter in the axial plane with histopathology.[8] They found that specificity, accuracy, and positive and negative predictive values were significantly higher for the visual score than for nodal diameter. A predictive model combining visual PET positivity with other parameters, including nodal SUV_{max}, ratio of node to aorta SUV_{max}, ratio of node to primary tumour SUV_{max}, and Hounsfield units, has been shown to improve the positive predictive value, specificity, and overall accuracy of ^{18}F-FDG PET/CT in the preoperative diagnosis of nodal metastases.[9] Thus, the visual score is a simple method with good inter-observer agreement, and has great value in nodal staging when combined with PET positivity and visual semi-quantification. Moreover, Ng et al[8] found that the visual score with a cut-off score of 3 achieved satisfactory areas under the curve values in the receiver operating characteristics curves to T stages, histology, epidermal growth factor receptor status, SUV_{max} of the primary tumour, and nodal stations. This implies the applicability of the visual score in patients with NSCLC.

In conclusion, accurate TNM staging is important to the direct management of NSCLC and bears prognostic implications for patients with NSCLC. ^{18}F-FDG PET/CT is currently the standard of care. Thoracic nodal staging is particularly important for early NSCLC in determining curative surgery. This retrospective local study proposed a simple visual scheme for nodal staging which has high

Correspondence: *Dr WSK Cheung, Department of Nuclear Medicine, Hong Kong Sanatorium & Hospital, Hong Kong*
Email: William.SK.Cheung@hksh.com

Contributors: The author contributed to the Editorial, approved the final version for publication, and takes responsibility for its accuracy and integrity.

Conflicts of Interest: The author has disclosed no conflicts of interest.

accuracy and good interobserver agreement, and thus can alleviate the robust semiquantitative assessment and application of diagnostic criteria among different scanners.

REFERENCE

1. Hospital Authority. Hong Kong Cancer Registry 2019. Overview of Hong Kong Cancer Statistics 2020. Available from: https://www3.ha.org.hk/cancereg/pdf/overview/Overview%20of%20HK%20Cancer%20Stat%202020.pdf. Accessed 13 Nov 2022.
2. Ettinger DS, Wood DE, Aisner DL, Akerley W, Bauman JR, Bharat A, et al. Non–small-cell lung cancer, version 3.2022, NCCN Clinical Practice Guidelines in Oncology. J Natl Compr Canc Netw 2022;20:497-530.
3. Silvestri GA, Gonzalez AV, Jantz MA, Margolis ML, Gould MK, Tanoue LT, et al. Methods for staging non–small-cell lung cancer: diagnosis and management of lung cancer, 3rd ed: American College of Chest Physicians evidence-based clinical practice guidelines. Chest 2013;143(5 Suppl):e211S-e250S.
4. Ravenel JG, Rosenzweig KE, Kirsch J, Ginsburg ME, Kanne JP, Kestin LL, et al. ACR Appropriateness Criteria non-invasive clinical staging of bronchogenic carcinoma. J Am Coll Radiol 2014;11:849-56.
5. Kandathil A, Kay FU, Butt YM, Wachsmann JW, Subramaniam RM. Role of FDG PET/CT in the eighth edition of TNM staging of non-small cell lung cancer. Radiographics. 2018;38:2134-49.
6. Walker CM, Chung JH, Abbott GF, Little BP, El-Sherief AH, Shepard JA, et al. Mediastinal lymph node staging: from noninvasive to surgical. AJR Am J Roentgenol 2012;199:W54-64.
7. Schmidt-Hansen M, Baldwin DR, Hasler E, Zamora J, Abraira V, Roqué I Figuls M. PET-CT for assessing mediastinal lymph node involvement in patients with suspected resectable non-small cell lung cancer. Cochrane Database Syst Rev. 2014;2014(11):CD009519.
8. Ng KS, Ng KK, Chu KS, Kung BT, Au Yong TK. Diagnostic accuracy of ^{18}F-fluorodeoxyglucose positron emission tomography/computed tomography in preoperative mediastinal/extramediastinal nodal staging of non–small-cell lung carcinoma. Hong Kong J Radiol. 2023;26:6-13.
9. Mathew B, Purandare NC, Pramesh CS, Karimundackal G, Jiwnani S, Agrawal A, et al. Improving accuracy of ^{18}F-fluorodeoxyglucose PET computed tomography to diagnose nodal involvement in non–small-cell lung cancer: utility of using various predictive models. Nucl Med Commun. 2021;42:535-44.

Hong Kong J Radiol. 2023;26:6-13 | https://doi.org/10.12809/hkjr2317503

ORIGINAL ARTICLE **CME**

Diagnostic Accuracy of ^{18}F-Fluorodeoxyglucose Positron Emission Tomography/Computed Tomography in Preoperative Mediastinal/ Extramediastinal Nodal Staging of Non–Small-Cell Lung Carcinoma

KS Ng, KK Ng, KS Chu, BT Kung, TK Au Yong

Nuclear Medicine Unit and Clinical PET Centre, Queen Elizabeth Hospital, Hong Kong

ABSTRACT

Introduction: *Lung cancer has the highest incidence and mortality among malignancies in many countries. ^{18}F-Fluorodeoxyglucose (^{18}F-FDG) positron emission tomography/computed tomography (PET/CT) is commonly indicated for the preoperative nodal staging of non–small-cell lung carcinoma. While maximum standardised uptake value (SUV_{max}), visual scoring systems and nodal diameter have been proposed to distinguish benign from malignant nodes, studies comparing the different measurements have been limited. Correct nodal staging is crucial in determining if treatment intent is curative or palliative. This study aimed to evaluate the accuracies of nodal staging in ^{18}F-FDG PET/CT based on different methods.*

Methods: *A total of 467 mediastinal/extramediastinal lymph nodes from 97 patients, who underwent staging ^{18}F-FDG PET/CT at our centre for non–small-cell lung carcinoma, were retrospectively reviewed. The nodes were evaluated based on SUV_{max}, five-point visual interpretation score, and diameter. Their sensitivities, specificities and accuracies were compared with histology using receiver operating characteristics curves and areas under the curves (AUCs). Subgroup analyses based on T staging, histology, epidermal growth factor receptor (EGFR) status, lymph node locations, and tumour SUV_{max} were also investigated.*

Results: *The diagnostic performance of visual score (at optimal cut-off of 3) yielded the highest specificity (0.932), accuracy (0.916), positive predictive value (0.623), and negative predictive value (0.972), results of which were similar to SUV_{max} of 2.5 and better than nodal diameter of 10 mm. Subgroup analyses showed that visual interpretation achieved satisfactory AUCs in different T stages, histologies, EGFR statuses, locations of lymph nodes, and tumour $SUVs_{max}$.*

Conclusion: *The five-point visual interpretation is a convenient diagnostic tool with performance better than nodal diameter, and similar to that of SUV_{max}.*

Key Words: *Carcinoma, non–small-cell lung; Fluorodeoxyglucose F18; Lung neoplasms; Mediastinum; Positron emission tomography computed tomography*

Correspondence: *Dr KS Ng, Nuclear Medicine Unit and Clinical PET Centre, Queen Elizabeth Hospital, Hong Kong*
Email: nks176@ha.org.hk

Submitted: 18 Nov 2021; Accepted: 1 Apr 2022.

Contributors: All authors designed the study, acquired the data, analysed the data, drafted the manuscript, and critically revised the manuscript for important intellectual content. All authors had full access to the data, contributed to the study, approved the final version for publication, and take responsibility for its accuracy and integrity.

Conflicts of Interest: As editors of the journal, KSN and TKAY were not involved in the peer review process. Other authors have disclosed no conflicts of interest.

Funding/Support: This research received no specific grant from any funding agency in the public, commercial, or not-for-profit sectors.

Data Availability: All data generated or analysed during the present study are available from the corresponding author on reasonable request.

Ethics Approval: This study was approved by the Research Ethics Committee (Kowloon Central/Kowloon East Cluster) of Hospital Authority, Hong Kong (Ref No.: KC/KE-19-0048-ER-4). Informed consent was waived because of the retrospective nature of the study.

中文摘要

^{18}F-氟脫氧葡萄糖正電子／電腦斷層掃描在非小細胞肺癌術前縱隔／縱隔外淋巴結分期中的診斷準確性

吳國勝、吳官橋、朱競新、龔本霆、歐陽定勤

簡介：肺癌在許多國家的惡性腫瘤中發病率和死亡率最高。^{18}F-氟脫氧葡萄糖（^{18}F-FDG）正電子發射斷層掃描／計算機斷層掃描（PET/CT）通常用於非小細胞肺癌的術前淋巴結分期。雖然已提出最大標準化攝取值（SUV_{max}）、視覺評分系統和淋巴結直徑來區分良性和惡性淋巴結，但比較不同測量值的研究不多。正確的淋巴結分期對於確定治療目的是治愈性還是姑息性至關重要。本研究旨在評估基於不同方法的^{18}F-FDG PET/CT淋巴結分期的準確性。

方法：本研究回顧性分析在本中心進行^{18}F-FDG PET/CT分期的非小細胞肺癌患者97例共467個縱隔／縱隔外淋巴結。淋巴結根據SUV_{max}、五級視覺判讀分數和直徑進行評估。我們使用接受者操作特徵曲線和曲線下面積（AUC）將它們的敏感性、特異性和準確性與組織學比較，並研究基於T分期、組織學、表皮生長因子受體（EGFR）狀態、淋巴結位置和腫瘤SUV_{max}的亞組分析。

結果：視覺分數（最佳截斷值為3）的診斷性能獲得最高特異性（0.932）、準確性（0.916）、陽性預測值（0.623）及陰性預測值（0.972），結果與SUV_{max}值2.5的結果相似，以及優於淋巴結直徑10 mm的結果。亞組分析顯示，視覺解釋在不同的T分期、組織學、EGFR狀態、淋巴結位置和腫瘤SUV_{max}中達到滿意的AUC。

結論：五級視覺判讀是一種方便的診斷工具，性能優於淋巴結直徑，並與SUV_{max}相似。

INTRODUCTION

In many countries, lung cancer has the highest incidence and mortality among all malignancies.[1] Mediastinal/extramediastinal nodal status is the most important factor determining the management of early non–small-cell lung carcinoma (NSCLC). For N0 or N1 disease, according to the 7th and 8th editions of American Joint Committee on Cancer staging,[2,3] curative surgical resection can be offered.[4] For N2 (subcarinal or ipsilateral mediastinal metastasis) disease, the usual treatment is chemoradiotherapy (CRT).[4] Accurate mediastinal nodal staging is critical but challenging. Whereas mediastinoscopy is the gold standard, this invasive procedure carries 0.5% life-threatening risks of major complications including arrhythmia, respiratory failure, and infection.[5] Although staging with computed tomography based on nodal diameter is non-invasive, it has limited accuracy.[6,7] ^{18}F-fluorodeoxyglucose (^{18}F-FDG) positron emission tomography/computed tomography (PET/CT) is useful in NSCLC staging.[8-11] Both semiquantitative assessment and qualitative visual interpretation are recommended for distinguishing benign from malignant lymph nodes (LNs).[10-14] In a semiquantitative approach, the maximum standardised uptake value (SUV_{max}) is used.[10-12] Yet, SUV_{max} depends on many physiological as well as technical factors, such as injection time, uptake period, and blood glucose level.[15,16] Thus, absolute SUV_{max} is difficult to compare between different PET/CT systems or subjects. Studies have compared the accuracies of simple SUV_{max} and visual score generated by different comparisons with the activity in the aorta and other locations, as well as with a simple unified windowing technique.[13,14] We aimed to evaluate the performance of ^{18}F-FDG PET/CT on mediastinal/extramediastinal nodal staging of NSCLC based on SUV_{max}, visual score, and nodal diameter. The disparity between radiological and pathological staging was also reviewed.

METHODS

Case Enrolment

Cases of newly diagnosed lung cancer patients who underwent whole-body ^{18}F-FDG PET/CT for staging in our centre at Queen Elizabeth Hospital from 1 January 2016 to 31 December 2016 were retrospectively analysed. Cases were included only if they had (1) histological

evidence of primary NSCLC and (2) histological mediastinal/extramediastinal LN staging. Cases were excluded if (1) the time interval between PET/CT and histological LN examination was >2 months, or (2) treatment was started before PET/CT.

Technical Aspects

All PET/CT examinations were acquired with a Discovery 710 (General Electric, Milwaukee [WI], US) according to the 2010 procedural protocol of the European Association of Nuclear Medicine for oncological PET imaging.[17] The mean ^{18}F-FDG activity administrated was 370 ± 44.4 MBq. After a mean uptake time of 60 minutes (standard deviation = 6.24), image data were acquired from the skull vertex to the mid-thighs in 7 to 8 bed positions (3 minutes per bed position) with mean axial bed coverage of 15.2 cm per bed and 9 sections bed overlap in the 2-dimensional acquisition mode. Reconstruction using optimisation of ordered subset expectation maximisation was performed with 4.2 mm section thickness in a 128 × 128 matrix and processed through a standard filter. Non-contrast CT was acquired for anatomical correlation and attenuation correction with the following parameters: 120 mA tube current, 140 kV tube voltage, 0.8 s gantry rotation speed, 0.75 pitch, 0.5 mm section thickness and 512 × 512 matrix. The mean blood glucose level was 5.5 mmol/L (standard deviation = 0.91).

Positron Emission Tomography/Computed Tomography Interpretation

This study evaluated the accuracy of staging PET/CT in the diagnosis of mediastinal/extramediastinal LNs. A nuclear medicine physician, blinded to the patients' clinical background and histological results, assessed the PET/CT images according to the Mountain and Dresler nodal station scheme[18] with an Advantage Workstation Volume Viewer 4.7 (General Electric, Milwaukee [WI], US). If the histologically evaluated LNs were identifiable on PET/CT, three nodal features were analysed: SUV_{max}, visual score (as illustrated below) and diameter (short axis in axial plane). SUV is defined as the activity measured in a volume of interest divided by the injected ^{18}F-FDG dose, based on body weight:

$$SUV = \frac{Activity_{VOI}\,(MBq/mL)}{Dose_{injected}\,(MBq/kg)}$$

A five-point visual score of LNs was used, with a standardised lower threshold set at 0 and the upper threshold at 2 times the liver's mean standardised uptake value (SUV_{mean}).[14] The LNs were rated based on the maximum intensity projection image with grey scale images (Figure 1):

- Score 0: No LN uptake
- Score 1: LN uptake < mediastinal blood pool
- Score 2: mediastinal blood pool ≤ LN uptake < SUV_{mean} of liver
- Score 3: SUV_{mean} of liver ≤ LN uptake <2 × SUV_{mean} of liver
- Score 4: LN uptake ≥2 × SUV_{mean} of liver

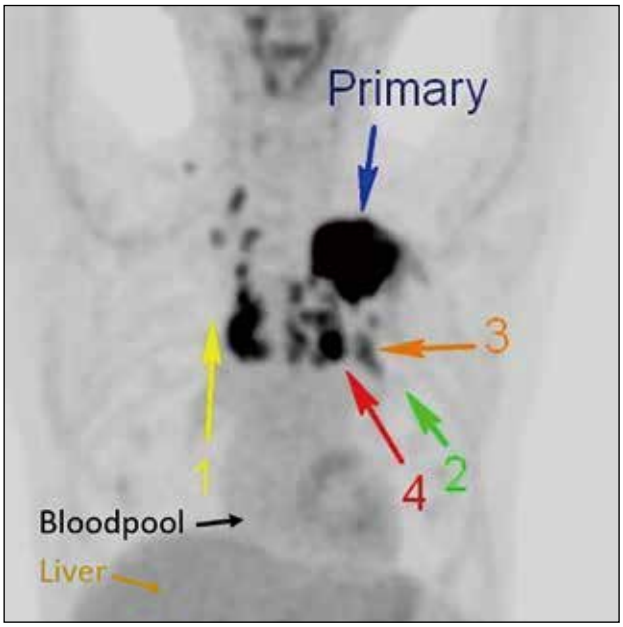

Figure 1. Representative maximum intensity projection for visual scores of 1 to 4, with bloodpool, liver, and primary tumour labelled (arrows).

For primary tumour with uptake similar to that of liver, the respective LNs were scored 4 if their uptakes were similar to the uptake of the primary.[14] If a LN was evaluated histologically but unidentifiable on PET/CT, a score of 0 was assigned and a 2-cm sphere was marked as a volume of interest in the corresponding anatomical location for SUV_{max}.

Histological Evaluation

Mediastinal/extramediastinal LNs were sampled by cardiothoracic surgeons or respiratory physicians via lobectomy (59%), mediastinoscopy (14%), video-assisted thoracoscopic surgery (11%), endobronchial ultrasound (8%), pneumonectomy (5%) or wedge resection (3%). Anatomical staging was evaluated by pathologists according to Mountain and Dresler scheme.[18]

Statistical Analysis

Statistical analysis was performed using SPSS (Window version 20.0; IBM Corp, Armonk [NY], US). Receiver operating characteristics (ROC) curves as well as corresponding areas under the curve (AUCs) based on SUV_{max}, visual score, and nodal diameter were compared. The optimal cut-off to distinguish benign from malignant LNs in PET/CT is the minimum of $\sqrt{(1-specificity)^2 + (1-sensitivity)^2}$. The respective sensitivities, specificities, accuracies, false negative and positive values were determined. Subgroup analyses were also examined according to primary tumour T stage (T1-2 vs. T3-4), histology (adenocarcinoma vs. squamous cell carcinoma), epidermal growth factor receptor (EGFR) status (wild type vs. mutated), primary tumour SUV_{max} (<10 vs. ≥10), and LN location (hilar vs. other mediastinal).

Table 1. Characteristics of the study population (n = 97).*

Variable	No. (%)
Gender	
Male	62 (63.9%)
Female	35 (36.1%)
Age, y	
Mean ± standard deviation	66 ± 8.4
Range	42-84
Histology	
Adenocarcinoma	63 (64.9%)
Squamous cell carcinoma	17 (17.5%)
Others	17 (17.5%)
T stage (tumour-node-metastasis)	
1	27 (27.8%)
2	45 (46.4%)
3	15 (15.5%)
4	10 (10.3%)
Primary tumour SUV_{max}	
Mean ± standard deviation	9.64 ± 4.99
Range	1.07-21.5
EGFR status	
Wild type	28 (28.9%)
Mutated	20 (20.6%)
Unspecific	49 (50.5%)

Abbreviations: EGFR = epidermal growth factor receptor; SUV_{max} = maximum standardised uptake value.
* Data are shown as No. (%) or mean ± standard deviation, unless otherwise specified.

Table 2. Properties of lymph nodes (n = 467).

	No. (%)
Metastatic (histology proven)	59 (12.6%)
Benign (histology proven)	408 (87.4%)
Cases (n = 97)	
Cases with nodal metastases	38 (39.2%)
Cases without nodal metastases	59 (60.8%)
Hilar	170 (36.4%)
Other mediastinal	297 (63.6%)

RESULTS

Histology Findings

A total of 467 mediastinal/extramediastinal LNs from 97 patients (62 male, 35 female) of mean age 66 ± 8.4 years were included. The characteristics of the study population are summarised in Table 1. Adenocarcinoma was the most commonly reported histological finding. The properties of LNs are outlined in Table 2.

Positron Emission Tomography/Computed Tomography Performance

Figure 2 shows the ROC curves based on visual score, SUV_{max}, and nodal diameter. Their corresponding AUCs are listed in Table 3. The visual score achieved the highest AUC of 0.901 (95% confidence interval [CI] = 0.870-0.926), compared with 0.897 (95% CI = 0.866-0.923) for SUV_{max} and 0.804 (95% CI = 0.737-0.872) for nodal diameter, respectively. Whereas the difference in AUCs for visual score and SUV_{max} were not statistically significant (p = 0.796), their AUCs were significantly greater than those for nodal diameter (p = 0.0003). Figure 3 shows $\sqrt{(1-specificity)^2 + (1-sensitivity)^2}$ against visual score (lower X-axis) and SUV_{max} (upper X-axis). As mentioned above, the optimal diagnostic cut-off corresponds to the minimum of $\sqrt{(1-specificity)^2 + (1-sensitivity)^2}$. The cut-off for visual score was 3, implying that LNs with uptakes greater than or equal to that of liver should be suspicious for metastases. The optimal cut-off for SUV_{max} was 2.5 as demonstrated in Figure 3. Similar analysis for nodal diameter (not shown) gave a cut-off of 10 mm.

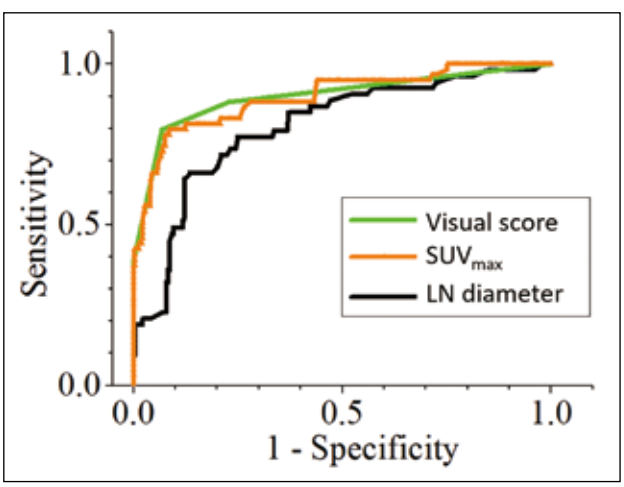

Figure 2. Receiver operating characteristics curves based on visual score, maximum standardised uptake value, and nodal diameter.
Abbreviations: LN = lymph node; SUV_{max} = maximum standardised uptake value.

Table 3. Diagnostic performance based on visual score, maximum standardised uptake value, and nodal diameter.

	Visual score (range)	SUV_{max} (range)	Nodal diameter (range)
Optimal cut-off	3	2.5	10 mm
AUC	0.901 (0.870-0.926)	0.897 (0.866-0.923)	0.804 (0.737-0.872)
p Value of AUC (compared with visual score)	-	0.796	0.0003
Sensitivity	0.810 (0.682-0.897)	0.810 (0.682-0.897)	0.660 (0.517-0.785)
Specificity	0.932 (0.901-0.953)	0.897 (0.868-0.924)	0.865 (0.813-0.906)
Accuracy	0.916 (0.880-0.953)	0.887 (0.845-0.929)	0.823 (0.778-0.867)
PPV	0.623 (0.507-0.733)	0.528 (0.420-0.633)	0.522 (0.398-0.644)
NPV	0.972 (0.949-0.985)	0.971 (0.950-0.984)	0.916 (0.869-0.948)

Abbreviations: AUC = area under the curve; NPV = negative predictive value; PPV = positive predictive value; SUV_{max} = maximum standardised uptake value.

Based on the cut-offs, the corresponding sensitivities, specificities, accuracies, positive predictive values (PPVs) and negative predictive values (NPVs) are evaluated in Table 3. Among SUV_{max}, visual score and nodal diameter, the visual score yielded the highest specificity (0.932, 95% CI = 0.901-0.953), accuracy (0.916, 95% CI = 0.880-0.953), PPV (0.623, 95% CI = 0.507-0.733), and NPV (0.972, 95% CI = 0.949-0.985). They were higher than those based on nodal diameter ($p = 0.0003$), although they had no statistically significant difference from the respective values of SUV_{max} ($p > 0.05$). On the other hand, the PET/CT achieved limited sensitivity based on nodal diameter (0.660, 95% CI = 0.517-0.785).

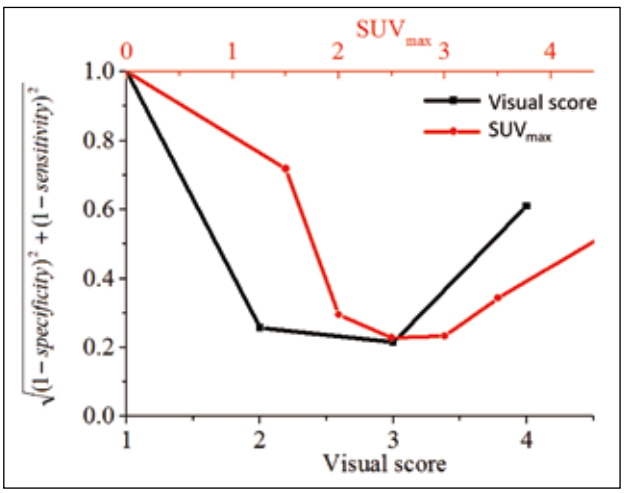

Figure 3. $\sqrt{(1-specificity)^2 + (1-sensitivity)^2}$ versus visual score (lower X-axis) and maximum standardised uptake value (upper X-axis).
Abbreviation: SUV_{max} = maximum standardised uptake value.

Subject-based staging rates are shown in Table 4. Based on visual interpretation, 77 subjects (79%) had correct nodal staging by visual score, whereas 12 subjects (12%) were false positive and eight (8%) were false negative. Based on SUV_{max}, 68 subjects (70%) had correct staging with 23 (24%) wrong upstaging and six (6%) wrong downstaging. Based on nodal diameter, 72 subjects (74%) had correct staging with 11 (11%) wrong upstaging and 14 (14%) wrong downstaging. The overall nodal staging performance achieved no significant difference between visual interpretation and nodal diameter in McNemar's test ($p = 0.190$), while that of SUV_{max} and nodal diameter had statistical significance ($p = 0.001$).

Table 4. Subject-based staging rates according to visual score, maximum standardised uptake value, and nodal diameter.

Subgroup	Visual score	SUV_{max}	Nodal diameter
Correct staging	79%	70%	74%
Wrong upstaging	12%	24%	11%
Wrong downstaging	8%	6%	14%

Abbreviation: SUV_{max} = maximum standardised uptake value.

Subgroup Analyses

Figure 4 shows the ROC curves of visual score according to T stage (T1-2 vs. T3-4), histology (adenocarcinoma vs. squamous cell carcinoma), EGFR status (wild type vs. mutated), primary tumour SUV_{max} (<10 vs. ≥10), and LN location (hilar vs. mediastinal). Their corresponding AUC values ranged from 0.838 to 0.961 (Table 6). For all subgroup analyses, the optimal cut-off of visual score was 3. To assess the significance of the difference between the AUCs, two-tailed tests were evaluated within the subgroups. The p values were > 0.05 for all subgroup analyses, except for histology, which had a p value of 0.0458.

DISCUSSION

Different radiological criteria have been proposed for nodal staging in NSCLC, including semiquantitative

SUV_{max},[10,11] qualitative visual interpretation,[13,14] and nodal diameter.[6,7] For visual interpretation, the current study focused on a five-point system[14] because of its convenient applicability (with reference to mediastinal blood pool and liver). We demonstrated good performance of the visual score. Subgroup analyses showed satisfactory AUCs in different T stages, histology, EGFR status, LN locations or primary SUV_{max}. There were no significant

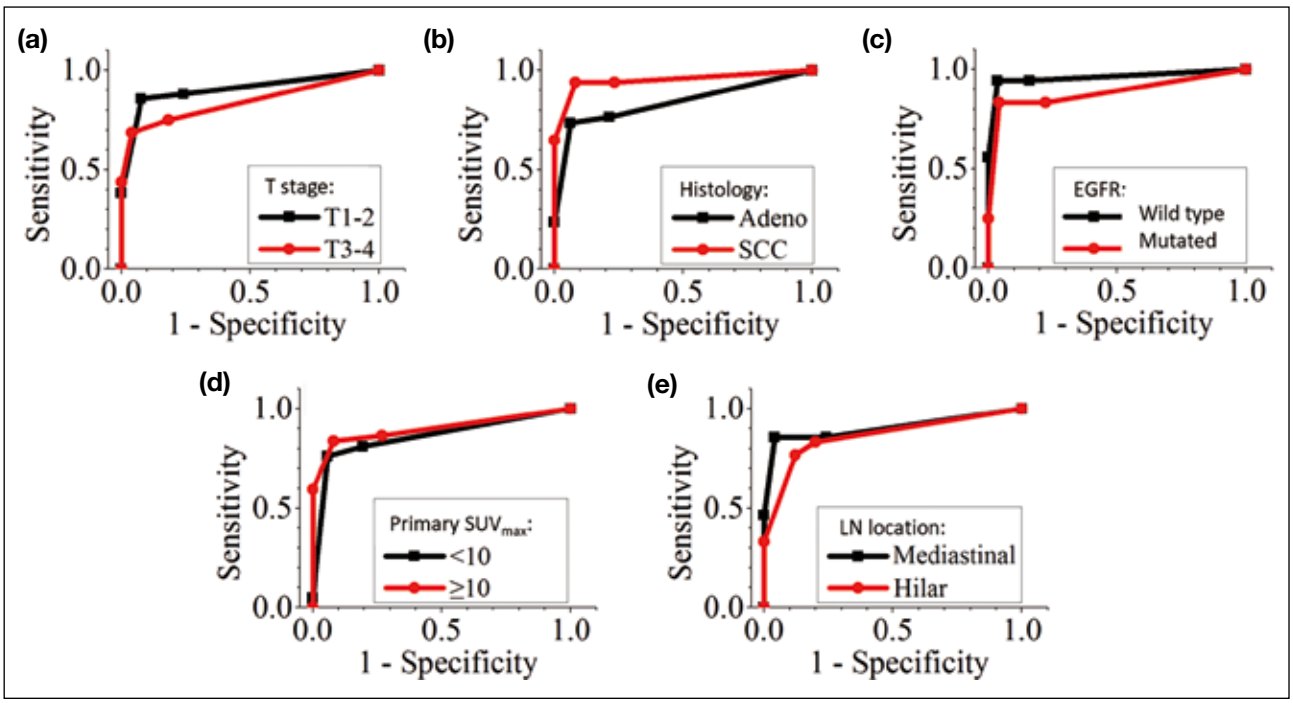

Figure 4. Subgroup receiver operating characteristics curves according to (a) T stage, (b) histology, (c) epidermal growth factor receptor status, (d) maximum standardised uptake value of primary tumour, and (e) lymph node location based on visual score.
Abbreviations: Adeno = adenocarcinoma; EGFR = epidermal growth factor receptor; LN = lymph node; SCC = squamous cell carcinoma; SUV_{max} = maximum standardised uptake value.

Table 5. Overall nodal staging performance with reference to histology.*

		Radiological nodal staging: 0 No. of cases based on		
		Visual score	SUV_{max}	Nodal diameter
Pathological nodal staging	0	49	39	50
	1	6	5	11
	2	2	1	3
		Radiological nodal staging: 1 No. of cases based on		
		Visual score	SUV_{max}	Nodal diameter
Pathological nodal staging	0	2	4	4
	1	10	10	5
	2	0	0	0
		Radiological nodal staging: 2 No. of cases based on		
		Visual score	SUV_{max}	Nodal diameter
Pathological nodal staging	0	8	16	5
	1	2	3	2
	2	18	19	17

Abbreviation: SUV_{max} = maximum standardised uptake value.
* Patients with N3 or N4 disease usually are not eligible for operation, therefore typically would not undergo histological lymph node staging.

Table 6. Subgroup areas under the curve according to T stage, histology, epidermal growth factor receptor status, primary maximum standardised uptake value, and nodal location.

Subgroup	AUC (95% confidence interval)
T stage	
1 & 2	0.904 (0.839-0.968)
3 & 4	0.84 (0.703-0.978)
p Value	0.370
Histology	
Adenocarcinoma	0.838 (0.745-0.93)
Squamous cell carcinoma	0.952 (0.877-1)
p Value	0.0458
EGFR status	
Wild type	0.961 (0.894-1)
Mutated	0.886 (0.747-1)
p Value	0.298
Primary SUV_{max}	
<10	0.86 (0.761-0.959)
≥10	0.9 (0.829-0.970)
p Value	0.523
Nodal location	
Hilar	0.863 (0.777-0.949)
Mediastinal	0.903 (0.818-0.989)
p Value	0.497

Abbreviations: AUC = area under the curve; EGFR = epidermal growth factor receptor; SUV_{max} = maximum standardised uptake value.

differences among the subgroups analyses, except for the histology, which had a borderline p value of 0.0458.

There were limited studies comparing the performance of visual score with SUV_{max} or nodal diameter.[13] Our study suggested that the visual interpretation achieved satisfactory AUC, specificity, accuracy, and NPVs. Such performance was statistically significant (p = 0.0003) compared with that of nodal diameter. While the cut-off for nodal diameter was 10 mm (axial plane), the smallest true positive LN identifiable by visual interpretation had a diameter of 7 mm with a SUV_{max} of 2.5 (corresponding primary tumour SUV_{max} = 11 and liver SUV_{mean} = 1.49). This example demonstrates the higher sensitivity of PET/CT to detect small malignant LNs compared with nodal diameter in CT alone. Although the visual score resulted in higher specificity, accuracy, PPV and NPV compared with SUV_{max} of 2.5, the differences were not statistically significant. A possible explanation is the similar cut-off magnitudes. A visual score with a cut-off of 3 corresponds to the liver's SUV_{mean} (range, 1.22-3.16). This is close to the SUV_{max} cut-off of 2.5 and therefore yields similar performance.

The limited sensitivity of 0.810 in visual interpretation was reviewed by examining the false negative cases.

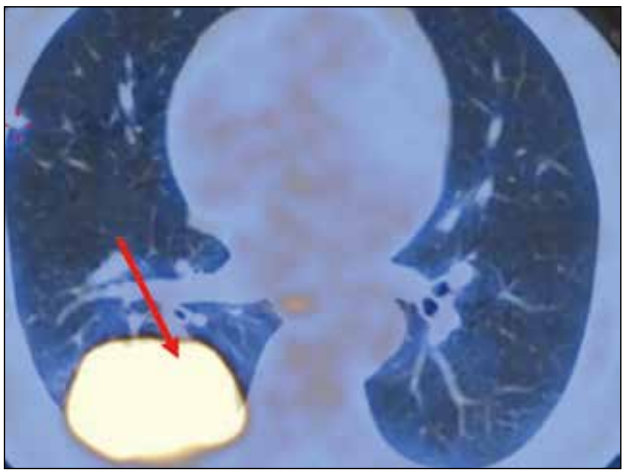

Figure 5. A large primary tumour can hinder the identification of an adjacent intrapulmonary lymph node (arrow), which was malignant in histology.

Among the eight false negative LNs, three (25%) may be explained by the limited PET/CT spatial resolution, as their pathology findings showed only a few clusters of tumour cells. Two cases (16.7%) may have been attributable to the close proximity of the primary tumour and LN. As illustrated in Figure 5, a large primary tumour limited the visualisation of the nearby intrapulmonary LN, which was proven to be malignant histologically. Whereas low ^{18}F-FDG uptake by the primary tumour may limit the identification of nodal metastases,[19] the 38 cases with nodal metastases all had ^{18}F-FDG–avid primaries. The least avid primary tumour with nodal metastasis had an SUV_{max} of 3.07, which was still distinguishable from the liver SUV_{mean} of 2.2. All nine (9.3%) cases with non–^{18}F-FDG avid primaries had no nodal metastases. We do not know what was behind the remaining seven false negative cases (58.3%).

Nodal staging is crucial for treatment of early-stage NSCLC.[4] For N1 and N2 disease treated with surgery, the adjuvant treatment is chemotherapy (N1) and sequential CRT (N2). For inoperable N2 disease, the primary treatment is CRT. Of the SUV_{max}, visual score and nodal diameter, the visual score achieved the most reliable overall staging, with an accuracy of 79% (Table 4). If a patient is mistakenly upstaged to N2 (10% subjects in the current report), his/her opportunity for curative surgery may be missed as they may receive CRT. If a patient is mistakenly downstaged from N2 disease (2% currently), his/her option for CRT instead of surgery may also be missed.

The cut-off of visual score in the current study was 3, implying that the LNs were suspicious for malignancy if their uptakes were greater than or equal to that of the liver (Figure 3). The identical cut-off of 3 was consistently observed in subgroup analyses (Figure 4). On the other hand, the cut-off in a previous study was >3,[14] implying malignancy if the uptake was >2 times the liver uptake or as elevated as that of the primary. The discrepancy of the two cut-offs may be due to different scanners, acquisition protocols, or reconstruction methods. Indeed, the same study suggested malignancy for a score of 3 as it was 3.3 times as likely to be malignant as a LN with a score of 2.[14]

In our study, the PPV based on visual interpretation was 0.623, which is less than the approximate value of 0.75 in the previous report.[14] This discrepancy may be explained by the fact that the lower the ratio of histologically malignant/total LNs, the lower the PPV. This ratio was 0.126 in the current study, which is lower than 0.194 in the previous report.[14]

The current study was limited by several factors. This was a retrospective study, thus it had no randomisation, and it was difficult to control confounders. The cases were all fit for histological workup and had no evidence of distant metastases. The study evaluated only 97 subjects and all were Chinese. The SUV depended on many factors, including scanner mode, acquisition protocol, and reconstruction method of the PET/CT.

CONCLUSION

PET/CT offers noninvasive preoperative nodal staging of NSCLC. A convenient visual interpretation is demonstrated to have diagnostic performance better than and similar to that of nodal diameter and SUV_{max}, respectively. The limited sensitivity can be attributed to the spatial resolution of PET/CT.

REFERENCES

1. Bray F, Ferlay J, Soerjomataram I, Siegel RL, Torre LA, Jemal A. Global cancer statistics 2018: GLOBOCAN estimates of incidence and mortality worldwide for 36 cancers in 185 countries. CA Cancer J Clin. 2018;68:394-424.
2. Edge SB, Compton CC. The American Joint Committee on Cancer: the 7th edition of the AJCC cancer staging manual and the future of TNM. Ann Surg Oncol. 2010;17:1471-4.
3. Detterbeck FC, Boffa DJ, Kim AW, Tanoue LT. The eighth edition lung cancer stage classification. Chest. 2017;151:193-203.
4. Ettinger DS, Wood DE, Aisner DL, Akerley W, Bauman J, Chirieac LR, et al. Non–small-cell lung cancer, version 5.2017, NCCN Clinical Practice Guidelines in Oncology. J Natl Compr Canc Netw. 2017;15:504-35.
5. Bacsa S, Czakó Z, Vezendi S. The complications of mediastinoscopy. Panminerva Med. 1974;16:402-6.
6. Bousema JE, Aarts MJ, Dijkgraaf MG, Annema JT, van den Broek FJ. Trends in mediastinal nodal staging and its impact on unforeseen N2 and survival in lung cancer. Eur Respir J. 2021;57:2001549.
7. Toloza EM, Harpole L, McCrory DC. Noninvasive staging of non–small-cell lung cancer: a review of the current evidence. Chest. 2003;123 (1 Suppl):137S-46S.
8. Schirrmeister H, Hetzel M, Buck A. Staging of non–small-cell lung cancer with integrated PET and CT. N Engl J Med. 2003;349:1188-90.
9. Antoch G, Stattaus J, Nemat AT, Marnitz S, Beyer T, Kuehl H, et al. Non–small-cell lung cancer: dual-modality PET/CT in preoperative staging. Radiology. 2003;229:526-33.
10. Bryant AS, Cerfolio RJ, Klemm KM, Ojha B. Maximum standard uptake value of mediastinal lymph nodes on integrated FDG-PET-CT predicts pathology in patients with non–small-cell lung cancer. Ann Thorac Surg. 2006;82:417-23.
11. Hellwig D, Graeter TP, Ukena D, Groeschel A, Sybrecht GW, Schaefers HJ, et al. ^{18}F-FDG PET for mediastinal staging of lung cancer: which SUV threshold makes sense? J Nucl Med. 2007;48:1761-6.
12. Hofman MS, Smeeton NC, Rankin SC, Nunan T, O'Doherty MJ. Observer variation in FDG PET-CT for staging of non–small-cell lung carcinoma. Eur J Nucl Med Mol Imaging. 2009;36:194-9.
13. Mathew B, Purandare NC, Pramesh CS, Karimundackal G, Jiwnani S, Agrawal A, et al. Improving accuracy of ^{18}F-fluorodeoxyglucose PET computed tomography to diagnose nodal involvement in non–small-cell lung cancer: utility of using various predictive models. Nucl Med Commun. 2021;42:535-44.
14. Rogasch JM, Apostolova I, Steffen IG, Steinkrüger FL, Genseke P, Riedel S, et al. Standardized visual reading of F18-FDG-PET in patients with non–small-cell lung cancer scheduled for preoperative thoracic lymph node staging. Eur J Radiol. 2016;85:1345-50.
15. Boellaard R. Standards for PET image acquisition and quantitative data analysis. J Nucl Med. 2009;50 Suppl 1:11S-20S.
16. Boellaard R, Krak NC, Hoekstra OS, Lammertsma AA. Effects of noise, image resolution, and ROI definition on the accuracy of standard uptake values: a simulation study. J Nucl Med. 2004;45:1519-27.
17. Boellaard R, Delgado-Bolton R, Oyen WJ, Giammarile F, Tatsch K, Eschner W, et al. FDG PET/CT: EANM procedure guidelines for tumour imaging: version 2.0. Eur J Nucl Med Mol Imaging. 2015;42:328-54.
18. Mountain CF, Dresler CM. Regional lymph node classification for lung cancer staging. Chest. 1997;111:1718-23.
19. Cloran FJ, Banks KP, Song WS, Kim Y, Bradley YC. Limitations of dual time point PET in the assessment of lung nodules with low FDG avidity. Lung Cancer. 2010;68:66-71.

Hong Kong J Radiol. 2023;26:14-23 | https://doi.org/10.12809/hkjr2317597

ORIGINAL ARTICLE **CME**

Neoadjuvant Treatment of Locally Advanced Rectal Cancer in Elderly Patients: Real-World Experience at a Tertiary Institution

GTC Cheung[1], EYH Chuk[1], KM Cheung[1], JCH Chow[1], L Fok[2], HL Leung[2], CC Law[1]

[1]Department of Clinical Oncology, Queen Elizabeth Hospital, Hong Kong
[2]Department of Oncology, United Christian Hospital, Hong Kong

ABSTRACT

Introduction: *The incidence of rectal cancer increases with age. Neoadjuvant radiotherapy, with or without concurrent chemotherapy, has been shown to improve outcomes. Elderly patients are underrepresented in clinical trials. In Hong Kong, there is a lack of consensus and local data to inform patient selection and formulate optimal treatment strategies for them. We sought to examine the outcomes of elderly patients undergoing neoadjuvant treatment for locally advanced rectal cancer.*

Methods: *Cases of patients with locally advanced rectal cancers who received neoadjuvant treatment in Department of Clinical Oncology, Queen Elizabeth Hospital from 2015 to 2018 were reviewed. 'Elderly patient' was defined as those ≥70 years at diagnosis. The key study endpoints were local relapse-free survival (RFS), regional RFS, distant RFS, overall RFS, and overall survival. Other endpoints included rate of downstaging, rate of conversion from threatened/involved margins to clear margins, and treatment-related toxicities.*

Results: *In all, 74 elderly patients and 142 non-elderly patients were identified. The proportion of patients receiving concurrent chemotherapy during radiotherapy was lower in the elderly patients ($p < 0.001$). Chemoradiation administered to patients of all ages did not result in statistically significant differences in any survival endpoint. Elderly patients deemed unfit for concurrent chemotherapy had a higher incidence of treatment toxicities. Age was not a significant prognostic factor in any categories of survival.*

Conclusion: *Age should not be a deterministic factor in treatment planning in locally advanced rectal cancer. Satisfactory oncological outcomes can be achieved in selected elderly patients. Utilisation of geriatric assessment and consideration of patients' preference are required to optimise treatment outcomes.*

Key Words: *Aged; Chemoradiotherapy; Neoadjuvant therapy; Radiotherapy; Rectal cancers*

Correspondence: *Dr GTC Cheung, Department of Clinical Oncology, Queen Elizabeth Hospital, Hong Kong*
Email: ctc069@ha.org.hk

Submitted: 14 Jun 2022; Accepted: 23 Oct 2022.

Contributors: GTCC designed the study and acquired the data. All authors analysed the data. GTCC, EYHC, KMC and JCHC drafted the manuscript. All authors critically revised the manuscript for important intellectual content. All authors had full access to the data, contributed to the study, approved the final version for publication, and take responsibility for its accuracy and integrity.

Conflicts of Interest: As an editor of the journal, GTCC was not involved in the peer review process. Other authors have disclosed no conflicts of interest.

Funding/Support: This research received no specific grant from any funding agency in the public, commercial, or not-for-profit sectors.

Data Availability: All data generated or analysed during the present study are available from the corresponding author on reasonable request.

Ethics Approval: This research was approved by the Research Ethics Committee (Kowloon Central/Kowloon East Cluster) of Hospital Authority, Hong Kong (Ref: KC/KE-21-0264/ER-3) and was conducted according to the Declaration of Helsinki. Informed consent of patients was waived because of the retrospective nature of the study.

中文摘要

局部晚期直腸癌年老病人的術前輔助治療：第三層醫療機構的實際經驗

張天俊、祝菀馨、張嘉文、周重行、霍善智、梁海量、羅志清

簡介：直腸癌發病率隨年齡增長而上升。已有研究顯示術前輔助放射治療（不論有否同步進行化學治療）能改善病情。年老病人在臨床測試中的代表性不足。在香港，在選取病人及為該類病人制訂最佳治療策略方面，醫學界尚未達成共識，本地數據亦不足。我們嘗試分析進行局部晚期直腸癌術前輔助治療的年老病人的病情。

方法：本研究回顧了於2015至2018年期間在伊利沙伯醫院臨床腫瘤科接受術前輔助治療的局部晚期直腸癌病人個案。「年老病人」的定義為於確診時年屆70歲或以上的病人。關鍵研究終點為無局部復發存活、無區域復發存活、無遠處轉移存活、整體無復發生存率及總生存率。其他研究終點包括癌症降期率、從受威脅／侵犯切緣轉為陰性切緣率及治療相關毒性。

結果：我們分析了74名年老病人及142名非年老病人。年老病人在接受放射治療期間同時進行化學治療的比例較低（$p < 0.001$）。為所有年齡的病人進行放化療在任何存活終點並沒有出現統計學上的顯著差異。不適合同時接受化學治療的年老病人，其治療毒性發生率較高。年齡並非任何類別存活的重要預後因素。

結論：在規劃局部晚期直腸癌的治療時，年齡不應被視為決定性因素。部分年老病人可以獲得令人滿意的腫瘤治療結果。要達至最佳治療結果，須使用老年評估及考慮病人的偏好。

INTRODUCTION

According to the latest Hong Kong Cancer Statistics 2019, colorectal cancer ranked second in annual incidence of neoplasms in Hong Kong.[1] Within the 5556 new cases in 2019, 2072 were rectal/anal malignancies. Age is an important risk factor for rectal cancers; over half of the newly diagnosed rectal/anal cancer patients in 2019 were >65 years old.[1]

Surgery is the mainstay of curative treatment for rectal adenocarcinomas. Extensive research efforts were made in search of the optimal neoadjuvant therapy modalities to improve outcomes. The German Rectal Cancer Study Group's phase III study published in 2004 set the standard of neoadjuvant chemoradiotherapy for clinical T3/4 or lymph node positive diseases,[2] and the role of concurrent chemotherapy during neoadjuvant radiotherapy (RT) was confirmed in a 2013 Cochrane review in lowering the incidence of local recurrence.[3] Mesorectal fascial involvement threatening the circumferential resection margin (CRM) and distal rectal tumours were included in international treatment guidelines as relative indications for neoadjuvant treatment.[4,5]

Elderly patients were underrepresented in these clinical trials. Ageing is associated with poor performance status, an increased incidence of comorbidities, and suboptimal treatment tolerance. Retrospective studies have investigated the outcomes of elderly patients undergoing rectal cancer treatments,[6-9] but conclusions were divided regarding the adequate methodology of patient selection, the optimal magnitude of neoadjuvant treatment in patients with marginal performance status, and the side-effect profile of this population. There is also a lack of local data specifically for this controversial topic. We therefore performed this study to examine the outcomes of elderly patients undergoing neoadjuvant treatment for locally advanced rectal cancers.

METHODS

We retrospectively reviewed the medical records of consecutive patients that received neoadjuvant treatment for rectal cancer in Department of Clinical Oncology, Queen Elizabeth Hospital during the period from 1 January 2015 to 31 December 2018. Patients were considered for neoadjuvant treatment if they satisfied the following inclusion criteria: (1) biopsy-proven adenocarcinoma of rectum (located ≤12 cm from anal verge); (2) staging by pelvic magnetic resonance imaging, and either computed tomography scan covering thorax, abdomen and pelvis, or positron emitted tomography/computed tomography of the

whole body, showing non-metastatic disease that was at local stage T3 or above by American Joint Committee on Cancer's Cancer Staging Manual 7th edition, or with involved or threatened mesorectal fascia; and (3) deemed fit for neoadjuvant treatment and subsequent surgery by the attending physician based on performance status, age, and comorbidities. The diagnostic scans and the decision to institute neoadjuvant treatment were discussed in a multidisciplinary team meeting involving clinical oncologists, colorectal surgeons, and diagnostic radiologists.

Neoadjuvant treatment consisted of pelvic RT with or without concurrent chemotherapy. For RT, gross tumour volume was determined from clinical data (physical examination, colonoscopy and imaging findings). Clinical target volume included gross tumour volume plus a 2-cm circumferential margin, the entire mesorectum, and high-risk nodal areas including presacral, mesorectal, obturator, and internal iliac nodes. A 1-cm circumferential margin was added to clinical target volume to form the planning target volume. Patients were treated with long-course RT with conformal, intensity-modulated radiotherapy or volumetric modulated arc therapy techniques. A minimum dose of 45 Gy in 25 fractions was prescribed to the 100% isodose line; an optional boost to the gross disease was allowed up to a total equivalent dose of 54 Gy in 30 fractions, either with two-phase techniques (in conformal RT) or simultaneous integrated boost (in intensity-modulated radiotherapy/volumetric modulated arc therapy).

Similar to reported local practice,[10] two regimens of concurrent chemotherapy were adopted: intravenous bolus 5-fluorouracil at 500 mg/m^2 on Days 1-3 and Days 29-31, or oral capecitabine at 825 mg/m^2 twice daily, 5 days per week. Omission of concurrent chemotherapy due to advanced age, comorbidities, or patient preference was allowed.

Cross-sectional imaging was repeated at around 4-6 weeks after completion of RT to evaluate treatment response after neoadjuvant treatment and to assess operability. If operable, total mesorectal excision was performed ideally 6-10 weeks after RT completion. Based on our institution protocol, further adjuvant chemotherapy was not routinely offered due to the lack of evidence supporting benefit of adjuvant chemotherapy in randomised controlled trials and meta-analyses.

After treatment, surveillance was performed with regular history taking, physical examination, carcinoembryonic antigen monitoring, and surveillance colonoscopy. Cross-sectional imaging with computed tomography or positron emitted tomography/computed tomography scan was arranged when clinically indicated.

In this study, we defined elderly patients as those ≥70 years old at the time of histological diagnosis. The key endpoints of this study were local relapse-free survival (RFS), regional RFS, distant RFS, overall RFS, and overall survival (OS). Other endpoints included rate of downstaging (both T and N stages) and rate of conversion from threatened/involved CRM to clear margins. Treatment-related toxicities were assessed by the National Cancer Institute Common Terminology Criteria for Adverse Events version 4.03 and 30-day postoperative mortality. Data were analysed using commercial software SPSS (Windows version 24.0; IBM Corp, Armonk [NY], United States). Baseline characteristics between groups were tabulated and compared using the Mann-Whitney *U* test for continuous data and the Chi squared test for categorical data. Survival endpoints were estimated by the Kaplan-Meier method. Prognostic significance of clinical predictors was analysed using the log-rank test in simple analysis and the Cox proportional hazards model in multivariable regression analysis.

RESULTS

A total of 238 cases of patients with rectal cancer who received neoadjuvant therapy were identified. Twenty-two cases were excluded for Stage IV disease at baseline. A total of 74 of the remaining 216 patients were elderly patients. Median ages of elderly patients and non-elderly patients were 76.0 and 61.2 years, respectively. In total, 91.7% of the patients had an Eastern Cooperative Oncology Group performance status (ECOG PS) score of 0-1; a higher proportion of ECOG PS score of 2 was noted in the elderly population (18.9% vs. 2.8%, $p = 0.011$). Elderly patients had a significantly higher prevalence of comorbidities (hypertension: 66.2% vs. 26.8%, $p < 0.001$; ischaemic heart disease: 16.2% vs. 4.9%, $p = 0.019$). No statistically significant difference was noted between elderly and non-elderly groups in clinical stage or CRM status. The full baseline demographics and comorbidities before treatment initiation are shown in Table 1.

A total of 53 elderly patients and six non-elderly patients had neoadjuvant RT alone; the proportion of patients who received concurrent chemotherapy was

Table 1. Baseline demographics by age-group and treatment.*

	Elderly patients (n = 74)			Non-elderly patients (n = 142)		
	Whole cohort	CRT (n = 21)	RT alone (n = 53)	Whole cohort	CRT (n = 136)	RT alone (n = 6)
Median age at diagnosis, y (range)	76.0 (70.0-89.4)	71.2 (70.2-75.3)	78.8 (70.0-89.4)	61.2 (39.1-69.8)	61.1 (39.1-69.8)	67.1 (53.7-69.2)
Gender						
Male	50 (67.6%)	18 (85.7%)	32 (60.4%)	102 (71.8%)	99 (72.8%)	3 (50.0%)
Female	24 (32.4%)	3 (14.3%)	21 (39.6%)	40 (28.2%)	37 (27.2%)	3 (50.0%)
Tobacco use						
Never	40 (54.1%)	9 (42.9%)	31 (58.5%)	69 (48.6%)	66 (48.5%)	3 (50.0%)
Active	11 (14.9%)	5 (23.8%)	6 (11.3%)	41 (28.9%)	40 (29.4%)	1 (16.7%)
Ex-user	22 (29.7%)	7 (33.3%)	15 (28.3%)	29 (20.4%)	27 (19.9%)	2 (33.3%)
Unknown	1 (1.4%)	0	1 (1.9%)	3 (2.1%)	3 (2.2%)	0
Alcohol use						
Never	54 (73.0%)	11 (52.4%)	43 (81.1%)	97 (68.3%)	91 (66.9%)	6 (100%)
Active	11 (14.9%)	6 (28.6%)	5 (9.4%)	30 (21.1%)	30 (22.1%)	0
Ex-user	6 (8.1%)	4 (19.0%)	2 (3.8%)	12 (8.5%)	12 (8.8%)	0
Unknown	3 (4.1%)	0	3 (5.7%)	3 (2.1%)	3 (2.2%)	0
Comorbidities						
Ischaemic heart disease	12 (16.2%)	1 (4.8%)	11 (20.8%)	7 (4.9%)	6 (4.4%)	1 (16.7%)
Diabetes mellitus	19 (25.7%)	2 (9.5%)	17 (32.1%)	31 (21.8%)	27 (19.9%)	4 (66.7%)
Hypertension	49 (66.2%)	11 (52.4%)	38 (71.7%)	38 (26.8%)	36 (26.5%)	2 (33.3%)
Hyperlipidaemia	23 (31.1%)	3 (14.3%)	20 (37.7%)	29 (20.4%)	26 (19.1%)	3 (50.0%)
ECOG PS score						
0-1	60 (81.1%)	21 (100%)	39 (73.6%)	138 (97.2%)	135 (99.3%)	3 (50.0%)
2	14 (18.9%)	0	14 (26.4%)	4 (2.8%)	1 (0.7%)	3 (50.0%)
Tumour distance from anal verge, cm						
0-5.0	39 (52.7%)	11 (52.4%)	28 (52.8%)	67 (47.2%)	64 (47.1%)	3 (50.0%)
5.1-10.0	35 (47.3%)	10 (47.6%)	25 (47.2%)	70 (49.3%)	67 (49.3%)	3 (50.0%)
10.1-15.0	0	0	0	5 (3.5%)	5 (3.7%)	0
Overall stage						
II	9 (12.2%)	3 (14.3%)	6 (11.3%)	13 (9.2%)	12 (8.8%)	1 (16.7%)
III	65 (87.8%)	18 (85.7%)	47 (88.7%)	129 (90.8%)	124 (91.2%)	5 (83.3%)
Clinical T staging						
2	3 (4.1%)	0	3 (5.7%)	6 (4.2%)	6 (4.4%)	0
3	61 (82.4%)	18 (85.7%)	43 (81.1%)	102 (71.8%)	98 (72.1%)	4 (66.7%)
4	10 (13.5%)	3 (14.3%)	7 (13.2%)	34 (23.9%)	32 (23.5%)	2 (33.3%)
Clinical N staging						
0	9 (12.2%)	3 (14.3%)	6 (11.3%)	13 (9.2%)	12 (8.8%)	1 (16.7%)
1	15 (20.3%)	3 (14.3%)	12 (22.6%)	25 (17.6%)	25 (18.4%)	0
2	50 (67.6%)	15 (71.4%)	35 (66.0%)	104 (73.2%)	99 (72.8%)	5 (83.3%)
CRM status						
Clear	16 (21.6%)	5 (23.8%)	11 (20.8%)	34 (23.9%)	34 (25.0%)	0
Involved/threatened	58 (78.4%)	16 (76.2%)	42 (79.2%)	108 (76.1%)	102 (75.0%)	6 (100%)
Carcinoembryonic antigen						
Normal	28 (37.8%)	9 (42.9%)	19 (35.8%)	44 (31.0%)	44 (32.4%)	0
Elevated	45 (60.8%)	12 (57.1%)	33 (62.3%)	97 (68.3%)	92 (67.6%)	5 (83.3%)
Unknown	1 (1.4%)	0	1 (1.9%)	1 (0.7%)	0	1 (16.7%)

Abbreviations: CRM = circumferential resection margin; CRT = chemoradiotherapy; ECOG PS = Eastern Cooperative Oncology Group Performance Status; RT = radiotherapy.
* Data are shown as No. (%), unless otherwise specified.

lower in elderly patients than non-elderly patients (28.4% vs. 95.8%, $p < 0.001$). The most common reasons for chemotherapy omission in elderly patients were advanced age (n = 44, 83%), poor performance status (n = 4, 7.5%), and patient refusal (n = 4, 7.5%). Technique of RT, boost dose frequency, and time of RT completion were similar between elderly and non-elderly groups.

After neoadjuvant treatments, 58 elderly cases (78.4%) and 128 non-elderly (90.1%) cases went on to undergo radical surgery as planned; 16 elderly patients (21.6%) and 14 non-elderly patients (9.9%) did not undergo radical surgery. The reasons are shown in Table 2. These patients were excluded from survival analyses but were included in toxicity and safety analyses.

Figure 1 illustrates the treatment scheme with number of cases involved. The time to radical surgery and the

Table 2. Reasons for radical surgery not being performed.*

	Elderly patients (16/74)			Non-elderly patients (14/142)		
	Whole cohort	CRT (3/21)	RT alone (13/53)	Whole cohort	CRT (13/136)	RT alone (1/6)
Inoperable disease	5 (6.8%)	1 (4.8%)	4 (7.5%)	9 (6.3%)	8 (5.9%)	1 (16.7%)
General condition deterioration thus unfit for operation/anaesthesia	5 (6.8%)	1 (4.8%)	4 (7.5%)	1 (0.7%)	1 (0.7%)	0
Patient refusal	6 (8.1%)	1 (4.8%)	5 (9.4%)	4 (2.8%)	4 (2.9%)	0

Abbreviations: CRT = chemoradiotherapy; RT = radiotherapy.
* Data are shown as No. (%), unless otherwise specified.

rate of sphincter preservation were similar between elderly and non-elderly patients. A total of 27 patients subsequently received further adjuvant chemotherapy after surgery. Treatment details are listed in the online supplementary Appendix.

No statistically significant difference in treatment outcomes was observed between elderly and non-elderly cases, or between the CRT and RT-alone arms. Eleven patients achieved a pathological complete response after neoadjuvant treatment, with all of them had received neoadjuvant CRT; the incidence was similar in the elderly and non-elderly CRT cohorts. Detailed treatment outcomes are listed in Table 3.

The 5-year local RFS, regional RFS, distant RFS, overall RFS and OS of the entire cohort were 88.0%, 88.7%, 63.9%, 57.1% and 70.2%, respectively. Elderly and non-elderly patients who underwent CRT did not demonstrate a statistically significant difference in any survival endpoints. Five patients in the elderly RT-alone subgroup died of non-cancer causes (12.5% of the subgroup; 3 due to infection, 1 due to acute myocardial infarction, and 1 due to cerebrovascular accident); no non-cancer mortality was documented in the elderly CRT subgroup. The Kaplan-Meier curves of the survival endpoints are demonstrated in Figure 2.

Elderly patients who underwent neoadjuvant CRT had noninferior toxicities and safety profiles in both neoadjuvant treatment and surgery when compared to their non-elderly counterparts. The incidence of grade ≥3 toxicities in neoadjuvant treatment in elderly and non-elderly CRT arms were 4.8% and 14.0%, respectively. Postoperative 30-day morbidities were 16.7% and 24.4%, respectively. Elderly patients who underwent neoadjuvant RT alone had higher incidence of significant treatment toxicities, with 7.5% having grade ≥3 RT toxicities, and 32.5% having significant morbidities after operation. No treatment-induced mortality was observed in this cohort. Table 4 shows the incidence of significant treatment toxicities.

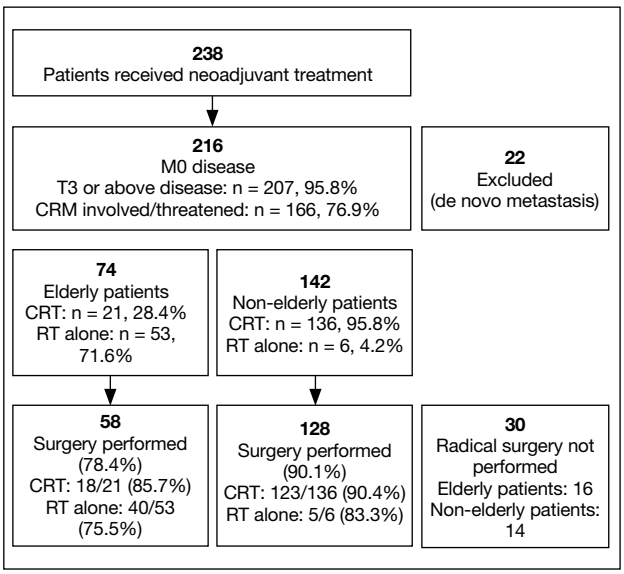

Figure 1. Treatment flowchart and number of patients involved.
Abbreviations: CRM = circumferential resection margin; CRT = chemoradiotherapy; RT = radiotherapy.

Analyses of prognostic factors indicated that older age was not a significant prognostic factor in any of the categories of survival on simple and multivariable analyses. After multivariable regression analysis, resection margin involvement and intramesorectal plane of excision were significantly associated with shorter local RFS. Presence of lymphovascular invasion and intramesorectal plane of excision were significantly associated with shorter distant RFS. Lymphovascular invasion, margin involved, and intramesorectal plane of excision were significantly associated with shorter overall RFS. Absence of concurrent chemotherapy, poorly differentiated histology, lymphovascular invasion, and intramesorectal plane of excision were significantly associated with shorter OS. The simple and multivariable analyses results are shown in Table 5.

Table 3. Treatment outcomes.*

		Elderly patients (n = 58)			Non-elderly patients (n = 128)		
		Whole cohort	CRT (n = 18)	RT alone (n = 40)	Whole cohort	CRT (n = 123)	RT alone (n = 5)
Pathological response							
ypT	0	2 (3.4%)	2 (11.1%)	0	11 (8.6%)	11 (8.9%)	0
	In situ	2 (3.4%)	0	2 (5.0%)	2 (1.6%)	2 (1.6%)	0
	1	2 (3.4%)	1 (5.6%)	1 (2.5%)	5 (3.9%)	5 (4.1%)	0
	2	9 (15.5%)	2 (11.1%)	7 (17.5%)	20 (15.6%)	19 (15.4%)	1 (20.0%)
	3	42 (72.4%)	12 (66.7%)	30 (75.0%)	81 (63.3%)	78 (63.4%)	3 (60.0%)
	4	1 (1.7%)	1 (5.6%)	0	9 (7.0%)	8 (6.5%)	1 (20.0%)
ypN	0	38 (65.5%)	11 (61.1%)	27 (67.5%)	77 (60.2%)	75 (61.0%)	2 (40.0%)
	1	14 (24.1%)	6 (33.3%)	8 (20.0%)	33 (25.8%)	31 (25.2%)	2 (40.0%)
	2	6 (10.3%)	1 (5.6%)	5 (12.5%)	18 (14.1%)	17 (13.8%)	1 (20.0%)
Resection margin	Clear	44 (75.9%)	12 (66.7%)	32 (80.0%)	101 (78.9%)	96 (78.0%)	5 (100%)
	Involved	14 (24.1%)	6 (33.3%)	8 (20.0%)	27 (21.1%)	27 (22.0%)	0
Pathological CR		2 (3.4%)	2 (11.1%)	0	9 (7.0%)	9 (7.3%)	0
T downstaging		18 (31.0%)	6 (33.3%)	12 (30.0%)	48 (37.5%)	47 (38.2%)	1 (20.0%)
N downstaging		43 (74.1%)	13 (72.2%)	30 (75.0%)	95 (74.2%)	91 (74.0%)	4 (80.0%)
CRM clearance from involved/threatened		32/43 (74.4%)	10/13 (76.9%)	22/30 (73.3%)	76/96 (79.2%)	71/91 (78.0%)	5/5 (100%)
Survival data							
3-year	Local RFS	88.5%	94.4%	85.7%	91.1%	90.8%	100%
	Regional RFS	94.5%	94.4%	94.5%	90.7%	90.3%	100%
	Distant RFS	69.8%	77.8%	66.2%	72.0%	71.1%	100%
	Overall RFS	65.0%	77.8%	59.3%	66.2%	65.6%	80.0%
	OS	77.5%	88.9%	72.3%	86.4%	86.7%	80.0%
5-year	Local RFS	85.3%	94.4%	80.6%	89.0%	88.6%	100%
	Regional RFS	94.5%	94.4%	94.5%	86.4%	86.0%	100%
	Distant RFS	64.7%	77.8%	58.4%	63.7%	62.6%	100%
	Overall RFS	60.1%	77.8%	51.9%	55.8%	55.0%	80.0%
	OS	62.5%	83.3%	52.4%	73.8%	73.6%	80.0%

Abbreviations: CR = complete response; CRM = circumferential resection margin; CRT = chemoradiotherapy; OS = overall survival; RFS = relapse-free survival; RT = radiotherapy; ypN = pathological nodal staging following therapy; ypT = pathological tumour staging following therapy.

* Data are shown as No. (%), unless otherwise specified.

DISCUSSION

Elderly rectal cancer patients were a heterogenous group with diverse outcomes after neoadjuvant treatment, as demonstrated by our study, which is to date the largest reported Hong Kong cohort, and with neoadjuvant CRT outcomes comparable to local and international data.[2,10-12]

Elderly patients deemed fit for neoadjuvant CRT had comparable outcomes compared to their non-elderly counterparts, including pathological complete response rate, rate of tumour downstaging, probability of conversion from involved/threatened CRM, survival endpoints, and adverse events. On simple and multivariable analyses, it was demonstrated that old age was not an independent prognostic factor in any categories of survival. This echoes the findings of Kang et al,[7] demonstrating an elderly subgroup treated with trimodality therapy with survival outcomes similar to those of younger patients.

Whereas less fit patients in this study underwent neoadjuvant RT alone, they tolerated the whole treatment course less well, despite treatment de-escalation, with 30.2% experiencing significant treatment toxicities, and 17.0% not completing treatment due to frailty and non-compliance. A total of five out of 40 patients (12.5% of the subgroup) that completed treatment died due to non-cancer causes. Our RT-alone cohort — mostly elderly patients — had poorer OS, which was in contrast to published data that suggested concurrent chemotherapy omission was not detrimental to RFS or OS.[3,13] The reason behind poorer OS in our RT-alone cohort was likely due to selection bias, as the patients were of more advanced age, with more comorbidities and a higher incidence of non-cancer mortalities, with limited choices for palliative systemic treatment of disease recurrence.

In our institution, patients' fitness for treatment was assessed based on ECOG PS score, age, and comorbidities. Inter-observer variability is inevitable,

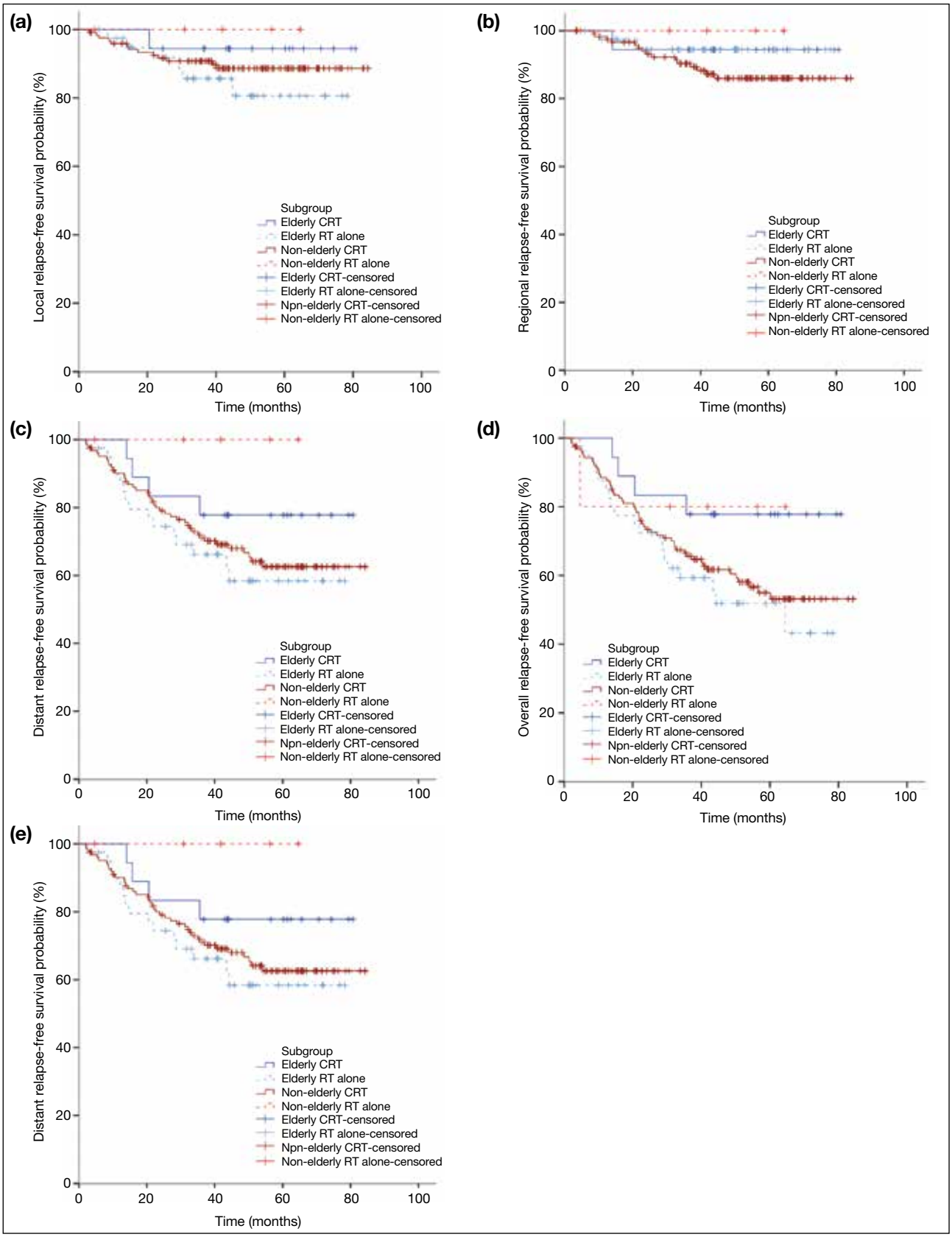

Figure 2. Kaplan-Meier curves illustrating different survival endpoints of elderly patients and non-elderly patients receiving chemoradiotherapy and radiotherapy alone: (a) local relapse-free survival, (b) regional relapse-free survival, (c) distant relapse-free survival, (d) overall relapse-free survival, and (e) overall survival.
Abbreviations: CRT = chemoradiotherapy; RT = radiotherapy.

Table 4. Significant treatment toxicities.*

		Elderly patients (n = 74)			Non-elderly patients (n = 142)		
		Whole cohort	CRT (n = 21)	RT alone (n = 53)	Whole cohort	CRT (n = 136)	RT alone (n = 6)
No. of patients who suffer from any significant treatment toxicities in any phase of treatment		20 (27.0%)	4 (19.0%)	16 (30.2%)	49 (34.5%)	48 (35.3%)	1 (16.7%)
		Neoadjuvant therapy (grade ≥3 toxicities)					
		Elderly patients (n = 74)			Non-elderly patients (n = 142)		
		Whole cohort	CRT (n = 21)	RT alone (n = 53)	Whole cohort	CRT (n = 136)	RT alone (n = 6)
All		5 (6.8%)	1 (4.8%)	4 (7.5%)	20 (14.1%)	19 (14.0%)	1 (16.7%)
RT toxicities	All categories	5 (6.8%)	1 (4.8%)	4 (7.5%)	10 (7.0%)	10 (7.4%)	0
	Dermatitis	2 (2.7%)	1 (4.8%)	1 (1.9%)	7 (4.9%)	7 (5.1%)	0
	Gastrointestinal	3 (4.1%)	0	3 (5.7%)	2 (1.4%)	2 (1.5%)	0
	Urinary	0	0	0	1 (0.7%)	1 (0.7%)	0
	Other	1 (1.4%)	0	1 (1.9%)	0	0	0
Chemo toxicities	All categories	-	0	-	-	10 (7.4%)	-
	Haematologic	-	0	-	-	6 (4.4%)	-
	Renal	-	0	-	-	2 (1.5%)	-
	Infection	-	0	-	-	2 (1.5%)	-
	Hand-foot syndrome	-	0	-	-	1 (0.7%)	-
		Surgery (30 days post-operation)					
		Elderly patients (n = 58)			Non-elderly patients (n = 128)		
		Whole cohort	CRT (n = 18)	RT alone (n = 40)	Whole cohort	CRT (n = 123)	RT alone (n = 5)
All		16 (27.6%)	3 (16.7%)	13 (32.5%)	31 (24.2%)	30 (24.4%)	1 (20.0%)
Wound healing >30 days		9 (15.5%)	1 (5.6%)	8 (20.0%)	17 (13.3%)	16 (13.0%)	1 (20.0%)
Abscess/collection requiring intervention		3 (5.2%)	1 (5.6%)	2 (5.0%)	7 (5.5%)	7 (5.7%)	0
Ileus/adhesive intestinal obstruction		4 (6.9%)	1 (5.6%)	3 (7.5%)	8 (6.3%)	8 (6.5%)	0
Second operation		4 (6.9%)	0	4 (10.0%)	1 (0.8%)	1 (0.8%)	0
Mortality		0	0	0	0	0	0

Abbreviations: CRT = chemoradiotherapy; RT = radiotherapy.
* Data are shown as No. (%), unless otherwise specified.

and discrepancies between physiological and chronological ages exist. Despite multidisciplinary team meeting endorsement, the treatments for a portion of less fit patients were futile on retrospective review, ranging from incapability to tolerate the whole treatment course to short lifespan after treatment completion. There is therefore a need for more accurate and objective tools to stratify patients' fitness for different intensities of neoadjuvant treatments, or even radical treatment at all.

Multidisciplinary participation in comprehensive geriatric assessment is recommended by the International Society of Geriatric Oncology when assessing frailty for tailoring the treatment plan in colorectal cancers.[14] However, it is a time- and resource-consuming process which hinders its routine use. Specific to rectal cancer, an international expert panel recommends patients aged ≥70 years to receive mandatory office-based frailty screening tests before being considered for usual care[15]; any presence of a frailty predictor requires a formal geriatric assessment and a geriatrician's presence in multidisciplinary decision making.

After careful assessment of fitness and frailty, treatment intent and its intensity should be adjusted accordingly. A review by Wang et al[16] proposed a treatment algorithm for locally advanced rectal cancer in elderly/comorbid patients based on degree of frailty. Elderly patients that are fully fit should undergo neoadjuvant treatment, either long-course CRT or short-course RT alone, before radical surgery. For less fit patients, different emerging nonsurgical treatment approaches, e.g., watch and wait approach or brachytherapy boost after CRT, should be considered. Palliative RT, or even symptomatic care, should be considered if patients are deemed frail. The adaptation of the abovementioned approaches will likely screen out unfit patients, avoid futile treatments in patients with limited life expectancies due to comorbidities, and

Table 5. Simple and multivariable analyses of prognostic factors.

	Simple analysis			Multivariable analysis		
	p Value	Hazard ratio	95% CI	p Value	Hazard ratio	95% CI
Local relapse-free survival						
Elderly patient (Yes vs. No)	0.658	1.23	0.49-3.09	0.727	0.77	0.18-3.38
Concurrent chemotherapy (No vs. Yes)	0.416	1.49	0.57-3.88	0.491	1.71	0.37-7.92
Poorly differentiated (Yes vs. No)	0.826	1.25	0.17-9.40	0.817	1.29	0.15-10.98
ypT4 disease (Yes vs. No)	0.041	3.61	1.06-12.32	0.396	1.83	0.45-7.37
yp node positive (Yes vs. No)	0.704	1.19	0.49-2.91	0.425	0.66	0.23-1.84
Lymphovascular invasion (Yes vs. No)	0.105	2.21	0.85-5.76	0.174	2.16	0.71-6.53
Margin involved (Yes vs. No)	0.001	4.42	1.84-10.63	0.032	3.06	1.10-8.54
Intramesorectal plane of excision (Yes vs. No)	<0.001	7.86	3.12-19.76	0.001	6.40	2.22-18.45
Regional relapse-free survival						
Elderly patient (Yes vs. No)	0.212	0.45	0.13-1.57	0.313	0.40	0.07-2.37
Concurrent chemotherapy (No vs. Yes)	0.268	0.44	0.10-1.89	0.614	0.63	0.10-3.87
Poorly differentiated (Yes vs. No)	0.480	1.75	0.37-8.29	0.952	1.07	0.14-8.41
ypT4 disease (Yes vs. No)	0.153	2.92	0.67-12.73	0.171	2.98	0.62-14.23
yp node positive (Yes vs. No)	0.002	5.13	1.83-14.40	0.052	3.15	0.99-10.02
Lymphovascular invasion (Yes vs. No)	0.006	3.94	1.49-10.38	0.090	2.56	0.86-7.59
Margin involved (Yes vs. No)	0.001	5.99	2.09-17.19	0.864	1.10	0.37-3.33
Intramesorectal plane of excision (Yes vs. No)	0.844	0.82	0.11-6.14	0.827	0.79	0.10-6.50
Distant relapse-free survival						
Elderly patient (Yes vs. No)	0.926	1.03	0.60-1.77	0.724	0.87	0.40-1.90
Concurrent chemotherapy (No vs. Yes)	0.663	1.14	0.63-2.04	0.648	1.21	0.53-2.76
Poorly differentiated (Yes vs. No)	0.048	2.53	1.01-6.36	0.378	1.61	0.56-4.62
ypT4 disease (Yes vs. No)	0.413	1.53	0.55-4.21	0.549	0.138	0.48-3.93
yp node positive (Yes vs. No)	<0.001	2.72	1.63-4.55	0.066	1.74	0.96-3.13
Lymphovascular invasion (Yes vs. No)	0.001	2.70	1.54-4.73	0.019	2.13	1.13-3.99
Margin involved (Yes vs. No)	<0.001	3.89	1.93-7.85	0.144	1.57	0.86-2.88
Intramesorectal plane of excision (Yes vs. No)	0.028	2.31	1.09-4.87	0.022	2.55	1.14-5.69
Overall relapse-free survival						
Elderly patient (Yes vs. No)	0.862	0.96	0.59-1.56	0.182	0.61	0.30-1.26
Concurrent chemotherapy (No vs. Yes)	0.419	0.81	0.49-1.35	0.203	1.62	0.77-3.39
Poorly differentiated (Yes vs. No)	0.010	2.85	1.28-6.14	0.115	2.03	0.84-4.89
ypT4 disease (Yes vs. No)	0.328	1.57	0.63-3.91	0.651	1.24	0.49-3.18
yp node positive (Yes vs. No)	0.001	2.09	1.33-3.30	0.607	1.15	0.68-1.94
Lymphovascular invasion (Yes vs. No)	0.025	2.03	1.09-3.77	0.003	2.33	1.32-4.09
Margin involved (Yes vs. No)	<0.001	2.74	1.70-4.42	0.016	1.97	1.14-3.44
Intramesorectal plane of excision (Yes vs. No)	0.016	2.28	1.17-4.45	0.011	2.54	1.24-5.20
Overall survival						
Elderly patient (Yes vs. No)	0.115	1.57	0.90-2.76	0.956	1.03	0.42-2.51
Concurrent chemotherapy (No vs. Yes)	0.012	2.09	1.17-3.71	0.046	2.47	1.02-6.00
Poorly differentiated (Yes vs. No)	0.001	4.42	1.87-10.43	0.002	5.07	1.83-14.09
ypT4 disease (Yes vs. No)	0.165	1.93	0.76-4.88	0.256	1.78	0.66-4.80
yp node positive (Yes vs. No)	0.003	2.33	1.34-4.05	0.311	1.39	0.73-2.65
Lymphovascular invasion (Yes vs. No)	<0.001	3.48	1.94-6.24	0.001	2.96	1.52-5.77
Margin involved (Yes vs. No)	0.001	2.65	1.50-4.69	0.189	1.58	0.80-3.13
Intramesorectal plane of excision (Yes vs. No)	0.004	2.89	1.40-5.97	0.001	4.10	1.79-9.41

Abbreviations: CI = confidence interval; T = tumour staging; yp = pathological staging following therapy.

minimise unbearable treatment toxicities.

Besides fitness for treatment, elderly patients' goals and preferences in treatment outcomes should be carefully respected during treatment planning. In our study, 9.4% of the elderly patients subsequently refused radical surgery after receiving neoadjuvant treatment. The specific reasons of treatment refusal were not documented in clinical notes, yet potential reasons may be due to fear of surgical/anaesthetic risk, or the subsequent inconvenience with a temporary/permanent stoma. Thorough counselling, before and during treatment, would be helpful to formulate a tailor-made treatment plan in respect of patients' preferences, and ensure compliance with treatment.

The concept of total neoadjuvant therapy for rectal cancers was introduced in recent years, with two phase III trials showing that such approach provided a superior pathological complete response rate and outcomes at 3 years (3-year disease-free survival in the UNICANCER-PRODIGE 23 trial, disease-related treatment failure at 3 years in the RAPIDO trial).[17,18] Although OS data were immature to demonstrate superiority of total neoadjuvant

therapy,[19] adding neoadjuvant chemotherapy is being increasingly adopted as a treatment option worldwide. This approach, however, will lead to more systemic chemotherapy exposure and may pose extra toxicities to patients. He et al[20] reported that the addition of neoadjuvant chemotherapy to neoadjuvant CRT in the elderly patients gave rise to similar disease-related survival rates and oncological outcomes with that of younger patients, but geriatric assessments and complications data were lacking in the study. It is expected that as we intensify the magnitude of our neoadjuvant treatment, there will be a growing importance in proper patient selection to balance the risk and benefits of treatment.

There were limitations to this study. The study data was collected retrospectively, limiting the completeness of data and introducing potential bias during data collection. There was selection bias during referral and initiation of neoadjuvant treatment, thus epidemiological data were limited. There was also selection bias when patients were assigned to different neoadjuvant treatment arms (i.e., with or without concurrent chemotherapy), thus confounding factors that were not identified in this study may be present. A short-course RT scheme was not adopted in this cohort, limiting our scope of analysis and subsequent recommendations. Absence of detailed parameters of elderly patients' conditions and the small sample size of this study limit the ability to identify prognostic factors to predict tolerance to treatment, and to derive further recommendations.

CONCLUSION

Age alone should not be a deterministic factor in treatment intensity consideration in locally advanced rectal cancer. Satisfactory oncological outcomes can be achieved in selected elderly patients with locally advanced rectal cancers who undergo standard neoadjuvant treatment and radical surgery, while the risk of shorter survival and toxicities is higher in less fit candidates. Utilisation of geriatric screening and assessment tools, and consideration of patients' preference and treatment objectives are required to achieve tailor-made treatment schemes and optimise treatment outcomes.

REFERENCES

1. Hong Kong Cancer Registry. Overview of Hong Kong Cancer Statistics of 2019. October 2021. Available from: https://www3.ha.org.hk/cancereg/pdf/overview/Overview%20of%20HK%20Cancer%20Stat%202019.pdf. Accessed 17 Apr 2022.
2. Sauer R, Becker H, Hohenberger W, Rödel C, Wittekind C, Fietkau R, et al. Preoperative versus postoperative chemoradiotherapy for rectal cancer. N Engl J Med. 2004;351:1731-40.
3. De Caluwé L, Van Nieuwenhove Y, Ceelen WP. Preoperative chemoradiation versus radiation alone for stage II and III resectable rectal cancer. Cochrane Database Syst Rev. 2013;(2):CD006041.
4. Glynne-Jones R, Wyrwicz L, Tiret E, Brown G, Rödel C, Cervantes A, et al. Rectal cancer: ESMO Clinical Practice Guidelines for diagnosis, treatment and follow-up. Ann Oncol. 2017;29(Suppl 4):iv22-40.
5. Benson AB, Venook AP, Al-Hawary MM, Azad N, Chen YJ, Ciombor KK, et al. Rectal cancer, version 2.2022, NCCN Clinical Practice Guidelines in Oncology. J Natl Compr Canc Netw. 2022;20:1139-67.
6. Choi Y, Kim JH, Kim JW, Kim JW, Lee KW, Oh HK, et al. Preoperative chemoradiotherapy for elderly patients with locally advanced rectal cancer — a real-world outcome study. Jpn J Clin Oncol. 2016;46:1108-17.
7. Kang S, Wilkinson KJ, Brungs D, Chua W, Ng W, Chen J, et al. Rectal cancer treatment and outcomes in elderly patients treated with curative intent. Mol Clin Oncol. 2021;15:256.
8. Mourad AP, De Robles MS, Putnis S, Winn RD. Current treatment approaches and outcomes in the management of rectal cancer above the age of 80. Curr Oncol. 2021;28:1388-401.
9. Tominaga T, Nagasaki T, Akiyoshi T, Fukunaga Y, Fujimoto Y, Yamaguchi T, et al. Feasibility of neoadjuvant therapy for elderly patients with locally advanced rectal cancer. Surg Today. 2019;49:694-703.
10. Lee SF, Chiang CL, Lee FA, Wong YW, Poon CM, Wong FC, et al. Outcome of neoadjuvant chemoradiation in MRI staged locally advanced rectal cancer: retrospective analysis of 123 Chinese patients. J Formos Med Assoc. 2018;117:825-32.
11. Yeung WW, Ma BB, Lee JF, Ng SS, Cheung MH, Ho WM, et al. Clinical outcome of neoadjuvant chemoradiation in locally advanced rectal cancer at a tertiary hospital. Hong Kong Med J. 2016;22:546-55.
12. Sauer R, Liersch T, Merkel S, Fietkau R, Hohenberger W, Hess C, et al. Preoperative versus postoperative chemoradiotherapy for locally advanced rectal cancer: results of the German CAO/ARO/AIO-94 randomized phase III trial after a median follow-up of 11 years. J Clin Oncol. 2012;30:1926-33.
13. Bosset JF, Collette L, Calais G, Mineur L, Maingon P, Radosevic-Jelic L, et al. Chemotherapy with preoperative radiotherapy in rectal cancer. N Engl J Med. 2006;355:1114-23.
14. Papamichael D, Audisio RA, Glimelius B, de Gramont A, Glynne-Jones R, Haller D, et al. Treatment of colorectal cancer in older patients: International Society of Geriatric Oncology (SIOG) consensus recommendations 2013. Ann Oncol. 2015;26:463-76.
15. Montroni I, Ugolini G, Saur NM, Spinelli A, Rostoft S, Millan M, et al. Personalized management of elderly patients with rectal cancer: Expert recommendations of the European Society of Surgical Oncology, European Society of Coloproctology, International Society of Geriatric Oncology, and American College of Surgeons Commission on Cancer. Eur J Surg Oncol. 2018;44:1685-702.
16. Wang SJ, Hathout L, Malhotra U, Maloney-Patel N, Kilic S, Poplin E, et al. Decision-making strategy for rectal cancer management using radiation therapy for elderly or comorbid patients. Int J Radiat Oncol Biol Phys. 2018;100:926-44.
17. Conroy T, Bosset JF, Etienne PL, Rio E, François É, Mesgouez-Nebout N, et al. Neoadjuvant chemotherapy with FOLFIRINOX and preoperative chemoradiotherapy for patients with locally advanced rectal cancer (UNICANCER-PRODIGE 23): a multicentre, randomised, open-label, phase 3 trial. Lancet Oncol. 2021;22:702-15.
18. Bahadoer RR, Dijkstra EA, van Etten B, Marijnen CA, Putter H, Kranenbarg EM, et al. Short-course radiotherapy followed by chemotherapy before total mesorectal excision (TME) versus preoperative chemoradiotherapy, TME, and optional adjuvant chemotherapy in locally advanced rectal cancer (RAPIDO): a randomised, open-label, phase 3 trial. Lancet Oncol. 2021;22:29-42.
19. Kasi A, Abbasi S, Handa S, Al-Rajabi R, Saeed A, Baranda J, et al. Total neoadjuvant therapy vs standard therapy in locally advanced rectal cancer: a systematic review and meta-analysis. JAMA Netw Open. 2020;3:e2030097.
20. He F, Chen M, Xiao WW, Zhang Q, Liu Y, Zheng J, et al. Oncologic and survival outcomes in elderly patients with locally advanced rectal cancer receiving neoadjuvant chemoradiotherapy and total mesorectal excision. Jpn J Clin Oncol. 2021;51:1391-9.

Hong Kong J Radiol. 2023;26:24-33 | https://doi.org/10.12809/hkjr2317620

ORIGINAL ARTICLE

^{90}Yttrium Selective Internal Radiation Therapy in Unresectable or Otherwise High-Risk Hepatocellular Carcinoma: Single-Centre Experience

KH Leung, MY Lim

Department of Oncology, Princess Margaret Hospital, Hong Kong

ABSTRACT

Objectives: *We reviewed prognostic factors and clinical outcomes of selective internal radiation therapy (SIRT) with ^{90}Yttrium (^{90}Y) microsphere using transarterial embolisation in unresectable hepatocellular carcinoma (HCC).*

Methods: *All cases of hepatocellular carcinoma patients who underwent ^{90}Y SIRT at Princess Margaret Hospital between July 2017 and September 2021 were retrospectively reviewed. Overall survival (OS), progression-free survival (PFS), and prognostic factors, as well as tumour response according to modified Response Evaluation Criteria in Solid Tumors criteria and safety, were evaluated.*

Results: *Thirty HCC patients were treated with ^{90}Y SIRT , of whom 26 (87%) were male. The median age of patients was 66.5 years (range, 40-93). Fifty-seven percent were chronic hepatitis B carriers and the majority (93%) had Child–Pugh class A liver disease. Patients had portal vein thrombosis, or tumour size >8 cm. After a median follow-up of 14.6 months, the objective response rate was 26.9% and the local control rate was 76.9%, including three complete responses, four partial responses and 13 cases of stable disease. The median PFS was 6.3 months and the 1-year PFS was 40.2%. Median OS was not yet reached and the 1-year OS was 57.5%. In multivariable analysis, alpha-fetoprotein level was a significant prognostic factor for OS (p = 0.045) and PFS (p = 0.011). Most side-effects were grades 1-2 only.*

Conclusion: *^{90}Y SIRT via transarterial embolisation is an effective and safe treatment for intermediate- to advanced-stage HCC patients which provides satisfactory local control with minimal toxicity. Longer survival was observed in patients with alpha-fetoprotein level <400 μg/L at baseline.*

Key Words: *Carcinoma, hepatocellular; Radiotherapy; Survival; Yttrium radioisotopes*

Correspondence: *Dr KH Leung, Department of Oncology, Princess Margaret Hospital, Hong Kong*
Email: lkh017@ha.org.hk

Submitted: 30 Jul 2022; Accepted: 20 Nov 2022.

Contributors: Both authors designed the study. KHL acquired the data. Both authors analysed the data, drafted the manuscript, and critically revised the manuscript for important intellectual content. Both authors had full access to the data, contributed to the study, approved the final version for publication, and take responsibility for its accuracy and integrity.

Conflicts of Interest: Both authors have disclosed no conflicts of interest.

Funding/Support: This research received no specific grant from any funding agency in the public, commercial, or not-for-profit sectors.

Data Availability: All data generated or analysed during the present study are available from the corresponding author on reasonable request.

Ethics Approval: The research was approved by the Kowloon West Cluster Research Ethics Committee of Hospital Authority, Hong Kong [Ref No.: KW/EX-22-027 (170-03)] and was conducted in compliance of Declaration of Helsinki. A waiver of patient consent was approved by the Committee.

中文摘要

不可切除或其他高危肝細胞癌的釔90選擇性內放射治療：單中心經驗

梁君豪、林美瑩

目的：本研究檢視在不可切除肝細胞癌使用經動脈栓塞術的釔90微粒選擇性內放射治療的預後因素及臨床結果。

方法：本研究回顧於2017年7月至2021年9月期間在瑪嘉烈醫院進行釔90選擇性內放射治療的所有肝細胞癌病人個案，評估了整體存活、疾病無惡化存活、預後因素及根據經修訂固體腫瘤反應評估標準的準則及安全程度評估的腫瘤反應。

結果：共30名病人接受了釔90選擇性內放射治療，當中26名（87%）為男性。病人年齡中位數為66.5歲（範圍，40-93）。57%病人為慢性乙型肝炎帶菌者，當中大部分（93%）為Child–Pugh分級A肝病病人。病人有肝門靜脈栓塞或腫瘤>8 cm。在覆診期中位數14.6個月後，客觀緩解率為26.9%，局部疾病控制率為76.9%，包括3個完全緩解、4個部分緩解及13個無變化個案。疾病無惡化存活中位數為6.3個月，一年疾病無惡化存活為40.2%。整體存活中位數尚未達到，一年整體存活為57.5%。在多變量分析中，甲型胎兒蛋白水平是整體存活（p = 0.045）及疾病無惡化存活（p = 0.011）的重要預後因素。大部分副作用只屬1-2級。

結論：對於中期至晚期肝細胞癌病人而言，使用經動脈栓塞術的釔90選擇性內放射治療是有效及安全的治療，能提供毒性最低而令人滿意的局部控制。本研究顯示，甲型胎兒蛋白基線水平<400 μg/L的病人的存活期較長。

INTRODUCTION

In Hong Kong, hepatocellular carcinoma (HCC) ranks fifth most common cancer and third among the most common causes of cancer death since 2014.[1] Transarterial embolisation or transarterial chemoembolisation (TACE) has been shown to improve the survival of patients with unresectable HCC.[2,3]

Selective internal radiation therapy (SIRT) is a directed liver therapy making use of the tumour vascularity in HCC in which the hepatic artery is usually the sole blood supply. SIRT involves the injection of beta emitters within resin or glass microspheres via the hepatic artery, where the spheres form microemboli, thus giving a very high radiation dose (100 to 1000+ Gy) to the tumour(s) while at the same time minimising the radiation exposure to normal liver tissue by not going through the hepatic veins or the portal system.

^{90}Yttrium (^{90}Y) is a pure beta-emitting isotope (maximum energy 2.28 MeV; mean energy 0.934 MeV), with a mean and maximum penetration range of 2.5 mm and 11 mm, respectively. It is commonly used to treat HCC.[4] ^{90}Y SIRT is effective, with one study showing an objective response rate up to 40.0% and a median overall survival (OS) of 16.4 months.[5] It has shown effectiveness in terms of survival, response rates, and safety profile similar to that with TACE in unresectable HCC in several studies and meta-analyses.[6-9] It was also shown to be an effective treatment to accomplish downstaging as a bridge to transplantation, surgical resection, or radiofrequency ablation.[10] Survival in patients receiving ^{90}Y SIRT for intermediate-advanced HCC can vary from 12-24 months (1-year pooled OS = 63%) to 6-12 months (1-year pooled OS = 37%), should portal vein thrombosis be present.[11,12]

Careful selection of suitable candidates for ^{90}Y SIRT is necessary. Several prognostic factors, including a low Child–Pugh score, percentage of liver replaced by tumour (≤50%) and alpha-fetoprotein (AFP) level (<400 μg/L) are associated with better survival.[13] Unilobar disease before SIRT and tumour response (complete response/partial response) have also been found to be significant predictors of survival.[14] It is believed that survival can be prolonged in unresectable HCC to a similar extent using TACE[15] with careful selection of candidates.

In our hospital (Princess Margaret Hospital), HCC patients are under the care of a multidisciplinary hepatoma team with oncologists, surgeons, and radiologists. Since 2012, ^{90}Y SIRT has been offered as a funded treatment by Hospital Authority, a statutory body managing the public healthcare services in Hong Kong, to high-risk HCC patients whose tumours are not resectable or ablatable, with portal vein thrombosis, or with tumour size >8 cm. Patients with infiltrative HCC, Child–Pugh class C disease, ascites, or inadequate liver reserve (with bilirubin level >34 μmol/L) are generally considered ineligible for SIRT. In this study, we report the outcome together with prognostic factors in the use of ^{90}Y in the treatment of these advanced cases of HCC in our centre.

METHODS

We retrospectively enrolled HCC patients who received ^{90}Y SIRT, either resin microspheres containing ^{90}Y (Sirtex, Australia) or ^{90}Y-impregnated glass microspheres (TheraSphere; MDS Nordion, Canada), at our hospital between July 2017 and September 2021. Before SIRT, patients underwent hepatic angiography, ^{99m}technetium-macroaggregated albumin scintigraphy, and computed tomography (CT) scans to estimate the potential doses to tumour, liver, and lung. A catheter was guided through the femoral artery and into the hepatic artery by an interventional radiologist. Blood vessels feeding the gastrointestinal tract and extrahepatic sites such as the pancreas were identified and prophylactically embolised if necessary. Patients were deemed ineligible when lung shunting was >20%. The dose activity calculation was based on a partition model.[16] The aim of the treatment was to administer a minimum dose of 120 Gy to the tumour while keeping the dose to normal liver at <40 Gy and to <50 Gy in patients with poor liver reserve. The lung dose was planned to be <20 Gy.

Treatment

Intrahepatic administration of radioactive ^{90}Y microspheres using either resin microspheres containing ^{90}Y or ^{90}Y-impregnated glass microspheres was performed. Understanding of radiation exposure of patients implanted with pure beta emitters is very limited. Patients were kept in a radiation isolation room to wait for assessment by physicists and considered safe if radiation activity was <1.5 GBq according to Radiation Ordinance of Hong Kong and Hospital Authority Code of Practice on Radiation Safety and Protection. They were discharged with medications including pantoprazole, ursodeoxycholic acid, prednisolone, and entecavir if they were viral hepatitis B carriers. A bremsstrahlung scan was performed on day 2 or 3 to document any extrahepatic reflux of ^{90}Y microspheres.

Outcome Assessment

Patients were followed up by surgeons after ^{90}Y treatment with liver function tests and AFP tumour marker test. The first follow-up was within 4 weeks after discharge to assess for any treatment-related toxicities. All patients had reassessment with triphasic CT at approximately 3 months after ^{90}Y treatment for an objective evaluation of treatment outcome according to mRECIST (modified Response Evaluation Criteria in Solid Tumors) based on combined assessment of target lesions, non-target lesions, and new lesions. Appearance of one or more new lesions was counted as progression regardless of the response of treated target and non-target lesions classified according to mRECIST. Subsequent follow-up was performed at approximately 1- to 3-month intervals with laboratory tests and/or CT at the discretion of surgeons. Any toxicity or adverse events noted during the first 6 months after completion of ^{90}Y treatment were reviewed and graded according to CTCAE (Common Terminology Criteria for Adverse Events) version 5.0 criteria.

Statistical Measures

Treatment responses were assessed radiologically according to mRECIST. Local control rate was defined as the proportion of patients with at least stable disease of an irradiated target lesion. Objective response rate was defined as the proportion of patients with partial or complete response in target lesions and at least stable disease in non-target lesions to ^{90}Y SIRT. Progression-free survival (PFS) was defined from the date of SIRT to the date of a radiological sign of progression or death from any cause. OS was calculated from the date of SIRT to the date of death from any cause. Survival curves were determined by the Kaplan-Meier method and comparison between different Barcelona Clinic Liver Cancer (BCLC) stages[17] and AFP levels was done by the log-rank test. Statistical significance was defined at $p < 0.05$. Univariate and multivariable analyses of different prognostic factors of survival outcomes, including patient and tumour factors, were performed using the Cox proportional hazards analysis. Only factors with p values < 0.05 were considered significant and included in the multivariable analysis. Commercial software SPSS (Windows version 28.0; IBM Corp, Armonk [NY], United States) was used to perform the statistical analyses.

Table 1. Baseline characteristics of the patients treated with ^{90}Yttrium (n = 29)*.

Characteristics	No. of patients (%)
Median age, y	66.5 (40-93)
Male	25 (86%)
Aetiology of cirrhosis	
Hepatitis B viral infection	16 (55%)
Hepatitis C viral infection	3 (10%)
Alcoholic cirrhosis	1 (3%)
Cryptogenic cirrhosis	6 (21%)
Non-B, non-C	3 (10%)
Child–Pugh class	
A5	9 (31%)
A6	19 (66%)
B8	1 (3%)
BCLC stage	
B	12 (41%)
C	17 (59%)
ECOG performance status score	
0	16 (55%)
1	11 (38%)
2	2 (7%)
Liver function	
Median total bilirubin, μmol/L	10 (6-29)
AFP level	
<400 μg/L	19 (66%)
≥400 μg/L	10 (34%)
Distribution of liver tumours	
Unilobar	19 (66%)
Bilobar	10 (34%)
Number of lesions	
Single	19 (66%)
Multifocal	10 (34%)
2-5	7 (24%)
5-10	2 (7%)
>10	1 (3%)
Median tumour size, cm	11.7 (4-19.7)
Tumour size	
<5 cm	1 (3%)
5-10 cm	10 (34%)
>10 cm	18 (62%)
Treatment lines	
First	26 (90%)
Second‡	1 (3%)
Third or beyond§	2 (7%)
Prior treatments received	
TACE	3 (10%)
Surgery	2 (7%)
Targeted therapy	1 (3%)
Post-SIRT surgery done	8 (28%)
Subsequent treatments received	
TACE	14 (48%)
Microwave or radiofrequency ablation	3 (10%)
Targeted therapy	9 (31%)
Immunotherapy	1 (3%)
Portal vein thrombosis	
Absent	19 (66%)
Present	10 (34%)
Site of portal vein thrombosis	
Main	4 (40%)
Left or right only	6 (60%)
Median prescribed dose, GBq	2.98 (1.1-6.09)
Median dose to tumour, Gy	174 (100-300)
Dose to tumour	
≤120 Gy	6 (21%)
>120 Gy	23 (79%)
Median dose to liver, Gy	22.94 (3.72-40.35)
Median tumour/normal liver ratio	7.96 (3.1-67.19)
Median lung shunting, %	5.8 (2.6-13.9)
Median lung dose, Gy	9.34 (2.44-31.23)

Abbreviations: AFP = alpha-fetoprotein; BCLC = Barcelona Clinic Liver Cancer; ECOG = Eastern Cooperative Oncology Group; SIRT = selective internal radiation therapy; TACE = transarterial chemoembolisation.

* One patient who had an ECOG performance status score of 3 and was classified as BCLC stage D (wheelchair bound with history of old haemorrhagic stroke) was excluded from analysis.

‡ Patient received prior TACE.

§ One patient received surgery and TACE while the other had prior surgery, TACE and targeted therapy.

RESULTS

Baseline Characteristics

From July 2017 to September 2021, 30 HCC patients were treated with ^{90}Y, of whom 26 (86.7%) were male. The median age was 66.5 years (range, 40-93). The majority of them (n = 17, 56.7%) were chronic hepatitis B carriers. Liver tumour sizes ranged from 4 cm to 19.7 cm, with a median size of 11.7 cm. Most of them had Child–Pugh class A liver disease (n = 28, 93.3%) and about one-third (n = 11, 36.7%) had AFP level ≥400 μg/L. Eleven (36.7%) patients had portal vein thrombosis with four (13.3%) having thrombosis involving the main portal vein. Half of the patients received TACE with cisplatin and one-third of them received targeted therapy (either sorafenib or lenvatinib) as subsequent treatment. Other characteristics and laboratory investigations are listed in Table 1.

Outcomes

Median follow-up time was 14.6 months. One patient with ECOG performance status score of 3 and BCLC stage D was excluded from the analysis. Of the 29 patients, 26 had assessable responses on CT (median time = 2.76 months after ^{90}Y treatment). Three patients had complete responses (11.5%), four with partial responses (15.4%), 13 with stable disease (50%), and six with progressive disease (23.1%). The objective response rate (defined as the sum of complete and partial responses) was 26.9% while the local control rate

(defined as the sum of complete and partial responses and stable disease) was 76.9%. Three patients were lost to follow-up. The median PFS was 6.3 months and 1-year PFS was 40.2% (Figure 1). Median OS was not yet reached and 1-year OS was 57.5% (Figure 2).

Eight out of 29 patients (27.6%) had surgery done after downstaging of disease (Table 2). Median time from ^{90}Y treatment to surgery was 6.1 months. One achieved a pathological complete response (Figure 3). Six of them had residual HCC completely resected and one resected with focally involved margin. Length of hospital stay was 5-24 days. One had significant intra-operative blood loss requiring massive blood transfusions. One had postoperative ileus and pulmonary embolism which resolved with anticoagulation. One died early postoperatively due to aspiration pneumonia.

Univariate and Multivariable Analyses

In univariate analysis (Table 3), BCLC stage C or above (hazard ratio [HR] = 5.733, p = 0.024), and AFP level ≥400 μg/L (HR = 4.270, p = 0.012) were significant prognostic factors for OS whereas BCLC stage C or above (HR = 3.652, p = 0.010), post-SIRT surgery (HR = 0.134, p = 0.008), AFP level ≥400 μg/L (HR = 3.527, p = 0.007), and treatment responder (defined as those with complete response or partial response) [HR = 0.203, p = 0.034; Figure 4] were significant prognostic factors for PFS. In multivariable analysis (Table 4), AFP level ≥400 μg/L remained as a significant

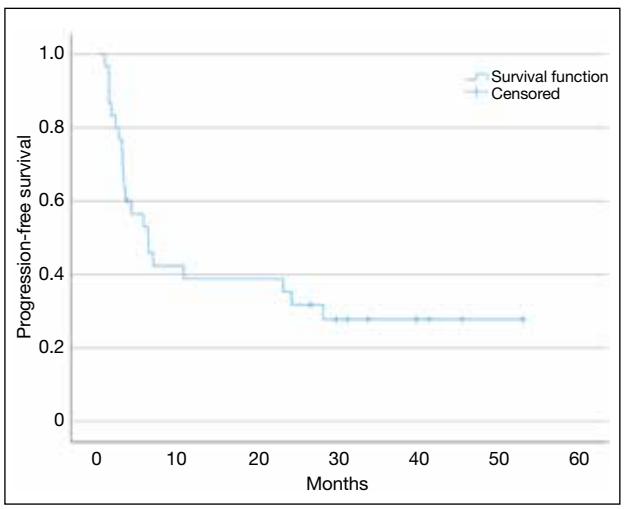

Figure 1. Kaplan-Meier curves showing progression-free survival (PFS) after ^{90}Yttrium selective internal radiation therapy. In all, 20 patients out of 29 had disease progression. Median PFS was 6.3 months. PFSs at 6, 12 and 24 months were 54.8%, 40.2% and 36.5%, respectively.

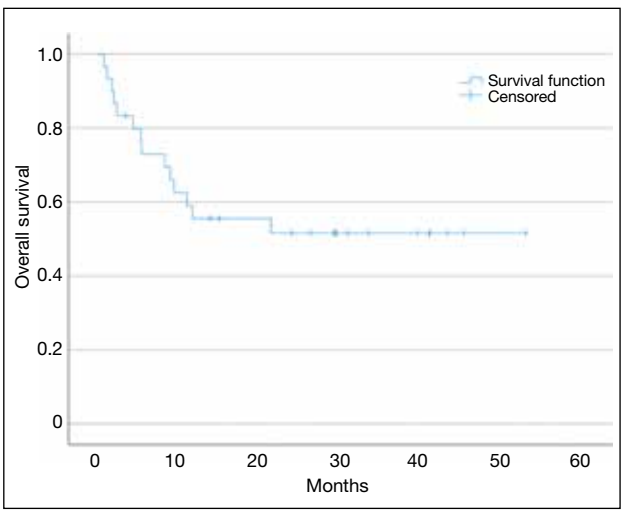

Figure 2. Kaplan-Meier curves showing overall survival (OS) after ^{90}Yttrium selective internal radiation therapy. In all, 13 died out of 29 patients. Median OS was not reached. OSs at 6 and 12 months were 75.4% and 57.5%, respectively.

Table 2. Demographics of patients amenable to surgery.

Patient No.	Sex/age	BCLC stage	Any PVT	No. of nodules	Size of target lesion, cm	AFP level, μg/L	Local response	Overall survival, mo
1	M/64	B	No	1	15.6	4.8	CR	29.63
2	M/66	B	No	2	10.2	9.5	PR	33.54
3	M/61	B	No	>10	13	1.6	PR	24.08
4	M/67	B	No	1	15	2.9	CR	52.87
5	M/64	C	Yes	1	4	87	CR	39.56
6	M/63	B	No	1	9	4.2	SD	41.11
7	F/53	B	No	1	8	7425	SD	31.01
8	M/61	B	No	1	9.2	13	SD	5.64*

Abbreviations: AFP = alpha-fetoprotein; BCLC = Barcelona Clinic Liver Cancer; CR = complete response; F = female; M = male; PR = partial response; PVT = portal vein thrombosis; SD = stable disease.
* Patient died of early postoperative complication.

Figure 3. Computed tomography images of pre-^{90}Yttrium selective internal radiation therapy (^{90}Y SIRT) [a] and post-^{90}Y SIRT (b) in a 67-year-old patient. The known right lobe tumour showed mild reduction in size with no abnormal arterial enhancement. It suggested complete response according to modified Response Evaluation Criteria in Solid Tumors guideline.

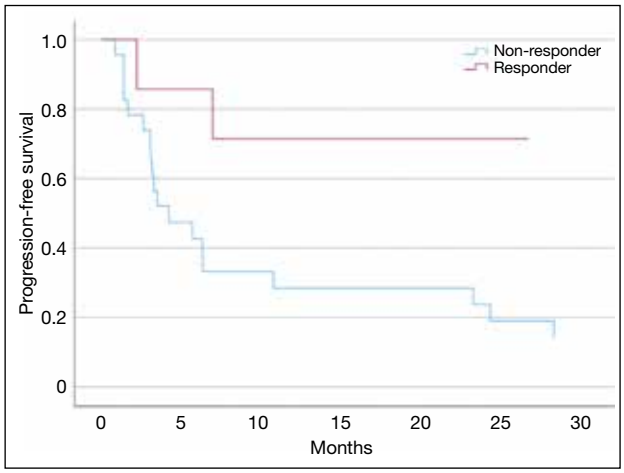

Figure 4. Kaplan-Meier curves showing progression-free survival (PFS) after ^{90}Yttrium selective internal radiation therapy in patients with responders and non-responders (median PFS not reached vs. 4.2 months, p = 0.034).

prognostic factor for OS (HR = 3.240, p = 0.045; Figure 5) as well as for PFS (HR = 3.930, p = 0.011; Figure 6).

In this series, there were four long-term survivors and three complete responders. Those with complete response achieved long survivals ranging from 29.6 to 52.9 months compared to a median of 11.2 months in non-responders. All of them had post-SIRT surgery done with clear resection margins. The median dose of ^{90}Y SIRT was higher in responders (200 Gy) than in non-responders (170 Gy). However, OS did not differ significantly with dose (lower dose: p = 0.268, 95% confidence interval = 0.983-1.005; higher dose: p = 0.456, 95% confidence interval = 0.201-2.056). Patient

Table 3. Univariate analysis.

Parameter	Overall survival		Progression-free survival	
	Hazard ratio (95% confidence interval)	p Value	Hazard ratio (95% confidence interval)	p Value
Prescribed dose >120 Gy	0.870 (0.239-3.171)	0.833	0.997 (0.333-2.985)	0.995
BCLC stage C or above	5.733 (1.262-26.042)	0.024	3.652 (1.369-9.748)	0.010
Presence of portal vein thrombosis	2.753 (0.918-8.255)	0.071	2.107 (0.836-5.307)	0.114
Post-SIRT surgery done	0.151 (0.020-1.169)	0.070	0.134 (0.030-0.591)	0.008
AFP level ≥400 μg/L	4.270 (1.379-13.217)	0.012	3.527 (1.406-8.845)	0.007
Multifocal tumour	2.610 (0.862-7.903)	0.090	1.647 (0.661-4.100)	0.284
Bilobed tumour	1.082 (0.353-3.314)	0.890	1.205 (0.492-2.953)	0.683
Treatment responder	0.197 (0.026-1.526)	0.120	0.203 (0.047-0.886)	0.034

Abbreviations: AFP = alpha-fetoprotein; BCLC = Barcelona Clinic Liver Cancer; SIRT = selective internal radiation therapy.

Table 4. Multivariable analysis.

Parameter	Overall survival		Progression-free survival	
	Hazard ratio (95% confidence interval)	p Value	Hazard ratio (95% confidence interval)	p Value
BCLC stage C or above	4.471 (0.958-20.873)	0.057	2.106 (0.704-6.298)	0.183
Post-SIRT surgery done	N/A	N/A	0.289 (0.042-1.999)	0.208
AFP level ≥400 μg/L	3.240 (1.025-10.246)	0.045	3.930 (1.378-11.212)	0.011
Treatment responder	N/A	N/A	0.463 (0.074-2.910)	0.412

Abbreviations: AFP = alpha-fetoprotein; BCLC = Barcelona Clinic Liver Cancer; SIRT = selective internal radiation therapy.

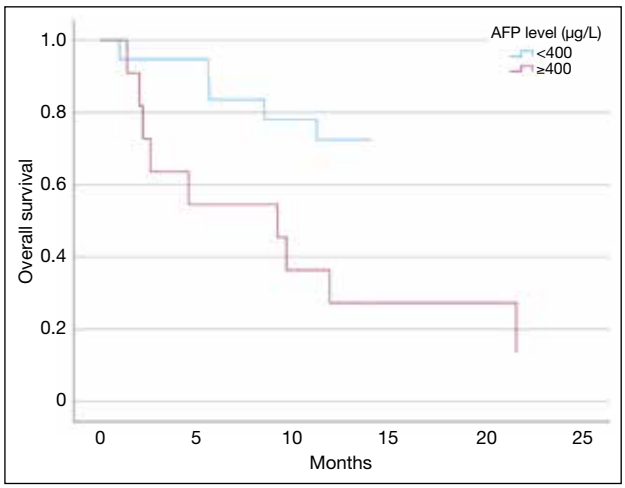

Figure 5. Kaplan-Meier curves showing overall survival (OS) after ^{90}Yttrium selective internal radiation therapy in patients with alpha-fetoprotein (AFP) level ≥400 μg/L and <400 μg/L (median OS = 9.2 months vs. not reached, p = 0.045).

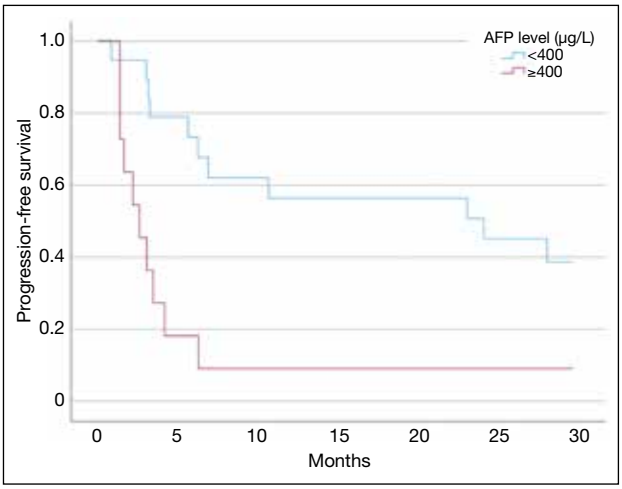

Figure 6. Kaplan-Meier curves showing progression-free survival (PFS) after ^{90}Yttrium selective internal radiation therapy in patients with alpha-fetoprotein AFP level ≥400 μg/L and <400 μg/L (median PFS = 2.2 months vs. 24.1 months, p = 0.011).

demographics and liver tumour baseline characteristics were investigated in treatment responders and non-responders together with those amenable to post-SIRT surgery and were compared to those that were not. The treatment responder group had better Eastern Cooperative Oncology Group (ECOG) performance status score (p = 0.039) and the group amenable to surgery had significantly more patients with BCLC stage B (p = 0.002) and better ECOG performance status score (p = 0.011).

Table 5. Radioembolisation-related toxicities (n = 29).*

Toxicities	All grades	Grade ≥3
Nausea	2 (6.9%)	0
Abdominal pain	7 (24.1%)	1 (3.4%)
Anorexia	3 (10.3%)	0
Fever	5 (17.2%)	0
Dyspepsia	1 (3.4%)	0
Deranged liver function	1 (3.4%)	0
Malaise	1 (3.4%)	0

* Data are shown as No. (%).

Toxicity

The median postoperative hospital stay was 6.5 days (range, 2-16). Twelve patients (41.4%) had some forms of post-^{90}Y treatment complications, in total 29 different kinds of toxicities experienced by them (Table 5). Most side-effects were mild with abdominal pain and fever being the most common. Only one patient had grade 3 abdominal pain requiring hospital admission 6 weeks after ^{90}Y SIRT. There was no identifiable cause found in work-up and the patient was discharged the next day after symptom subsided with analgesics. Abnormal liver function with grade 1 hyperbilirubinemia occurred in one patient and was self-limited.

There was one case of suspected radiation pneumonitis occurring approximately 7 weeks post-SIRT. The patient was a non-smoker and presented with fever and shortness of breath. The lung dose by the ^{90}Y SIRT was 24.4 Gy. Chest CT showed extensive ground-glass opacities and patchy consolidation, which may have represented oedema or infection. Multiple antibiotics and systemic steroids were administered but patient succumbed due to respiratory failure. Since the diagnosis was doubtful, it was not regarded as post-SIRT toxicity.

DISCUSSION

In this study, it was demonstrated that ^{90}Y SIRT was a feasible and effective treatment option in our local population who had intermediate- and advanced-stage HCC without serious adverse events. The response rate to ^{90}Y SIRT was high and the results were comparable to other Asian series that reported OS and PFS of patients receiving ^{90}Y SIRT ranging from 11 to 16.4 months and 2.4 to 11 months, respectively.[5,18-20] The wide range of survivals represents heterogeneity of patients' demographics and disease status, thus making direct comparison of survivals across different studies difficult. In our study, 59% and 34% of patients belong to BCLC stage C and had AFP level ≥400 μg/L, respectively. Both were found to be poor prognostic factors, which is consistent with the findings in a European multicentre analysis.[21] Despite this, the results of our cohort were impressive with encouraging results of local control, PFS, and OS.

TACE is commonly used in intermediate-stage HCC but is contraindicated in presence of portal vein thrombosis due to the potential risk of precipitating liver necrosis and failure by its effects on the already compromised hepatic vascular supply. This limitation can be overcome by ^{90}Y SIRT due to the small size of the ^{90}Y particles which exert microembolic effects on hepatic vascular dynamics.[22] Also, easy application in the left or right hepatic arteries of ^{90}Y SIRT makes it attractive for patients compared to superselective TACE with longer intervention times and repeated hospital admissions.[23] Yet, presence of portal vein thrombosis was shown to be associated with worse survival in treatment of ^{90}Y SIRT.[24] This was reconfirmed in our study in which the OS after SIRT was shorter in those with portal vein thrombosis compared to those without (median OS = 9.2 months vs. 26.4 months, $p = 0.045$).

In advanced HCC, targeted therapies are the mainstay of treatment with a median survival of approximately 13.6 months with lenvatinib and 12.3 months with sorafenib.[25] Although ^{90}Y SIRT failed to demonstrate a statistically significant difference in OS compared with sorafenib in two recent phase III trials, SARAH[26] and SIRveNIB[27], it had significantly fewer severe adverse events and better health-related quality of life. Most of the patients were classified as BCLC stage C in SARAH study, 68% in the ^{90}Y group and 67% in the sorafenib group, whereas respective rates were 48.4% and 44.9% in SIRveNIB study. Targeted therapy is associated with numerous side-effects, namely hypertension, diarrhoea, and hand-foot syndrome, and are known to lead to treatment discontinuation permanently in approximately 11% of patients.[28] On the other hand, ^{90}Y SIRT has better toxicity profiles with most side-effects being only mild as grades 1 to 2. This is also consistent with the observation in our cohort with the most common side-effects being grades 1 to 2 abdominal pain (23.3%) followed by fever (16.7%). There was only one grade 3 abdominal pain in our study with no identifiable causes. Symptom subsided quickly with analgesics and the patient was discharged the next day with no further complaints noted.

^{90}Y SIRT is also effective in bridging to liver surgery through tumour shrinkage and inducing future liver remnant hypertrophy in initially unresectable HCC.[29] In our study, 90% of the subjects underwent SIRT as the initial treatment and eight (30%) of them had surgery afterwards. They enjoyed a significantly longer survival (ranging from 24 to 52 months, excluded one died of postoperative complications). One of them demonstrated radiological and pathological complete response in his initial 4-cm tumour in subsequent hepatectomy after SIRT. He remains well without any disease recurrence for over 3 years by now. One of the long survivors received ^{90}Y SIRT twice to the right lobe of liver. Radiological complete response was achieved. Right hepatectomy was performed 2 months after the second ^{90}Y treatment. Pathology showed residual pT1 grade III HCC with clear resection margins. He has enjoyed >4 years of survival by now without disease recurrence. The above finding illustrated the potential role of downstaging and facilitating curative resection. ^{90}Y SIRT outperforms TACE in the role of downstaging from T3 to T2 HCC[30] and patients enjoyed better quality of life with ^{90}Y treatment.[31] Our series also showed ^{90}Y SIRT is safe with very low rates of grade ≥3 adverse events. Based on our study results, those amenable to surgery mostly were with ECOG performance status score of 0, classified as BCLC stage B with low AFP level, and without portal vein thrombosis, which could further guide our selection

of ^{90}Y SIRT candidates aiming for surgical resection.

The retrospective nature and the small sample size in this cohort might affect survival analysis and determination of the significance of different prognostic factors. Also, the survival is not mature yet where longer follow-up of patients is necessary. Another limitation was the time of the reassessment of CT scans. The mean time to the first response assessment CT was 2.35 months after SIRT and not all patients had regular scans afterwards. Later response might then be underreported. Yet, the first CT was chosen to assess the treatment response to ^{90}Y SIRT as most of the patients had subsequent treatment which might confound the response solely due to ^{90}Y SIRT. In fact, most of the subjects only had one CT scan done within 6 months of ^{90}Y treatment. Furthermore, 23 out of 26 patients had ^{90}Y SIRT alone whereas only three cases had planned combination treatment with SIRT and TACE or systemic therapy. Two patients had concurrent TACE and one was taking sorafenib during radioembolisation. Hence, it is believed the CT could reflect the treatment response of ^{90}Y SIRT.

Our study confirmed the role of ^{90}Y SIRT in intermediate- to advance-stage HCC patients. However, careful patient selection is of utmost importance to optimise treatment benefits. There has been evidence suggesting that AFP level ≥400 μg/L predicts a higher rate of dual-tracer positron emission tomography/CT–detected metastasis.[32] Our study further confirms it as a negative prognostic factor, probably due to occult extrahepatic metastases. With discreet use of incorporating staging dual tracer positron emission tomography/CT scan in high-risk cases with AFP level ≥400 μg/L, we might screen out those with extensive distant metastases whom ^{90}Y SIRT is not advised as the initial therapy.

The result of the series further consolidated the role of ^{90}Y SIRT in our local practice. In locally advanced HCC, selection of appropriate treatment modalities has been challenging. The study reflects the importance of careful selection of candidates for ^{90}Y SIRT. Good ECOG performance status score and the classification as BCLC stage B HCC are shown to be favourable factors for this expensive radioisotope treatment and should be prioritised when it comes to selection of suitable candidates in multidisciplinary meetings. Other local ablative treatments such as radiofrequency ablation and stereotactic radiotherapy should be reserved for solitary or lower volume disease, whereas systemic therapy is for clearly disseminated disease.

CONCLUSION

^{90}Y SIRT is an effective and safe treatment for intermediate- to advanced-stage HCC which provides satisfactory local control with minimal toxicity. Longer survival was observed in patients with AFP level <400 μg/L.

REFERENCES

1. Hong Kong Cancer Registry. Top ten cancers. Available from: https://www3.ha.org.hk/cancereg/topten.html. Accessed 1 May 2022.
2. Llovet JM, Bruix J. Systematic review of randomized trials for unresectable hepatocellular carcinoma: chemoembolization improves survival. Hepatology. 2003;37:429-42.
3. D'Avola D, Iñarrairaegui M, Pardo F, Rotellar F, Marti P, Bilbao JI, et al. Prognosis of hepatocellular carcinoma in relation to treatment across BCLC stages. Ann Surg Oncol. 2011;18:1964-71.
4. Levillain H, Bagni O, Deroose CM, Dieudonné A, Gnesin S, Grosser OS, et al. International recommendations for personalised selective internal radiation therapy of primary and metastatic liver diseases with yttrium-90 resin microspheres. Eur J Nucl Med Mol Imaging. 2021;48:1570-84.
5. Hilgard P, Hamami M, Fouly AE, Scherag A, Müller S, Ertle J, et al. Radioembolization with yttrium-90 glass microspheres in hepatocellular carcinoma: European experience on safety and long-term survival. Hepatology. 2010;52:1741-9.
6. Kooby DA, Egnatashvili V, Srinivasan S, Chamsuddin A, Delman KA, Kauh J, et al. Comparison of yttrium-90 radioembolization and transcatheter arterial chemoembolization for the treatment of unresectable hepatocellular carcinoma. J Vasc Interv Radiol. 2010;21:224-30.
7. Carr BI, Kondragunta V, Buch SC, Branch RA. Therapeutic equivalence in survival for hepatic arterial chemoembolization and yttrium 90 microsphere treatments in unresectable hepatocellular carcinoma: a two-cohort study. Cancer. 2010;116:1305-14.
8. Pitton MB, Kloeckner R, Ruckes C, Wirth GM, Eichhorn W, Wörns MA, et al. Randomized comparison of selective internal radiotherapy (SIRT) versus drug-eluting bead transarterial chemoembolization (DEB-TACE) for the treatment of hepatocellular carcinoma. Cardiovasc Intervent Radiol. 2015;38:352-60.
9. Facciorusso A, Serviddio G, Muscatiello N. Transarterial radioembolization vs chemoembolization for hepatocarcinoma patients: a systematic review and meta-analysis. World J Hepatol. 2016;8:770-8.
10. Kulik LM, Atassi B, van Holsbeeck L, Souman T, Lewandowski RJ, Mulcahy MF, et al. Yttrium-90 microspheres (TheraSphere) treatment of unresectable hepatocellular carcinoma: downstaging to resection, RFA and bridge to transplantation. J Surg Oncol. 2006;94:572-86.
11. Rognoni C, Ciani O, Sommariva S, Facciorusso A, Tarricone R, Bhoori S, et al. Trans-arterial radioembolization in intermediate-advanced hepatocellular carcinoma: systematic review and meta-analyses. Oncotarget. 2016;7:72343-55.
12. Salem R, Lewandowski RJ, Mulcahy MF, Riaz A, Ryu RK, Ibrahim S, et al. Radioembolization for hepatocellular carcinoma using yttrium-90 microspheres: a comprehensive report of long-term outcomes. Gastroenterology. 2010;138:52-64.
13. Geschwind JF, Salem R, Carr BI, Soulen MC, Thurston KG, Goin KA, et al. Yttrium-90 microspheres for the treatment of hepatocellular carcinoma. Gastroenterology. 2004;127(5 Suppl 1):S194-205.

14. Van Thai N, Thinh NT, Ky TD, Bang MH, Giang DT, Ha LN, et al. Efficacy and safety of selective internal radiation therapy with yttrium-90 for the treatment of unresectable hepatocellular carcinoma. BMC Gastroenterol. 2021;21:216.
15. Llovet JM, Real MI, Montaña X, Planas R, Coll S, Aponte J, et al. Arterial embolisation or chemoembolisation versus symptomatic treatment in patients with unresectable hepatocellular carcinoma: a randomised controlled trial. Lancet. 2002;359:1734-9.
16. Ho S, Lau WY, Leung TW, Chan M, Ngar YK, Johnson PJ, et al. Partition model for estimating radiation doses from yttrium-90 microspheres in treating hepatic tumours. Eur J Nucl Med. 1996;23:947-52.
17. Llovet JM, Brú C, Bruix J. Prognosis of hepatocellular carcinoma: the BCLC staging classification. Semin Liver Dis. 1999;19:329-38.
18. Lee VH, Leung DK, Luk MY, Tong CC, Law MW, Ng SC, et al. Yttrium-90 radioembolization for advanced inoperable hepatocellular carcinoma. Onco Targets Ther. 2015;8:3457-64.
19. Chaikajornwat J, Tanasoontrarat W, Phathong C, Pinjaroen N, Chaiteerakij R. Clinical outcome of yttrium-90 selective internal radiation therapy (Y-90 SIRT) in unresectable hepatocellular carcinoma: experience from a tertiary care center. Liver Res. 2022;6:30-8.
20. Mazzaferro V, Sposito C, Bhoori S, Romito R, Chiesa C, Morosi C, et al. Yttrium-90 radioembolization for intermediate-advanced hepatocellular carcinoma: a phase 2 study. Hepatology. 2013;57:1826-37.
21. Sangro B, Carpanese L, Cianni R, Golfieri R, Gasparini D, Ezziddin S, et al. Survival after yttrium-90 resin microsphere radioembolization of hepatocellular carcinoma across Barcelona clinic liver cancer stages: a European evaluation. Hepatology. 2011;54:868-78.
22. Quirk M, Kim YH, Saab S, Lee EW. Management of hepatocellular carcinoma with portal vein thrombosis. World J Gastroenterol. 2015;21:3462-71.
23. Kloeckner R, Ruckes C, Kronfeld K, Wörns MA, Weinmann A, Galle PR, et al. Selective internal radiotherapy (SIRT) versus transarterial chemoembolization (TACE) for the treatment of intrahepatic cholangiocellular carcinoma (CCC): study protocol for a randomized controlled trial. Trials. 2014;15:311.
24. Floridi C, Pesapane F, Angileri SA, De Palma D, Fontana F, Caspani F, et al. Yttrium-90 radioembolization treatment for unresectable hepatocellular carcinoma: a single-centre prognostic factors analysis. Med Oncol. 2017;34:174.
25. Kudo M, Finn RS, Qin S, Han KH, Ikeda K, Piscaglia F, et al. Lenvatinib versus sorafenib in first-line treatment of patients with unresectable hepatocellular carcinoma: a randomised phase 3 non-inferiority trial. Lancet. 2018;391:1163-73.
26. Vilgrain V, Pereira H, Assenat E, Guiu B, Ilonca AD, Pageaux GP, et al. Efficacy and safety of selective internal radiotherapy with yttrium-90 resin microspheres compared with sorafenib in locally advanced and inoperable hepatocellular carcinoma (SARAH): an open-label randomised controlled phase 3 trial. Lancet Oncol. 2017;18:1624-36.
27. Chow PK, Gandhi M, Tan SB, Khin MW, Khasbazar A, Ong J, et al. SIRveNIB: selective internal radiation therapy versus sorafenib in Asia-Pacific patients with hepatocellular carcinoma. J Clin Oncol. 2018;36:1913-21.
28. Llovet JM, Ricci S, Mazzaferro V, Hilgard P, Gane E, Blanc JF, et al. Sorafenib in advanced hepatocellular carcinoma. N Engl J Med. 2008;359:378-90.
29. Bekki Y, Marti J, Toshima T, Lewis S, Kamath A, Argiriadi P, et al. A comparative study of portal vein embolization versus radiation lobectomy with yttrium-90 microspheres in preparation for liver resection for initially unresectable hepatocellular carcinoma. Surgery. 2021;169:1044-51.
30. Lewandowski RJ, Kulik LM, Riaz A, Senthilnathan S, Mulcahy MF, Ryu RK, et al. A comparative analysis of transarterial downstaging for hepatocellular carcinoma: chemoembolization versus radioembolization. Am J Transplant. 2009;9:1920-8.
31. Salem R, Gilbertsen M, Butt Z, Memon K, Vouche M, Hickey R, et al. Increased quality of life among hepatocellular carcinoma patients treated with radioembolization, compared with chemoembolization. Clin Gastroenterol Hepatol. 2013;11:1358-65.e1.
32. Chu KK, Chan AC, Ma KW, She WH, Dai WC, Chok KS, et al. Role of C11-FDG dual-tracer PET-CT scan in metastatic screening of hepatocellular carcinoma — a cost-effectiveness analysis. Hepatobiliary Surg Nutr. 2021;10:301-7.

Hong Kong J Radiol. 2023;26:34-41 | https://doi.org/10.12809/hkjr2317444

ORIGINAL ARTICLE

Prevalence and Clinical Significance of Incidental Extracardiac Findings during Cardiac Magnetic Resonance Imaging: a Retrospective Study

HS Abdel Rahman[1], AM Shawky[2], EM Mehana[3]

[1]Department of Radiology, Faculty of Medicine, Ain Shams University, Egypt
[2]Department of Cardiology, Al-Azhar University, Egypt
[3]Department of Radiology, Medical Research Institute, Alexandria University, Egypt

ABSTRACT

Introduction: *We sought to assess the prevalence and significance of incidental findings during cardiovascular magnetic resonance imaging (CMRI) and to investigate their impact on patient management.*

Methods: *We performed a retrospective evaluation of the CMRI images of all 131 referred patients suitable for inclusion who presented to our radiology department between July 2017 and May 2019. Their images were evaluated for any extracardiac findings beyond the pericardium detected and reported at the time of examination and classified in terms of the effects of these findings on the patients' treatment plans.*

Results: *A total of 109 incidental findings were detected in 53% of the scanned population, of which 27 (24.8%) were clinically significant and potentially significant, including pulmonary consolidation (n = 11), extracardiac vascular lesions (n = 3), and other chest and abdominal abnormalities. Among the 27 cases, four (all male; 3% of the study population) showed clinically significant extracardiac findings, namely fibrocavitary tuberculosis, lymphoma, and pericardial mesothelioma, as well as one case of patent ductus arteriosus, as patients were referred to other specialists to treat the primary disease that was causative of the secondary cardiac problem.*

Conclusions: *Incidental extracardiac findings were common in CMRI, and although the prevalence of significant lesions was low, they changed patient management. Thus, it is important to identify extracardiac findings and clarify their significance during CMRI reporting.*

Key Words: *Cardiovascular system; Heart; Incidental findings; Magnetic resonance imaging*

Correspondence: *Dr EM Mehana, Department of Radiology, Medical Research Institute, Alexandria University, Egypt*
Email: sayedmehana9@gmail.com

Submitted: 29 Jul 2021; Accepted: 5 Oct 2021.

Contributors: HSAR designed the study. All authors acquired and analysed the data. HSAR and EMM drafted the manuscript. All authors critically revised the manuscript for important intellectual content. All authors had full access to the data, contributed to the study, approved the final version for publication, and take responsibility for its accuracy and integrity.

Conflicts of Interest: All authors have disclosed no conflicts of interest.

Funding/Support: This study received no specific grant from any funding agency in the public, commercial, or not-for-profit sectors.

Data Availability: All data generated or analysed during the present study are available from the corresponding author on reasonable request.

Ethics Approval: This study was approved by the ethics committee of Saudi German Hospital, Jeddah, Saudi Arabia. The committee identified no ethical problem and granted a waiver on patient consent as this study was a retrospective description of clinical cases and no experiments or trials were done related to this study.

中文摘要

心臟磁共振成像時意外心臟外發現的發病率和臨床意義：回顧性研究

HS Abdel Rahman、AM Shawky、EM Mehana

簡介：我們評估心血管磁共振成像（CMRI）時偶然發現病變的普遍性和重要性，並調查它們對患者處理的影響。

方法：我們對2017年7月至2019年5月期間就診於我們放射科的所有131名適合納入的轉介患者的CMRI 圖像進行了回顧性評估，評估其圖像是否存在心包結構以外的任何心臟外發現，並根據這些發現對患者的治療計劃的影響進行分類。

結果：在53%的研究族群中共檢測到109項偶然發現，其中27項（24.8%）有臨床意義或具有潛在意義，包括肺實變（n = 11）、心外血管病變（n = 3）和其他胸部和腹部異常。患者總數中有四人（全部為男性；佔研究族群的3%）顯示有臨床意義的心外發現，即纖維腔結核、淋巴瘤和心包間皮瘤，以及一例動脈導管未閉。因為有導致繼發性心臟問題的原發性疾病，這些患者被轉介至其他專科醫生治療。

結論：意外的心外發現在CMRI中很常見，儘管顯著病變的發生率很低，但它們改變了患者的處理。因此，在CMRI報告中識別心外發現並闡明其意義非常重要。

INTRODUCTION

Cardiovascular magnetic resonance imaging (CMRI) has proven to be one of the most established noninvasive techniques to assess cardiac structure and performance in multiple heart diseases, and hundreds of CMRI studies have been performed subsequently.[1] During CMRI acquisition, parts of the adjacent anatomical regions within the thorax, upper abdomen, and root of the neck are also imaged, especially in initial multi-section axial and coronal images. These images can reveal a wide range of pathologies outside the cardiovascular system. Although many of these pathologies may represent benign lesions of no clinical importance, others may represent significant clues for new diagnoses, further investigations, or early treatment.[2,3]

The potential challenges and benefits associated with these incidental extracardiac findings have been investigated in multiple studies, the results of which differed in terms of the prevalence of the findings and their impact on the diagnosis and management plans for patients.[1-17] However, these studies are in agreement regarding the importance of incidental extracardiac findings. Moreover, the importance of these extracardiac findings has been recognised and implemented within the European Association of Cardiovascular Imaging core syllabus for the European Cardiovascular Magnetic Resonance certification examination.[4-7]

Extracardiac findings are also being increasingly focused on while reporting CMRI findings at our centre. Therefore, we performed this audit to retrospectively evaluate the prevalence of incidental extracardiac findings in clinically indicated CMRI examinations performed at our institution and to assess their impact on the patients' diagnosis and management. Using the obtained data, we hoped to provide recommendations for changes to reporting of CMRI studies.

METHODS

Patient Population

In this study, we performed a retrospective evaluation of the CMRI images of all patients referred to the radiology department at Saudi German Hospital, Jeddah, Saudi Arabia between July 2017 and May 2019 for clinically indicated CMRI to evaluate the prevalence of incidental extracardiac findings in these cases. We excluded patients with extended imaging, examinations with inadequate image quality, and follow-up imaging assessments and repeat scans. An incidental extracardiac finding was defined as any change found beyond the pericardium, e.g., great vessels, lung, pleural, or abdominal pathology.

Cardiovascular Magnetic Resonance Imaging Protocol

All CMRI examinations were performed on a 1.5T Avanto MRI system (Siemens Healthcare, Germany)

equipped with a 32-element cardiac coil array. All scans were electrocardiography-gated for synchronisation with the cardiac cycle and performed in end-expiration, and were performed in accordance with a local standard CMRI protocol that included the following sequences:

1. Three localising single-shot steady-state sequences in the three orthogonal planes, followed by axial, sagittal, and coronal multi-section half-Fourier acquisition single-shot turbo spin-echo (HASTE). These sequences were acquired from the top of the aortic arch to the diaphragm in the axial plane, from the sternum to the spine in the coronal plane, and from the right to left cardiac borders in the sagittal plane. The field of view (FOV) chosen was based on patient size and ranged from 340 × 233 mm^2 to 390 × 344 mm^2. Base and phase resolutions were 256 and 59%, respectively. Section thickness and section gap were 8 and 2 mm, respectively, yielding spatial resolutions from 2.3 mm × 1.3 mm × 8 mm to 2.5 mm × 1.5 mm × 8 mm.
2. Cine sequences with steady-state free precession (SSFP)–oriented 2-chamber vertical long-axis view, 4-chamber horizontal long-axis view, 3-chamber view, and short axis for studying the kinetics of the right and left ventricles (acquisition time, 7-12 s for each section; matrix, 192 × 192; flip angle, 180°; echo time, 1.69 ms).
3. Phase-contrast sequence to review valvular flow. This sequence was planned using a 3-chamber view and coronal aortic view, with one section perpendicular to the ascending aorta just distal to the valve leaflet tips, velocity encoding = 150 cm/s for normal flow (or greater for stenosis), retrospective gating, and short echo time for optimal flow sensitivity.
4. Phase-sensitive inversion recovery (PSIR) sequences for studying late gadolinium enhancement performed 10 to 15 minutes after intravenous administration of gadolinium (0.1-0.2 mmol/kg). FOV, 244 × 300 mm^2; matrix, 156 × 256.

Data Interpretation

Two radiologists with at least 5 years of experience in reporting and supervising cardiovascular MR imaging and without prior knowledge of the objectives of the study reinterpreted the CMRI examinations. All extracardiac findings were recorded as incidental findings and formed the basis for diagnosis. To assess the clinical implications of the incidental extracardiac findings, clinical data were analysed by reviewing the electronic medical records database of the hospital. All those findings were characterised and classified into three categories: (1) non-significant, which are findings that did not warrant further action; (2) potentially significant, which are findings with possible clinical significance that warranted further imaging or specialist consultation but did not warrant a change of the treatment plan or primary diagnosis; and (3) significant, which are findings with major clinical significance that warranted a change in the patient's treatment plan and primary diagnosis. The prevalence of incidental extracardiac findings and their sites were evaluated and reported. Evaluation of the previous radiological reports for the patients was also performed to assure that significant and potentially significant findings had not been missed and qualified for a change of the treatment plan of the patients, if any.

RESULTS

A total of 140 patients underwent CMRI examinations during the study period; of these, we included 131 patients after excluding nine patients for the following reasons: extended imaging (e.g., cardiac MR and abdominal MR in one session; 2 patients), examinations with inadequate image quality (e.g., artifacts, arrhythmia, or incomplete examination because of patient-related factors; 4 patients), and follow-up imaging assessments and repeat scans (3 patients). The patients' ages ranged from 1 to 84 years (mean, 44). The study population included 14 children (one aged 1 year and 13 adolescents aged 10-19 years). The 131 patients included 104 males (79%) and 27 females (21%).

An analysis of the clinical indications for our study cohort is presented in Table 1. Most of our patients were referred for evaluation of myocardial viability (63 patients, 48.1%), followed by non-ischaemic cardiomyopathy (25 patients, 19.1%) and myocarditis (15 patients, 11.5%); other indications included congenital heart

Table 1. Clinical indications for cardiovascular magnetic resonance imaging (CMRI) in the current study cohort (n = 131).

Indications for CMRI	No. (%)
Myocardial viability	63 (48.1%)
Non-ischaemic cardiomyopathy	25 (19.1%)
Myocarditis	15 (11.5%)
Congenital heart disease	8 (6.1%)
Right ventricular evaluation	5 (3.8%)
Pericardium	4 (3.1%)
Valvular disease	3 (2.3%)
Anatomy and function evaluation	2 (1.5%)
Ascending aorta evaluation	2 (1.5%)
Extracardiac mass	2 (1.5%)
Intracardiac mass	1 (0.8%)
Persistent atrial fibrillations	1 (0.8%)

disease, right ventricular evaluation, valvular disease, and intra- or extracardiac masses.

A total of 109 incidental extracardiac findings were recorded in 70 patients (53.4% of the study population), while 61 patients (46.6%) did not show any extracardiac findings. Of these findings, 82 (75.2% of the findings) were mild or of no clinical significance (Table 2) and 27 (24.8% of the findings) warranted further diagnostic workup or consultation since they were considered significant or potentially significant (Table 3).

Out of the 109 incidental extracardiac findings, four findings in four patients had a clinically significant impact on patient diagnosis and management (prevalence among incidental extracardiac findings, 3.7%) but were not clinically significant before imaging. These were as follows:

1. Right upper lobe consolidation and cavitation (fibrocavitary tuberculosis) in a patient presenting with dilated cardiomyopathy. This was confirmed by radiography and laboratory tests (Figure 1). The patient was referred to a pulmonologist, and the cardiac problem was treated as secondary, not primary, dilated cardiomyopathy as the dilation of the cardiac chamber was secondary to the inflammatory process caused by tuberculosis which may be reversable after treating the cause.
2. Marked mediastinal lymph node enlargement, moderate pericardial effusion, and enhancement (pericardial mesothelioma) in a patient with persistent haemorrhagic pericardial effusion. This was diagnosed by an open biopsy in cardiopulmonary surgery (Figure 2). The patient was subsequently referred to an oncologist to receive treatment for the condition in conjunction with the cardiology management.
3. Multiple left lung patchy consolidations, enlarged left supraclavicular lymph node, and marked abdominal paraaortic lymphadenopathy (B-cell lymphoma) in a patient with a large anterior mediastinal mass. This was confirmed by biopsy (Figure 3) and the patient was referred to an oncologist for treatment of the primary condition.
4. Patent ductus arteriosus in an adult patient with dilated right ventricle and pulmonary artery and suspected pulmonary hypertension. The pulmonary-to-systemic blood flow ratio was 0.6:1, while the estimated shunted blood volume through the patent ductus arteriosus was 111 mL. He was referred to undergo cardiothoracic surgery for adequate management (Figure 4).

Table 2. Non-significant incidental extracardiac findings in the current study cohort (n = 82).

Findings	No. of cases	Prevalence
Pleural effusion	28	21.4%
Mediastinal lymphadenopathy	11	8.4%
Axillary lymphadenopathy	23	17.6%
Thymus	1	0.8%
Simple renal cysts	3	2.3%
Spine degeneration	2	1.5%
Splenules	4	3.1%
Breast implant	2	1.5%
Diaphragm eventration	2	1.5%
Bovine arch	1	0.8%
Hiatus hernia	1	0.8%
Shoulder effusion	1	0.8%
Ascites	3	2.3%

Table 3. Potentially significant and significant findings in the current study cohort (n = 27).

Findings	No. of cases	Prevalence
Pulmonary consolidation	11	8.3%
Thyroid lesion	2	1.5%
Renal lesion	2	1.5%
Significant mediastinal lymph nodes	3	2.3%
Thymus	1	0.8%
Abdominal lymphadenopathy	1	0.8%
Extracardiac vascular lesions	3	2.3%
Breast mass	1	0.8%
Spine fracture	1	0.8%
Pulmonary fibrosis	1	0.8%
Large splenic cysts	1	0.8%

Among the anatomical sites where incidental extracardiac findings were detected, the chest showed the highest prevalence of findings among the whole patient population, including pleural effusion (n = 28, 21.4%), axillary lymphadenopathy (n = 23, 17.6%) or mediastinal lymphadenopathy (n = 14, 10.7%), followed by pulmonary parenchymal lesions (n = 12, 9.2%), thymus (n = 2, 1.5%), breast lesions (n = 3, 2.3%), spine abnormalities (n = 3, 2.3%), vascular extracardiac lesions (n = 4, 3.1%), and a shoulder effusion (n = 1, 0.8%). In contrast, abdominal findings were less prevalent and included ascites (n = 3, 2.3%), diaphragmatic hiatal hernia (n = 1, 0.8%), splenic lesions (n = 5, 3.8%), renal lesions (n = 5, 3.8%), abdominal lymphadenopathy (n = 1, 0.8%), and diaphragmatic eventration (n = 2, 1.5%). The site showing the lowest prevalence of findings was the root of the neck with only two thyroid nodules reported (1.5%).

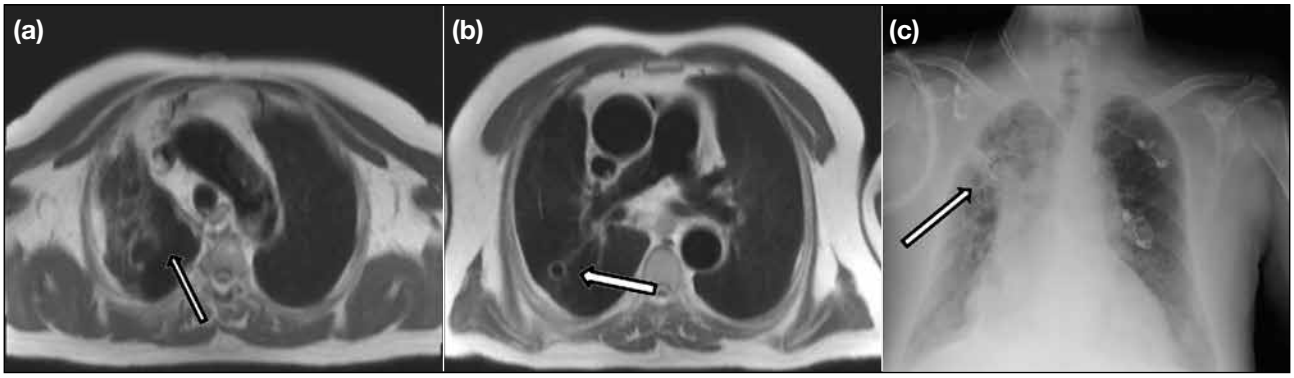

Figure 1. A 62-year-old male presented with atrial fibrillation and dilated cardiomyopathy. He was found to have viable myocardium in cardiovascular magnetic resonance imaging and normal coronaries in coronary angiography. (a and b) Axial black-blood magnetic resonance imaging showing fibrosis and cavitation in the right upper lobe (arrows). (c) Radiography of the chest confirms the diagnosis, with the arrow indicating the cavitary changes in (a) and (b). The patient was diagnosed with fibrocavitary tuberculosis by laboratory tests.

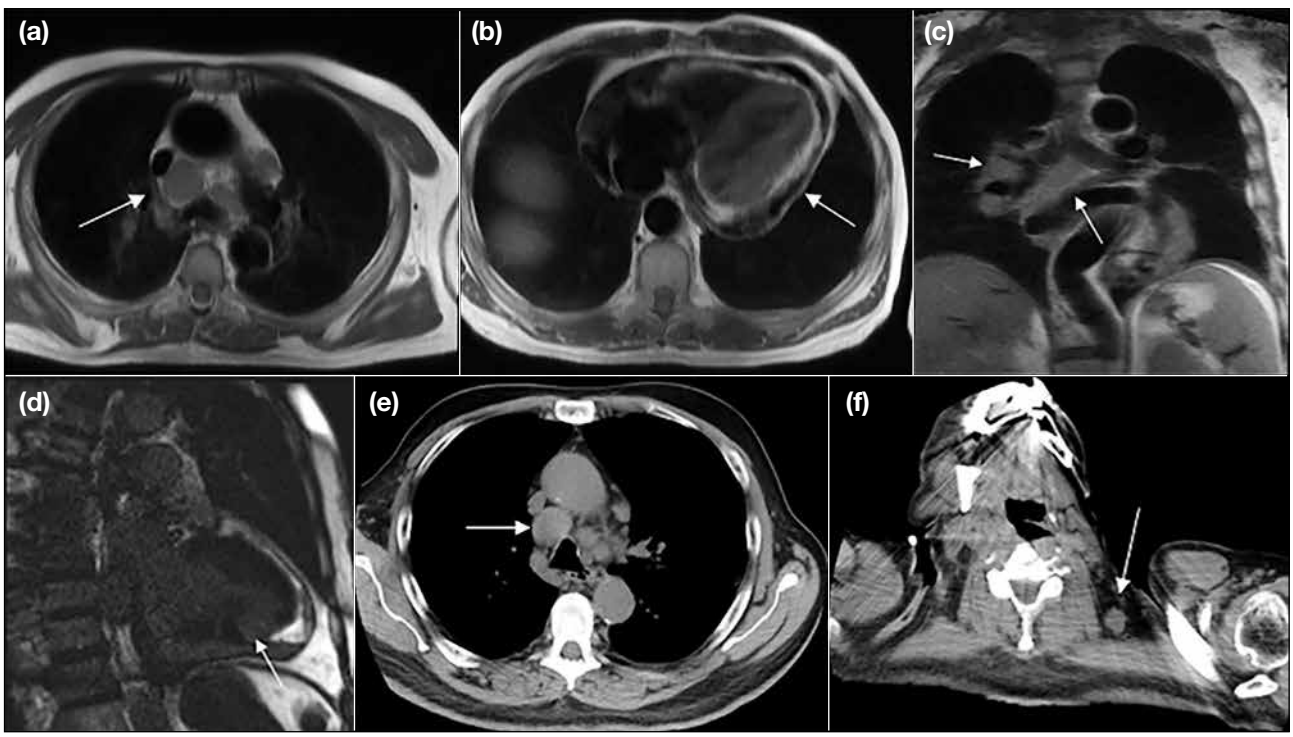

Figure 2. A 61-year-old male presented with dysarthria and facial weakness, pericardial effusion, and tamponade. (a) Axial black-blood image showing significant mediastinal lymphadenopathy (arrow). (b) Axial black-blood image showing pericardial thickening and collection (arrow). (c) Coronal black-blood image showing subcarinal and right hilar lymphadenopathy (arrows). (d) Long-axis phase-sensitive inversion recovery image with abnormal inferior wall myocardial enhancement (arrow). (e and f) Axial computed tomography images confirm the pathological lymph nodes (arrows). The patient underwent an open biopsy that revealed pericardial mesothelioma.

The most relevant sequences that detected extracardiac findings were the initial localiser sequences (HASTE) within the three orthogonal planes that allowed a global view, with all incidental extracardiac findings visualised in this sequence. Other relevant sequences were the morphological post-contrast PSIR sequences in which 10 out of 109 of the findings were visualised, and cine-SSFP sequences in which five findings were visualised.

DISCUSSION

CMRI is a highly reproducible tool to assess cardiovascular diseases. In CMRI examinations, an

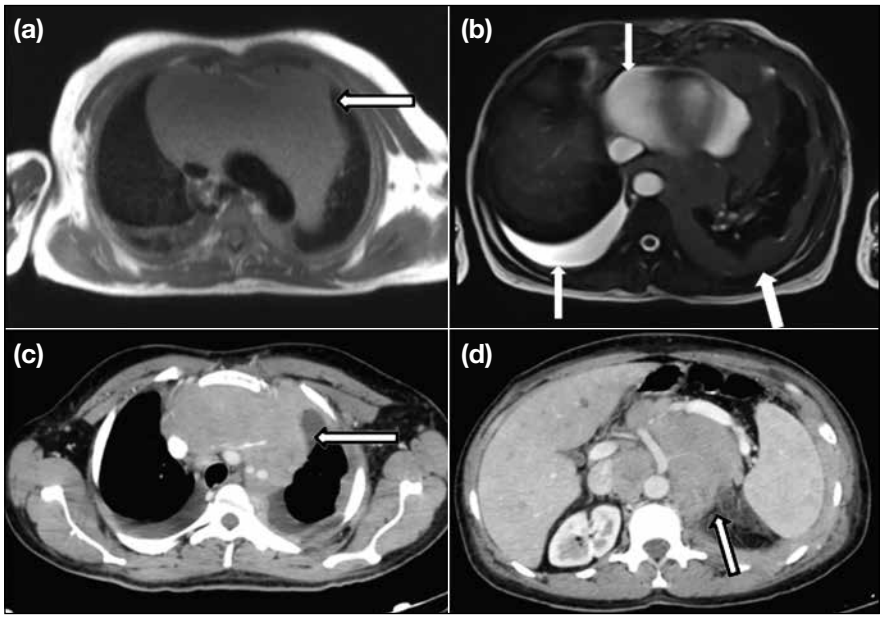

Figure 3. A 36-year-old male with B-cell lymphoma. (a) Axial black-blood cardiovascular magnetic resonance imaging showing a large anterior mediastinal mass surrounding and displacing the great vessels (arrow). (b) True fast imaging with steady-state free precession magnetic resonance imaging axial image showing lobulated soft tissue thickening of the left pleural cavity with pericardial and right pleural effusion (arrows). (c) Axial computed tomography (CT) image at the level of the chest confirms the findings in (a) [arrow]. (d) Axial CT image at the abdomen shows prominent paraaortic lymphadenopathy (arrow).

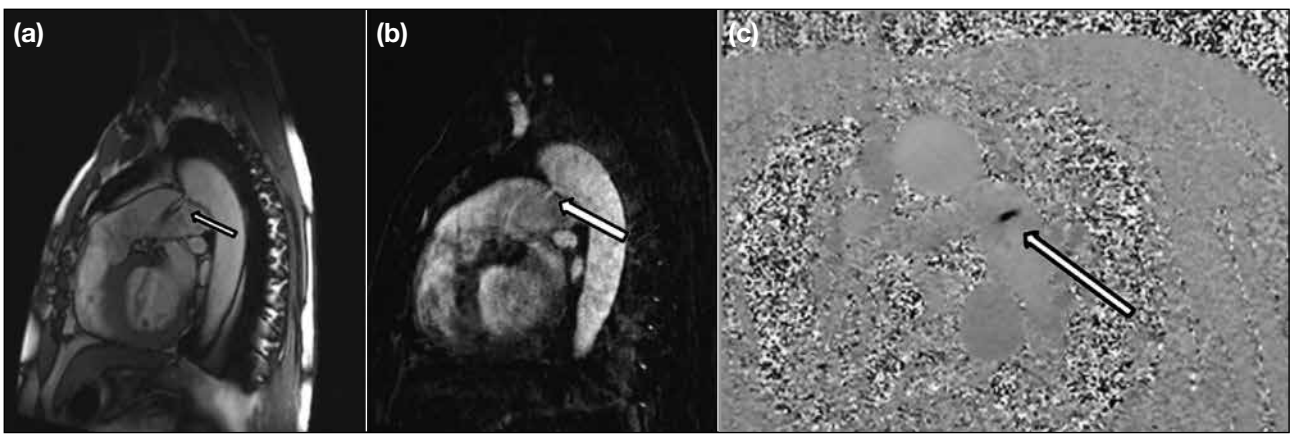

Figure 4. A 61-year-old man presented with wheezing and was suspected to have an aortic valvular disease. (a) Sagittal true fast imaging with steady-state free precession localiser magnetic resonance imaging (MRI) showing a 3-mm patent ductus arteriosus jet flow (arrow). A dilated pulmonary artery and ascending aorta can also be seen. (b) Sagittal post-contrast dynamic MRI with flow across patent ductus arteriosus (arrow). (c) Axial phase-contrast image marking the flow across the patent ductus arteriosus (arrow).

informed assessment of extracardiac structures can help detect multiple non-cardiac diseases. However, few studies in the literature have reported the prevalence and nature of incidental extracardiac findings on CMRI; although the comparisons of these studies are difficult because of different study designs (i.e., the study cohorts, clinical setting, sequences applied, and reading session format), the general agreement is that missing these incidental extracardiac findings can result in a significant delay in the appropriate management of the patients, which may be associated with progressive morbidity, as well as legal consequences and costs.[3,8,9]

For the classification of incidental extracardiac findings, we adopted the scheme proposed by Gravina et al,[3] who divided incidental extracardiac findings into three groups: (1) findings with mild or no clinical significance; (2) findings with possible clinical significance; and (3) clinically significant findings that required further diagnostic workup or the initiation of a new specific treatment different from the current treatment or ended by a non-cardiac diagnosis of the disease process of the patient. However, some other studies categorised incidental extracardiac findings as relevant if they required further diagnostic workup or the initiation

of a new specific treatment different from the current treatment or clinically irrelevant/insignificant if they necessitated no change in the patient's management.[1,9-11] Previous studies have also differed in their considerations for relevant findings. For example, Jacobs et al[12] considered pleural effusion as a potentially relevant finding, whereas other studies[10,13,14] performed a separate assessment in each case to classify the significance of the findings. In our study, we also assessed the patients individually and found that pleural effusion in all the patients was non-significant and was related to their cardiac condition since a large group of our patients had ischaemic heart disease.

Our study is consistent with other studies with regard to the significant lesions. However, the difference between our study and those of other studies was rooted in the non-significant lesions, which did not influence patient management. In our retrospective cross-sectional study with a focused review of 131 CMRI examinations (based on an image review), extracardiac abnormal findings were prevalent in 53% of the study population. Similar studies reported the rates of extracardiac abnormal findings from 10 to 62%.[7,8,15] This great variability may be attributed to differences in study designs, the use of different definitions of incidental extracardiac findings, as well as the differences in the number of patients included within the studies. In this study, we found that 3.7% of incidental extracardiac findings were clinically significant, which was comparable to other studies with reported rates of 2 to 5%.[3,10] However, a much lower prevalence of 0.9% was reported.[7] This variation could be attributed to the larger patient population included in their study, the differences in the study protocols, variations in the FOV coverage, and, possibly, the differences in the number of sections per sequence.[9]

In our evaluation of the site of prevalence of extracardiac findings either in the lower neck, chest, or upper abdomen, we found that most were localised in the chest, such as pleural effusion; this may be because most of our patients were referred for ischaemic cardiomyopathy (48.1%). Sokolowski et al[7] also reported a high association between vascular and congenital heart disease indications and a high prevalence of vascular findings and a low prevalence of major findings. Despite a male predominance in our study compared with other reports,[1,3] the overall prevalence of incidental extracardiac findings was higher in female patients (77.8% vs. 47.1%).

With regard to the influence of MRI sequences on detection of incidental extracardiac findings, we found that while the lesions could be detected in multiple sequences, 100% of such findings were identified in the HASTE sequence due to its large FOV and tissue coverage, despite the lower spatial resolution, while the single-section cine-SSFP and multi-section post-contrast PSIR sequences were useful in confirming some of these findings or limiting the differential diagnosis on the basis of signal intensity and enhancement characteristics. This is in agreement with other reports[3,16] but with the difference that they used multiplane SSFP localisers instead of HASTE. Another study[17] compared these two large-FOV sequences and stated that the transaxial balanced SSFP (bSSFP) sequence with a wide FOV is more accurate in the detection of incidental extracardiac findings than the HASTE localiser images due to its better spatial resolution. In our study, we depended on HASTE localiser images for evaluation of incidental extracardiac findings since all of these were detected in these large-FOV images, with confirmation or clarification of some of the findings in other sequences such as late post-contrast images, as a result of the poorer resolution of HASTE localiser images.

One limitation of our study and a potential source of bias is its small size, which hindered evaluation of the incidental extracardiac finding prevalence by age-group. Another limitation was the absence of histologic confirmation since many lesions were managed on the basis of suspected imaging diagnoses alone. We should also mention that our routine localised large-FOV sequence was the HASTE sequence, and we would have preferred to compare these findings to those obtained with the large-FOV bSSFP sequence, which has a higher spatial resolution and provides greater coverage in a very short time.

We recommend adding a subtitle to CMRI reports to include the extracardiac findings encountered during reporting and their significance or the further recommended management. We also recommend the use of bSSFP sequences with a wide FOV during routine CMRI in the axial and coronal planes to replace the HASTE localising sequences at the beginning of the CMRI study owing to their better resolution.

CONCLUSION

Incidental extracardiac findings are common in cardiac MRI, and, despite the low prevalence of significant

lesions (around 3% of patients), they changed patient management and facilitated the delivery of an accurate diagnosis. Hence, it is important to identify incidental extracardiac findings and clarify their significance during CMRI reporting.

REFERENCES

1. Ulyte A, Valeviciene N, Palionis D, Kundrotaite S, Tamosiunas A. Prevalence and clinical significance of extracardiac findings in cardiovascular magnetic resonance. Hellenic J Cardiol. 2016;57:256-60.
2. Rodrigues JC, Lyen SM, Loughborough W, Amadu AM, Baritussio A, Dastidar AG, et al. Extra-cardiac findings in cardiovascular magnetic resonance: what the imaging cardiologist needs to know. J Cardiovasc Magn Reson. 2016;18:26.
3. Gravina M, Stoppino LP, Casavecchia G, Moffa AP, Vinci R, Brunetti ND, et al. Incidental extracardiac findings and their characterization on cardiac MRI. Biomed Res Int. 2017;2017:2423546.
4. Dunet V, Barras H, Boulanger X, Monney P, Qanadli SD, Meuli R, et al. Impact of extracardiac findings during cardiac MR on patient management and outcome. Med Sci Monit. 2015;21:1288-96.
5. Dunet V, Schwitter J, Meuli R, Beigelman-Aubry C. Incidental extracardiac findings on cardiac MR: systematic review and meta-analysis. J Magn Reson Imaging. 2016;43:929-39.
6. Petersen SE, Almeida AG, Alpendurada F, Boubertakh R, Bucciarelli-Ducci C, Cosyns B, et al. Update of the European Association of Cardiovascular Imaging (EACVI) core syllabus for the European Cardiovascular Magnetic Resonance Certification Exam. Eur Heart J Cardiovasc Imaging. 2014;15:728-9.
7. Sokolowski FC, Karius P, Rodríguez A, Lembcke A, Wagner M, Hamm B, et al. Extracardiac findings at cardiac MR imaging: a single-centre retrospective study over 14 years. Eur Radiol. 2018;28:4102-10.
8. Wyttenbach R, Médioni N, Santini P, Vock P, Szucs-Farkas Z. Extracardiac findings detected by cardiac magnetic resonance imaging. Eur Radiol. 2012;22:1295-302.
9. Mora-Encinas JP, Martín-Martín B, Nogales-Montero J, Mora-Monago R, Romero JA. Prevalence and significance of extracardiac findings in cardiac magnetic resonance imaging. Rev Argent Radiol. 2016;80:171-7.
10. Atalay MK, Prince EA, Pearson CA, Chang KJ. The prevalence and clinical significance of noncardiac findings on cardiac MRI. AJR Am J Roentgenol. 2011;196:W387-93.
11. McKenna DA, Laxpati M, Colletti PM. The prevalence of incidental findings at cardiac MRI. Open Cardiovasc Med J. 2008;2:20-5.
12. Jacobs PC, Mali WP, Grobbee DE, van der Graaf Y. Prevalence of incidental findings in computed tomographic screening of the chest: a systematic review. J Comput Assist Tomogr. 2008;32:214-21.
13. Sohns JM, Schwarz A, Menke J, Staab W, Spiro JE, Lotz J, et al. Prevalence and clinical relevance of extracardiac findings at cardiac MRI. J Magn Reson Imaging. 2014;39:68-76.
14. Irwin RB, Newton T, Peebles C, Borg A, Clark D, Miller C, et al. Incidental extra-cardiac findings on clinical CMR. Eur Heart J Cardiovasc Imaging. 2013;14:158-66.
15. Chan PG, Smith MP, Hauser TH, Yeon SB, Appelbaum E, Rofsky NM, et al. Noncardiac pathology on clinical cardiac magnetic resonance imaging. JACC Cardiovasc Imaging. 2009;2:980-6.
16. Khosa F, Romney BP, Costa DN, Rofsky NM, Manning WJ. Prevalence of noncardiac findings on clinical cardiovascular MRI. AJR Am J Roentgenol. 2011;196:W380-6.
17. Mantini C, Mastrodicasa D, Bianco F, Bucciarelli V, Scarano M, Mannetta G, et al. Prevalence and clinical relevance of extracardiac findings in cardiovascular magnetic resonance imaging. J Thorac Imaging. 2019;34:48-55.

Hong Kong J Radiol. 2023;26:42-8 | https://doi.org/10.12809/hkjr2317477

PERSPECTIVE

Contrast-Enhanced Ultrasonography and Its Application in Liver Interventions

CH Ho, SM Wong, HL Wong, JCW Siu, KCH Yu, JCX Chan, HY Lau, CB Tan, YC Wong

Department of Radiology, Tuen Mun Hospital, Hong Kong

ABSTRACT

Ultrasound (US) guidance has been a fundamental tool for interventionalists to perform percutaneous procedures. A limitation to US guidance is poor lesion visibility on conventional B-mode (brightness mode) US. Contrast-enhanced US (CEUS) is an adjunct technique that facilitates the visualisation and localisation of lesions. We review the use of CEUS and its application in liver interventions and describe the experience in our institution in using CEUS in these procedures.

Key Words: *Contrast media; Radiology, interventional; Ultrasonography, interventional*

中文摘要

超聲造影檢查及其在肝臟介入中的應用綜述

何卓謙、王先民、黃皓廉、蕭志偉、余俊鴻、陳積聖、劉顯宇、陳崇文、王耀忠

超聲引導一直是介入醫生開展經皮手術的基本工具，它的其中一個局限性是傳統B模式（亮度模式）超聲對於病變的可見性欠佳。對比增強超聲這種輔助技術可幫助病變的檢出和定位。本文檢視對比增強超聲的使用及其在肝臟介入中的應用，並描述本院在有關操作中使用對比增強超聲的實踐。

Correspondence: *Dr CH Ho, Department of Radiology, Tuen Mun Hospital, Hong Kong*
Email: hch1931@ha.org.hk

Submitted: 22 Sep 2021; Accepted: 4 Feb 2022.

Contributors: All authors designed the study. CHH, SMW, HLW and JCWS acquired and analysed the data. CHH drafted the manuscript. SMW, HLW, JCWS, KCHY, JCXC, HYL, CBT and YCW critically revised the manuscript for important intellectual content. All authors had full access to the data, contributed to the study, approved the final version for publication, and take responsibility for its accuracy and integrity.

Conflicts of Interest: The authors have no conflict of interest to declare.

Funding/Support: This study received no specific grant from any funding agency in the public, commercial, or not-for-profit sectors.

Data Availability: All data generated or analysed during the present study are available from the corresponding author on reasonable request.

Ethics Approval: This study was approved by New Territories West Cluster Research Ethics Committee of Hospital Authority, Hong Kong (Ref No.: NTWC/REC/21086). Informed consent was waived by the Committee.

INTRODUCTION

Ultrasound (US) guidance has been a fundamental tool for interventionalists for various percutaneous procedures. It has the advantages of real-time imaging, lack of ionising radiation, and wide availability. However, the role of US guidance is greatly limited if the lesion has a poor visibility on conventional B-mode (brightness mode) US.

To overcome this limitation, contrast-enhanced ultrasound (CEUS) is an adjunct technique to facilitate the localisation of lesions.[1] In this article, we review the background information of US contrast agents and techniques for performing CEUS. We also describe the application of CEUS in liver interventions and our experience with this technique in our institution.

ULTRASOUND CONTRAST AGENTS

US contrast agents consist of gaseous microbubbles enclosed within shells.[2] They are injected intravenously. The size of microbubbles ranges from 1 to 10 μm.[3] Microbubbles respond differently under different acoustic energies. When microbubbles are subjected to low acoustic energy (mechanical index [MI] = 0.1-0.3), they oscillate and produce non-linear harmonic resonances.[2,3] Separation of the non-linear resonances from microbubbles and linear resonances from background soft tissue forms the basis of CEUS. These two signals can be separated using one of several soft tissue cancellation techniques, such as pulse inversion, frequency, and amplitude modulation.[2,4] Microbubbles are vulnerable to higher acoustic energies (MI > 0.3-0.6), which can cause cavitation and fragmentation.[2]

US contrast agents are classified into first and second generations, depending on the solubility of the gaseous content.[3,5] The first-generation US contrast agents, which consisted mostly of air, are largely obsolete due to their instability (as they will burst easily) and high solubility in blood. Most of the currently used second-generation contrast agents are composed of encapsulated inert gases with high stability and low solubility (e.g., perfluorobutane, perfluoropropane, and sulphur hexafluoride).[5] Currently, there are four agents that are available internationally for use in liver imaging, including sulphur hexafluoride within a phospholipid shell (SonoVue; Bracco Suisse SA, Switzerland), octafluoropropane within a bilayer phospholipid shell (Luminity; Lantheus Medical Imaging, Inc, North Billerica [MA], United States), perfluorobutane gas coated with a chicken egg–derived surfactant hydrogenated egg phosphatidylserine sodium [Optison; GE HealthCare, United Kingdom], and perflubutane enclosed in a phospholipid shell, which has immediate blood pool and delayed Kupffer cell uptake in the liver, which can last up to a few hours (Sonazoid[6-8]; GE HealthCare, Norway). In Asian countries, SonoVue and Sonazoid are more commonly used.[7]

SonoVue is taken up by the blood pool. It is the only registered US contrast agent in Hong Kong.[9] It is currently registered in 44 countries[10] and is available in Japan, Korea, Norway, Singapore and China, etc.[7] It is currently an unregistered drug in Hong Kong, and the relevant legal requirement needs to be observed before use.[8] Details can be obtained from the Drug Office of the Department of Health.[11]

Intravenous use of US contrast agents has a very safe profile. They are excreted via the lungs. The outer shells are biodegradable in general owing to the fact that they will be engulfed by macrophages in the reticuloendothelial system.[2] They are not nephrotoxic, and therefore can be administered in patients with renal failure.[5,6] It also has no effect on thyroid function as it does not contain iodine.[5] US contrast agents have a very low rate of anaphylactic reactions (1 in 7000 patients or 0.014%) compared to iodinated contrast agents or gadolinium-based contrast agents.[5,6]

Contraindications vary among different US contrast agents. For SonoVue, contraindications include, but are not limited to, hypersensitivity to the active substance or to any of the excipients (including polyethylene glycol), known right-to-left shunts, severe pulmonary hypertension, uncontrolled systemic hypertension, and adult respiratory distress syndrome.[12] For Sonazoid, contraindications include hypersensitivity to the active substances (including perfluorobutane gas and hydrogenated egg phosphatidylserine sodium) or to any of the excipients. Sonazoid is derived from egg. For patients with egg or egg products allergy, Sonazoid should only be used if the benefit clearly outweighs the potential hazard.[7] Care should be taken in patients with right-to-left shunts, unstable heart conditions, serious coronary arterial diseases or serious pulmonary diseases.[13] Readers are advised to read the relevant product information and package insert carefully before use.

TECHNIQUE OF CONTRAST-ENHANCED ULTRASOUND

One of the unique features of CEUS is that real-time imaging of contrast enhancement is enabled. The arterial phase usually occurs from 10-20 seconds to 30-45 seconds after injection. The portal venous phase ensues 30-45 seconds to 2 minutes post-injection and is followed by late phase, which ends when there is clearance of microbubbles from the circulation which is about 4-6 minutes.[4] For Sonazoid, the Kupffer cell uptake (post-vascular) phase usually starts 10 minutes post-injection and can persist up to a few hours.[7,10]

MI is the measure of acoustic power of an US beam. To minimise the disruption of the microbubbles, CEUS imaging is performed at low acoustic pressures with MI ranging from 0.05 to 0.3.[4] Different contrast agents may require different machine settings for optimal signals; for example, SonoVue can be used with a lower MI (<0.1) due to its softer shell, while a higher MI is needed for Sonazoid due to its stiffer outer shell.[9,14] Optimal MI settings may vary from machine to machine.

The dose of US contrast agent varies with different brands. The current recommended dose is 2.4 mL for SonoVue (peripheral vascular use), and 0.015 mL/kg body weight for Sonazoid.[12,13] Both SonoVue and Sonazoid need to be reconstituted before administration and readers are referred to the relevant package insert for detail information. A reminder on reconstituting Sonazoid from our experience is although an ampoule of 10 mL sterile water is provided in the package, only 2 mL is required for reconstitution. Using a 20G or larger catheter for contrast injection is recommended to minimise microbubble destruction. Slow hand injection of contrast agent over 2 to 3 seconds followed by a 5- to 10-mL saline flush is suggested.[4] Repeated contrast injection of the recommended dose can be considered if necessary.[15]

Dual-screen display with low MI B-mode and contrast-mode images side-by-side is commonly used during CEUS. A timer is also displayed to record the time after contrast injection (Figure 1). Depth of penetration of CEUS is usually less than that seen with conventional B-mode imaging due to low MI settings. The focal zone should be placed just deep to the target lesion.[4,15] It is important to avoid excessive or continuous scanning in a single plane in order to prevent microbubble destruction, which causes loss of contrast signal.[15] Again, repeated contrast injection can be considered to characterise a washed-out region for any arterial phase enhancement.[15]

Key features of hepatocellular carcinoma with SonoVue are arterial phase hyperenhancement followed by late and mild washout (Figure 2). Similarly for Sonazoid, hepatocellular carcinoma typically shows arterial phase hyperenhancement and a defect in the Kupffer cell phase.

There are many guidelines and publications describing the use of CEUS in characterising focal liver lesions. A complete description of lesion enhancement patterns

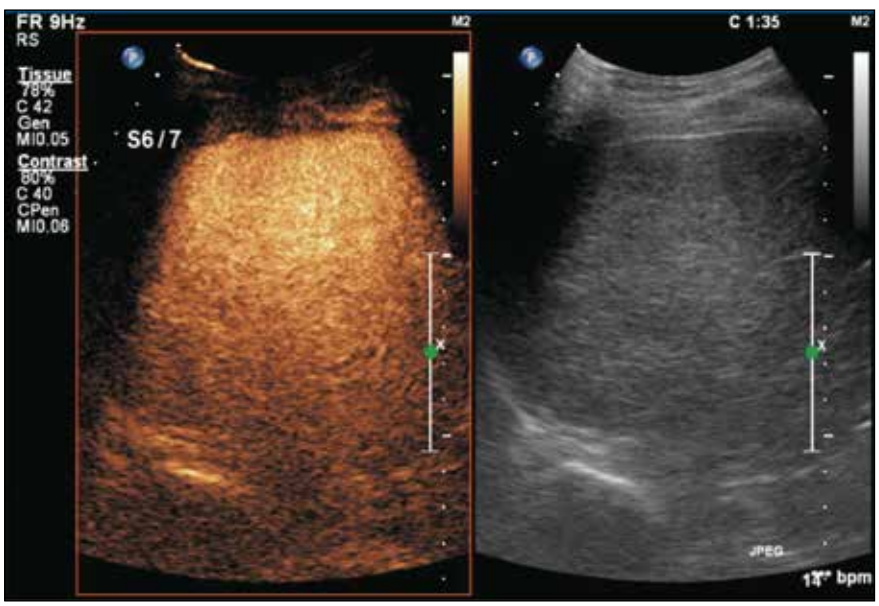

Figure 1. Dual-screen display with contrast-mode image on the left and low mechanical index B-mode (brightness mode) ultrasound image on the right side-by-side when performing contrast-enhanced ultrasound. A scanner timer is also displayed at the upper right corner of the screen.

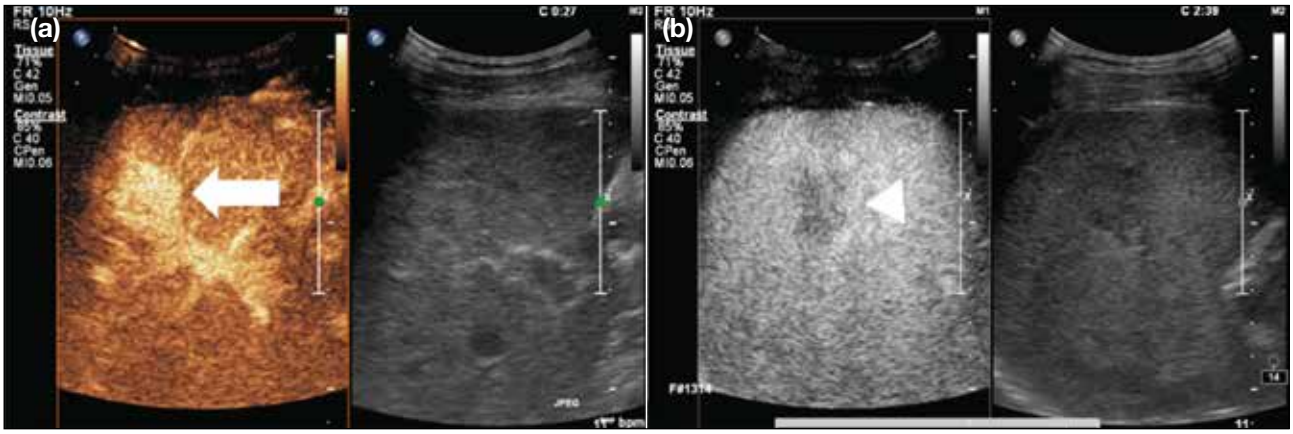

Figure 2. Case of typical hepatocellular carcinoma. (a) Contrast-enhanced ultrasound (CEUS) with SonoVue showed non-rim arterial phase hyperenhancement of the target lesion in segment V of liver (white arrow). The lesion measured 2.8 cm in maximal diameter (not shown). (b) In the late phase, this lesion demonstrated mild contrast washout (white arrowhead). This lesion was classified as CEUS LR-5 lesion (i.e., definitely hepatocellular carcinoma) according to the CEUS Liver Imaging Reporting and Data System version 2017.

and a lexicon are beyond the scope of this article. Readers are referred to the Guidelines and Good Clinical Practice Recommendations for CEUS in the Liver from WFUMB (World Federation for Ultrasound in Medicine and Biology), and CEUS of the liver: technical and lexicon recommendations from the American College of Radiology CEUS Liver Imaging Reporting and Data System working group for further information.[4,6] The current American College of Radiology CEUS Liver Imaging Reporting and Data System (LI-RADS) version 2017 only described the use of pure blood pool agents, and the use of Sonazoid will be addressed in the next version.[4]

APPLICATION OF CONTRAST-ENHANCED ULTRASOUND IN LIVER INTERVENTIONS

CEUS can enhance lesion conspicuity for percutaneous interventions, especially when they are not well depicted on conventional B-mode US.[16] Common uses of CEUS in liver interventions include guiding percutaneous biopsy and tumour ablation.

For indeterminate lesions on computed tomography (CT) or magnetic resonance (MR) imaging, CEUS may provide further diagnostic information to characterise the lesions. For example, indeterminate lesions showing absence of arterial hyperenhancement on CT or MR may be due to mistiming of the arterial phase imaging. Using CEUS can eliminate this problem since it is real-time continuous imaging.[4,6,7,17] Therefore, CEUS can be a problem-solving tool and may obviate the need for biopsy for indeterminate lesions on CT or MR.

CEUS is often employed in guiding percutaneous biopsy of focal liver lesions. It is helpful in both increasing lesion conspicuity and evaluating the viable vascularised portion of the lesion. In the recent guidelines issued by WFUMB, CEUS guidance for focal liver lesion biopsy should be attempted when the lesions are invisible or inconspicuous on conventional B-mode imaging and should be considered in lesions with potential necrotic areas or if previous biopsy resulted in necrotic material.[6] A two-dose procedure is recommended. The first dose of US contrast is used for characterising the target lesion and planning the needle path, and the second dose is used for the real-time CEUS guidance during interventions.[6] The safety and feasibility of using CEUS with SonoVue and Sonazoid in focal liver lesion biopsy have been reported in multiple studies.[16,18,19] With the use of CEUS, the need to abort the procedure and convert to CT guidance is potentially reduced. It also helps to confirm the target lesion in cases of advanced cirrhosis where multiple background cirrhosis-related nodules are common or of concurrent benign liver lesions (e.g., haemangioma), and therefore minimises mistargeting. Vascular complications after biopsy, such as pseudoaneurysm formation, can be detected by CEUS, avoiding the need for contrast-enhanced CT.[20]

CEUS is also valuable in guiding liver tumour ablation. Similar to guiding percutaneous biopsy of focal liver lesions, CEUS can increase lesion conspicuity, allow real-time needle guidance to the lesion during the procedure, and minimise mistargeting to other lesions. In a randomised controlled trial reported by Minami et al,[21] there was a significantly higher complete ablation rate

(94.7% vs. 65.0%) and a smaller number of treatment sessions when using CEUS guidance with Levovist in liver tumour ablation for lesions poorly depicted on conventional B-mode US. After ablation, gas clouds form in the treatment bed; they are markedly echogenic and obscure the ablation zone, but usually resolve after 10 to 15 minutes, and CEUS can then be performed post-ablation to evaluate for residual disease around the ablation zone.[22-25] Re-intervention can be performed in the same setting if indicated. Performing immediate

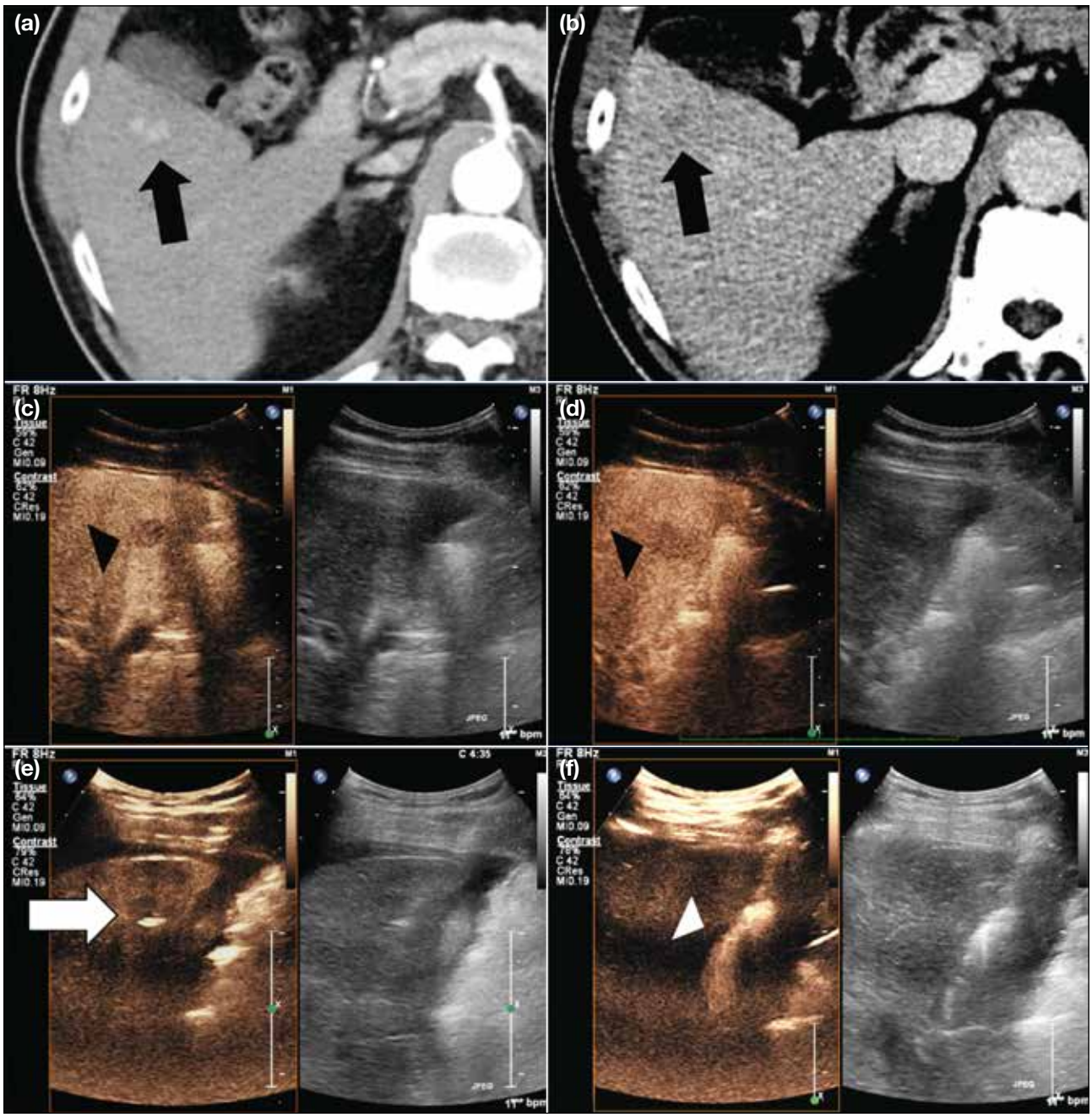

Figure 3. This patient had chronic hepatitis B viral infection and cirrhosis. (a and b) Axial contrast computed tomography (CT) liver showed two small arterial enhancing lesions in segment V of the liver with contrast washout in the delayed phase suspicious for hepatocellular carcinoma (black arrows). (c and d) The patient was referred to our team for percutaneous ablation of the lesions. On conventional B-mode (brightness mode) ultrasound, both of the lesions could not be well visualised (image not captured). Contrast-enhanced ultrasound (CEUS) with Sonazoid was then performed, with two nodular parenchymal defects in segment V of liver closely abutting each other during the Kupffer phase corresponding to the CT-detected lesions (black arrowheads). (e and f) Subsequent percutaneous ablation was performed under CEUS with Sonazoid during the Kupffer phase. The lesions were first targeted with a 22G spinal needle (white arrow) and then a microwave antenna was inserted with parallel technique under CEUS guidance (white arrowhead).

postprocedural CEUS with Definity can significantly reduce the incidence of residual tumour (0% vs. 16.7%) shown in a retrospective study by Lekht et al.[24] Mauri et al[25] also reported using CEUS with Sonovue after liver tumour ablation, detecting residual tumour in 29.0% of the ablations. They were able to repeat ablation immediately, with later CT showing 96.6% success. Nishigaki et al[23] reported the successful use of Sonazoid in detecting residual tumour and securing minimal ablative margins immediately after ablation. These show the effectiveness of immediate post-ablation CEUS in determining the adequacy of the ablation, which can potentially improve patient survival and clinical outcome.

SonoVue is the only registered US contrast agent in Hong Kong.[9] It can be used in guiding different liver interventions as described. However, its short enhancement period may not be ideal for liver interventions, especially in liver tumour ablation where the procedural time is usually long. Sonazoid provides a unique advantage with the prolonged Kupffer cell phase, which can last up to a few hours, providing a longer time window for real-time CEUS guidance.

We have recently introduced CEUS with Sonazoid in our institution. For patients referred to us for percutaneous liver tumour ablation, we would carry out a consultation in our interventional radiology clinic. During the consultation, we routinely perform a US of the index lesion for preprocedural planning. CEUS can be considered at the same juncture if the lesion cannot be clearly visualised on conventional B-mode US. If the lesion becomes more conspicuous after contrast administration and the time window of visibility appears technically feasible for percutaneous ablation, then CEUS-guided percutaneous ablation is scheduled. In our experience, the early Kupffer phase (10-30 minutes post-injection) provides a good intervention window. Avoiding unnecessary continuous scanning is important to minimise microbubble destruction. A second dose of contrast injection is also helpful if contrast signal loss occurs. CEUS with Sonazoid during interventional radiology clinic consultation can be safely performed in outpatient setting. In our institution, patients would be discharged following a 10- to 15-minute observation after administration of Sonazoid.

In our experience, CEUS with Sonazoid improves the detection and conspicuity of liver lesions (Figure 3). It enables real-time US guidance for lesions that are not conspicuous on conventional B-mode US when performing percutaneous liver procedures, obviating the need for CT guidance. This reduces the radiation exposure to patients, and possibly decreases the procedural time and complexity. CEUS has also a role in percutaneous liver tumour ablation to detect any residual tumour immediate post-ablation (Figure 4),

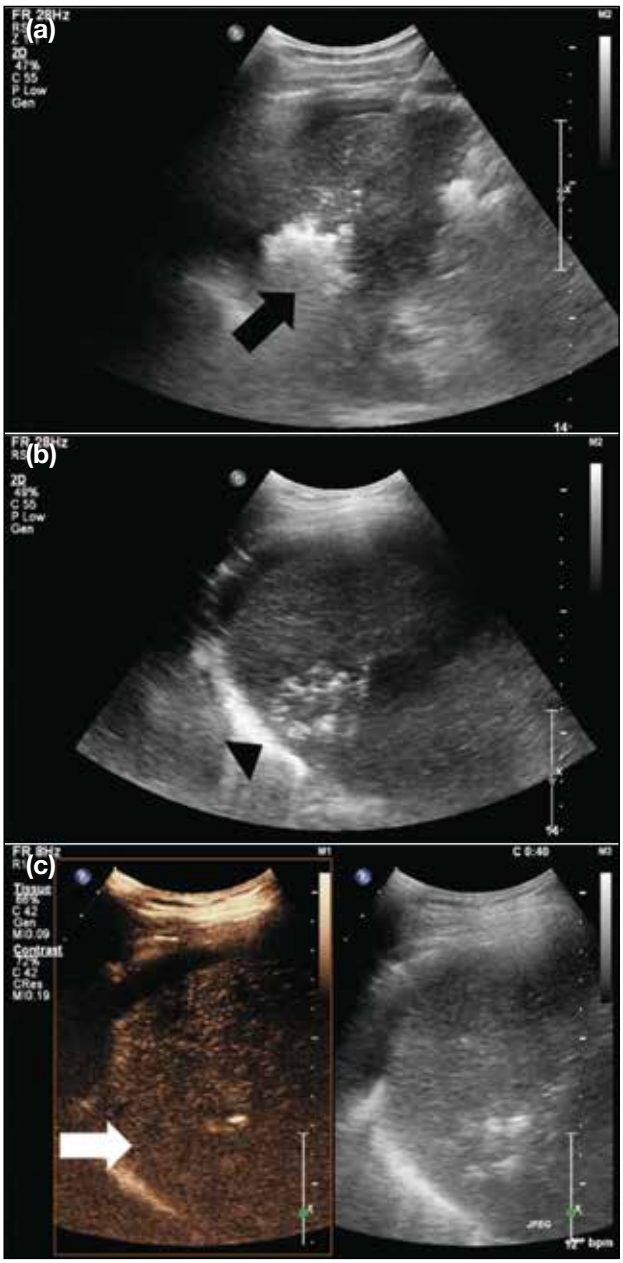

Figure 4. This patient had a hepatocellular carcinoma in segment VII of the liver. Percutaneous microwave ablation was performed. (a) Immediately after ablation, the ablation zone was largely obscured by a gas cloud (black arrow). (b) Twenty minutes after the ablation, the gas cloud had largely subsided and the ablation zone could be clearly demonstrated on ultrasound (black arrowhead). (c) Contrast-enhanced ultrasound performed with Sonazoid showed no marginal nodular enhancement adjacent to the ablation zone to suggest the presence of residual tumour (white arrow).

and re-intervention can be easily performed in the same setting if any residual tumour is detected. There are also no serious adverse reactions reported after intravenous administration of Sonazoid in our institution.

However, there are still some limitations of CEUS in guiding liver interventions from our experience. CEUS has a detection limit for deep lesions since the penetration may not be adequate with the presence of microbubbles and low MI settings. Similar to conventional B-mode US, there is also limitation for CEUS to detect lesions located at the liver dome.

CONCLUSION

CEUS is a safe and effective tool for liver interventions. It improves the visibility of lesions for needle guidance and is particularly useful when the lesions are small or not conspicuous on conventional B-mode US. The unique feature of Kupffer cell uptake of Sonazoid provides a longer time window for real-time guidance during liver interventions.

REFERENCES

1. Kim YJ, Lee MW, Park HS. Small hepatocellular carcinomas: ultrasonography guided percutaneous radiofrequency ablation. Abdom Imaging. 2013;38:98-111.
2. Baun J. Contrast-enhanced ultrasound: a technology primer. J Diagn Med Sonogr. 2017;33:446-52.
3. Ignee A, Atkinson NS, Schuessler G, Dietrich CF. Ultrasound contrast agents. Endosc Ultrasound. 2016;5:355-62.
4. Lyshchik A, Kono Y, Dietrich CF, Jang HJ, Kim TK, Piscaglia F, et al. Contrast-enhanced ultrasound of the liver: technical and lexicon recommendations from the ACR CEUS LI-RADS working group. Abdom Radiol (NY). 2018;43:861-79.
5. Chung YE, Kim KW. Contrast-enhanced ultrasonography: advance and current status in abdominal imaging. Ultrasonography. 2015;34:3-18.
6. Dietrich CF, Nolsøe CP, Barr RG, Berzigotti A, Burns PN, Cantisani V, et al. Guidelines and Good Clinical Practice Recommendations for Contrast-Enhanced Ultrasound (CEUS) in the Liver–update 2020 WFUMB in cooperation with EFSUMB, AFSUMB, AIUM, and FLAUS. Ultrasound Med Biol. 2020;46:2579-604.
7. Lee JY, Minami Y, Choi BI, Lee WJ, Chou YH, Jeong WK, et al. The AFSUMB consensus statements and recommendations for the clinical practice of contrast-enhanced ultrasound using Sonazoid. Ultrasonography. 2020;39:191-220.
8. Shunichi S, Hiroko I, Fuminori M, Waki H. Definition of contrast enhancement phases of the liver using a perfluoro-based microbubble agent, perflubutane microbubbles. Ultrasound Med Biol. 2009;35:1819-27.
9. Drug Office, Department of Health, Hong Kong SAR Government. List of Registered Pharmaceutical Products. SONOVUE FOR INJ 8MCL/ML. Available from: https://www.drugoffice.gov.hk/eps/drug/productDetail/en/consumer/120026. Accessed 21 Dec 2021.
10. Barr RG, Huang P, Luo Y, Xie X, Zheng R, Yan K, et al. Contrast-enhanced ultrasound imaging of the liver: a review of the clinical evidence for SonoVue and Sonazoid. Abdom Radiol (NY). 2020;45:3779-88.
11. Drug Office, Department of Health, Hong Kong SAR Government. Frequently asked questions. Available from: https://www.drugoffice.gov.hk/eps/do/en/pharmaceutical_trade/guidelines_forms/faq.html. Accessed 21 Dec 2021.
12. European Medicines Agency. SonoVue: EPAR — product information. Available from: https://www.ema.europa.eu/en/documents/product-information/sonovue-epar-product-information_en.pdf. Accessed 19 Dec 2021.
13. Health Sciences Authority of Singapore. Summary report of benefit-risk assessment: Sonazoid powder and solvent for dispersion for injection, 16 microlitre per vial. Available from: https://www.hsa.gov.sg/docs/default-source/hprg-tpb/summary-reports/sonazoid-summary-report-06-jan-21.pdf. Accessed 19 Dec 2021.
14. Numata K, Luo W, Morimoto M, Kondo M, Kunishi Y, Sasaki T, et al. Contrast enhanced ultrasound of hepatocellular carcinoma. World J Radiol. 2010;2:68-82.
15. Dietrich CF, Averkiou M, Nielsen MB, Barr RG, Burns PN, Calliada F, et al. How to perform contrast-enhanced ultrasound (CEUS). Ultrasound Int Open. 2018;4:E2-15.
16. Yoon SH, Lee KH, Kim SY, Kim YH, Kim JH, Lee SH, et al. Real-time contrast-enhanced ultrasound-guided biopsy of focal hepatic lesions not localised on B-mode ultrasound. Eur Radiol. 2010;20:2047-56.
17. Jo PC, Jang HJ, Burns PN, Burak KW, Kim TK, Wilson SR. Integration of contrast-enhanced US into a multimodality approach to imaging of nodules in a cirrhotic liver: how I do it. Radiology. 2017;282:317-31.
18. Park HS, Kim YJ, Yu MH, Jung SI, Jeon HJ. Real-time contrast-enhanced sonographically guided biopsy or radiofrequency ablation of focal liver lesions using perflurobutane microbubbles (Sonazoid): value of Kupffer-phase imaging. J Ultrasound Med. 2015;34:411-21.
19. Spârchez Z, Radu P, Kacso G, Spârchez M, Zaharia T, Al Hajjar N. Prospective comparison between real time contrast enhanced and conventional ultrasound guidance in percutaneous biopsies of liver tumors. Med Ultrason. 2015;17:456-63.
20. Huang DY, Yusuf GT, Daneshi M, Husainy MA, Ramnarine R, Sellars ME, et al. Contrast-enhanced US-guided interventions: improving success rate and avoiding complications using US contrast agents. Radiographics. 2017;37:652-64.
21. Minami Y, Kudo M, Chung H, Kawasaki T, Yagyu Y, Shimono T, et al. Contrast harmonic sonography-guided radiofrequency ablation therapy versus B-mode sonography in hepatocellular carcinoma: prospective randomized controlled trial. AJR Am J Roentgenol. 2007;188:489-94.
22. Bansal S, Gui J, Merrill C, Wong JK, Burak KW, Wilson SR. Contrast-enhanced US in local ablative therapy and secondary surveillance for hepatocellular carcinoma. Radiographics. 2019;39:1302-22.
23. Nishigaki Y, Hayashi H, Tomita E, Suzuki Y, Watanabe N, Watanabe S, et al. Usefulness of contrast-enhanced ultrasonography using Sonazoid for the assessment of therapeutic response to percutaneous radiofrequency ablation for hepatocellular carcinoma. Hepatol Res. 2015;45:432-40.
24. Lekht I, Gulati M, Nayyar M, Katz MD, Ter-Oganesyan R, Marx M, et al. Role of contrast-enhanced ultrasound (CEUS) in evaluation of thermal ablation zone. Abdom Radiol (NY). 2016;41:1511-21.
25. Mauri G, Porazzi E, Cova L, Restelli U, Tondolo T, Bonfanti M, et al. Intraprocedural contrast-enhanced ultrasound (CEUS) in liver percutaneous radiofrequency ablation: clinical impact and health technology assessment. Insights Imaging. 2014;5:209-16.

Hong Kong J Radiol. 2023;26:49-52 | https://doi.org/10.12809/hkjr2317235

CASE REPORT

Eosinophilic Meningitis and Pneumonitis due to Angiostrongyliasis: a Case Report

YM Leng, Allen Li

Department of Radiology and Nuclear Medicine, Tuen Mun Hospital, Hong Kong

INTRODUCTION

Angiostrongylus cantonensis infection is one of the most common causes of eosinophilic meningitis in Southeast Asia and the Pacific Basin.[1] The organism was first described in 1935 by Chinese parasitologist Hsin-tao Chen. It was first found in the cerebrospinal fluid (CSF) of a Japanese patient who died of eosinophilic meningoencephalitis in Taiwan in 1944.[2] Since then, there has been an increase in the global distribution of reported cases. Sporadic cases in travellers who have returned from endemic areas have been reported.

Infection with *A cantonensis* can arise from ingestion of food items contaminated by intermediate or definitive hosts. Neural tissue can be targeted after infection. Lung involvement is less commonly encountered clinically. To the best of our knowledge, this is the first reported local case of *A cantonensis* infection with both central nervous system and lung involvement.

CASE PRESENTATION

A 29-year-old Chinese man with a history of epileptic seizure since childhood was admitted to Tuen Mun Hospital with a 5-day history of severe cerebellar ataxia, preceded by a 3-day history of fever and mild dry cough after travelling to Japan. On admission, he was afebrile with a right-hand intentional tremor, pass pointing sign, and tandem walking instability. No neck rigidity was detected. His Glasgow Coma Scale score was 15. Computed tomography (CT) of the brain on admission was essentially normal.

Initial lumbar puncture revealed elevated opening pressure and a CSF white blood count of 257/μL, with 96% lymphocytes and 4% polymorphonuclear leucocytes. Cryptococcal antigen, bacterial culture and sensitivity test, CSF Japanese encephalitis virus antigen, *Mycobacterium tuberculosis* polymerase chain reaction (PCR), and CSF viral PCR test results were all negative. Subsequent magnetic resonance imaging (MRI) of the brain (Figure 1) showed diffusely increased leptomeningeal enhancement, suggestive of meningitis. MRI of the whole spine showed no abnormal signal along the spinal cord. A new lumbar puncture revealed escalating white cell count from 257 to 2049/μL. Repeat CSF viral, bacterial, and fungal test results were again all negative.

Correspondence: *Dr YM Leng, Department of Radiology and Nuclear Medicine, Tuen Mun Hospital, Hong Kong*
Email: ly108@ha.org.hk

Submitted: 22 May 2020; Accepted: 7 Oct 2020.

Contributors: Both authors designed the study, acquired the data, analysed the data, drafted the manuscript, and critically revised the manuscript for important intellectual content. Both authors had full access to the data, contributed to the study, approved the final version for publication, and take responsibility for its accuracy and integrity.

Conflicts of Interest: Both authors have disclosed no conflicts of interest.

Funding/Support: This study received no specific grant from any funding agency in the public, commercial, or not-for-profit sectors.

Data Availability: All data generated or analysed during the present study are available from the corresponding author on reasonable request.

Ethics Approval: The study was approved by New Territories West Cluster Research Ethics Committee of Hospital Authority (Ref No.: NTWC/REC/20052). The patient was treated in accordance with the tenets of the Declaration of Helsinki and has provided written informed consent for all treatments and procedures. Patient consent for this study was waived by the Committee.

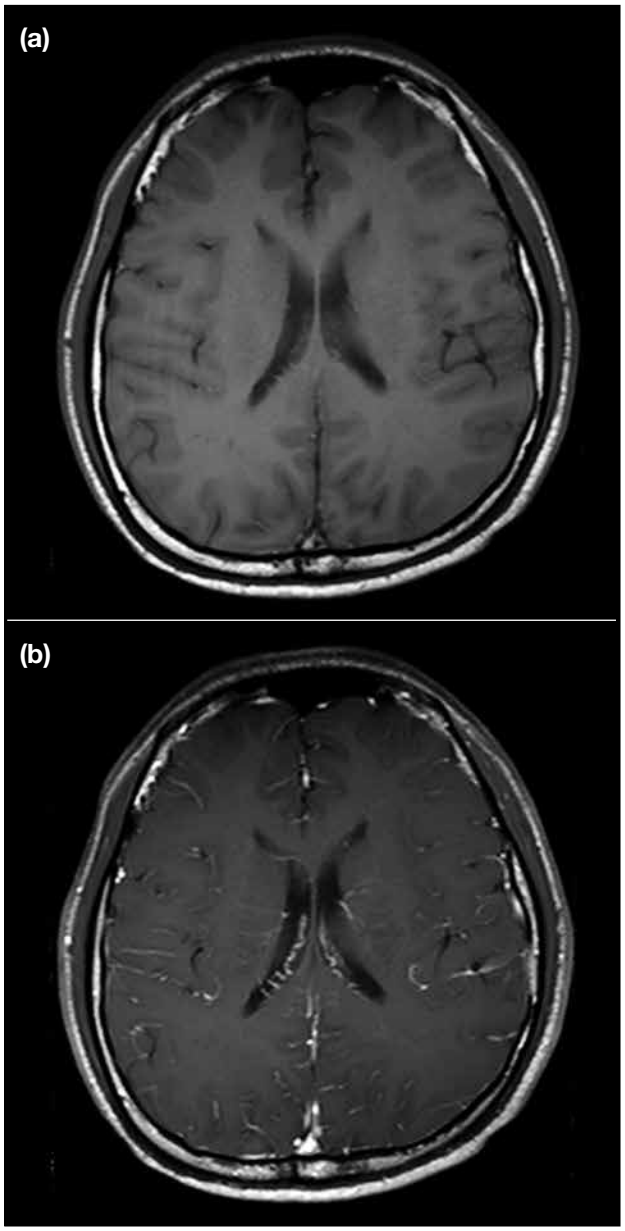

Figure 1. (a) T1-weighted and (b) T2-weighted post-contrast magnetic resonance images showing diffuse leptomeningeal enhancement over the brain, suggestive of meningitis.

However, peripheral blood eosinophil count progressively increased to 33.3% (normal <6%). A third lumbar puncture demonstrated eosinophilia, and a PCR test for *Angiostrongylus* spp. was positive. Plain chest radiograph on admission had revealed patchy infiltrates over peripheral lung fields (Figure 2). CT scan of the thorax showed bilateral subpleural consolidation and ground-glass opacities (Figure 3). Of note was the presence of the halo sign in some areas, that is ground-glass opacity surrounding some of the consolidative lesions.

The patient was prescribed empirical antibiotics, antiviral treatment, and analgesics with gradual clinical improvement. He was not immunocompromised after

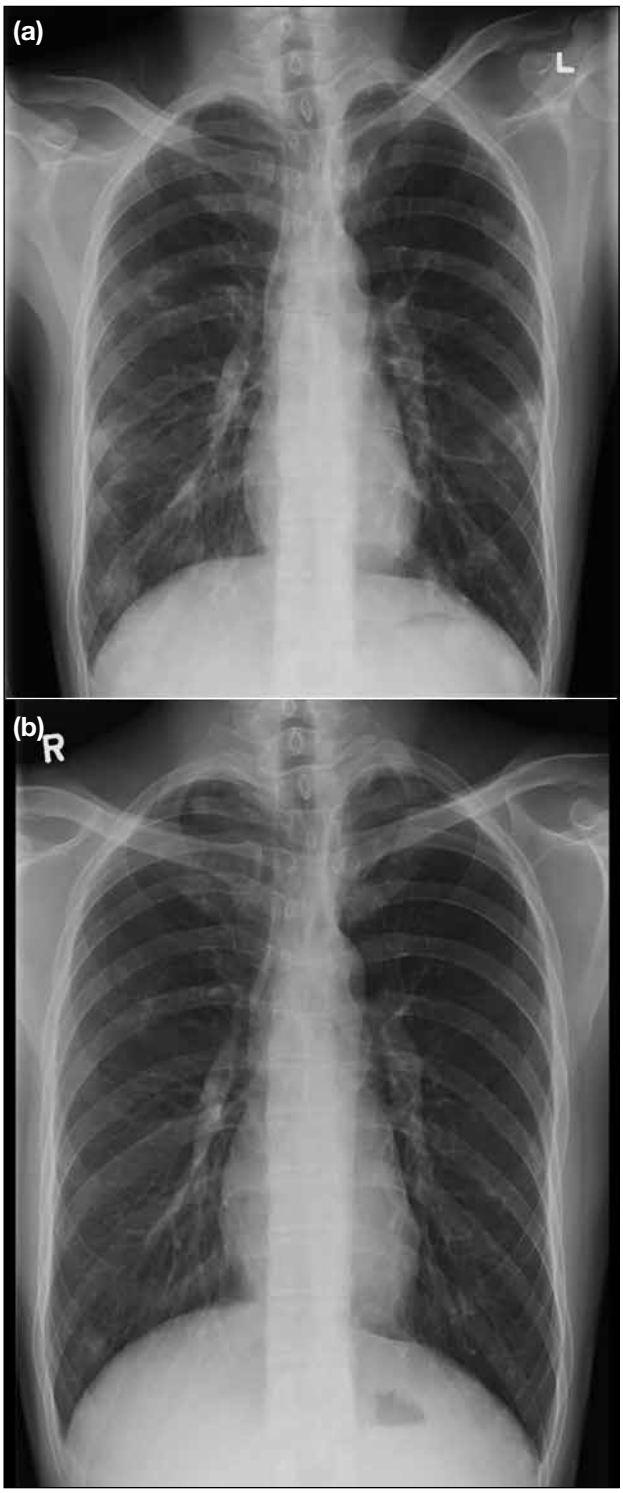

Figure 2. (a) Early plain radiograph of the chest revealed patchy air-space opacities over lung peripheries. (b) Plain radiograph of the chest taken 3 months later showed resolution of bilateral lung consolidation.

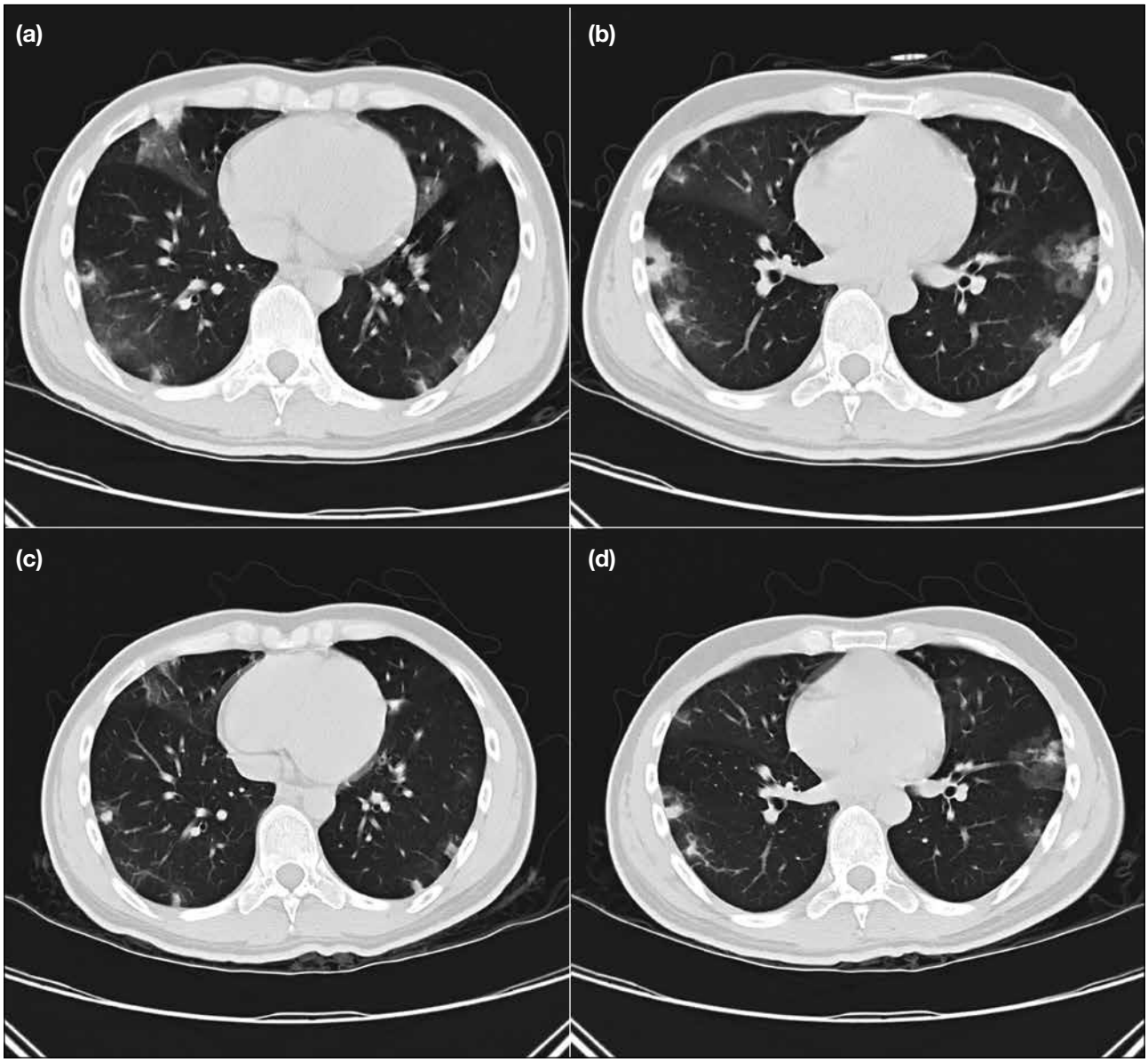

Figure 3. (a) & (b) Initial computed tomography scans of the thorax showed bilateral subpleural consolidation and ground-glass opacities. (c) & (d) New computed tomography scans of the thorax taken 4 days later showed a mild decrease in size of bilateral lung consolidative subpleural lesions.

work-up and was discharged after 4 weeks, with follow-up CT scan of the thorax during admission (Figure 3) and chest radiograph after discharge showing resolution of the lung lesions (Figure 2). His fever had resolved, and no headache or neurological signs were evident. Peripheral eosinophil count was decreasing.

DISCUSSION

A cantonensis primarily infects rat lungs. First-stage larvae migrate to the pharynx where they are swallowed and excreted via the faeces. Intermediate hosts such as snails ingest the faeces of rodents contaminated by these first-stage larvae that then moult twice within the mollusc to develop into second- and third-stage larvae. The third-stage larva is the infecting form of the parasite. Human infection can occur after ingestion of undercooked snails, or through ingestion of unwashed salads or raw vegetable juice contaminated with infective third-stage larvae.[3]

Once infective third-stage larvae are ingested, they can invade the gastrointestinal system and cause enteritis. The larvae then pass through the liver and lungs before reaching the nervous system. Symptoms that include

cough, sort throat, and fever develop as the nematode moves through the lungs. The neurological manifestations of *A cantonensis* infection include eosinophilic meningitis, encephalitis or encephalomyelitis, radiculitis, cranial nerve abnormalities, and ataxia.

Angiostrongyliasis should be considered in patients with high eosinophil count in blood and/or CSF. The diagnosis of angiostrongyliasis is confirmed by detection of *A cantonensis* antigen or antibody in blood or CSF. PCR for antigen detection in CSF has recently been developed and may help to confirm diagnosis at an earlier stage.[4] In our case, the patient had a high eosinophil count in blood and CSF. The CSF PCR confirmed the diagnosis.

MRI examination of the brain and spinal cord in our patient showed diffuse leptomeningeal enhancement of the brain only. There was no abnormal enhancement of the spinal cord on MRI study. In a case series with 17 MRI examinations of the brain and spinal cord in five patients with angiostrongyliasis, multiple enhancing nodules in the brain and linear enhancement in the leptomeninges were the main imaging findings.[5] Spinal cord involvement with enhancement of the nerve roots can also occur but is rare.[5] In a study of 27 patients who were clinically diagnosed with angiostrongyliasis, MRI findings included leptomeningeal enhancement, thickening of the meninges, intracranial nodules, and perimeningeal vascular thickening.[6]

The CT thorax in our patient showed diffuse bilateral subpleural consolidations with ground-glass halo sign. In another study, CT thorax in 15 patients revealed pulmonary nodular lesions and ground-glass opacity lesions located in the subpleural area, which are characteristic signs of the disease.[7] In a case series of 12 patients with lung involvement, CT findings included small nodules with or without a halo of ground-glass attenuation, patchy areas of ground-glass attenuation and focal thickening of bronchovascular bundles located mainly in the peripheral lungs.[8] A large series of 81 patients with *A cantonensis* infection showed concordant imaging findings of focal leptomeningeal enhancement on MRI brain (n = 36) and lung nodules and ground-glass opacity (n = 18).[9]

The diagnosis of angiostrongyliasis can be difficult and requires a high level of suspicion. Clinical history is very important, particularly a history of travel to endemic regions or ingestion of commonly infested host. The diagnosis should be suspected in patients with eosinophilic meningoencephalitis with elevated eosinophils in the blood and/or CSF. MRI brain finding of leptomeningeal enhancement is non-specific. *A cantonensis* can be associated with focal brain lesions on imaging but less commonly than with other helminthic infections of the central nervous system (gnathostomiasis or neurocysticercosis).[10-12] Lung findings of subpleural consolidation and ground-glass opacities, some with halo sign, are also non-specific and can be found in various diseases ranging from infection or neoplasia to inflammatory conditions. Although many cases are self-limiting, severe neurological sequelae and even death may occur.

In summary, we report a case of angiostrongyliasis involvement of the brain and lung. Early recognition and accurate detection of *A cantonensis* can improve patient outcomes. It is important to raise public awareness of disease risk factors in endemic areas and international travellers to prevent further transmission.

REFERENCES

1. Baheti NN, Sreedharan M, Krishnamoorthy T, Nair MD, Radhakrishnan K. Neurological picture. Eosinophilic meningitis and an ocular worm in a patient from Kerala, south India. J Neurol Neurosurg Psychiatry. 2008;79:271.
2. Nomura S, Lin H. First clinical case of Haemostrongylus ratti. Taiwan No Ikai. 1945;3:589-92.
3. Tsai HC, Lee SS, Huang CK, Yen CM, Chen ER, Liu YC. Outbreak of eosinophilic meningitis associated with drinking raw vegetable juice in southern Taiwan. Am J Trop Med Hyg. 2004;71:222-6.
4. Ansdell V, Wattanagoon Y. *Angiostrongylus cantonensis* in travelers: clinical manifestations, diagnosis, and treatment. Curr Opin Infect Dis. 2018;31:399-408.
5. Jin E, Ma D, Liang Y, Ji A, Gan S. MRI findings of eosinophilic myelomeningoencephalitis due to *Angiostrongylus cantonensis*. Clin Radiol. 2005;60:242-50.
6. Yang B, Yang L, Chen Y, Lu G. Magnetic resonance imaging findings and clinical manifestations in cerebral angiostrongyliasis from Dali, China. Brain Behav. 2019;9:e01361.
7. Cui Y, Shen M, Meng S. Lung CT findings of angiostrongyliasis cantonensis caused by *Angiostrongylus cantonensis*. Clin Imaging. 2011;35:180-3.
8. Cheng J, Huang H, Wang X, Wu A, Yu Z, Xu F, et al. *Angiostrongylus cantonensis*: chest CT findings [in Chinese]. Chin J Radiol. 1999;33:371-3.
9. Wang J, Zheng X, Yin Z, Qi H, Li X, Ji A, et al. A clinical analysis of 81 cases of *Angiostrongylus cantonensis* in Beijing [in Chinese]. Chin J Intern Med. 2008;1:50-1.
10. Diaz JH. Recognizing and reducing the risks of helminthic eosinophilic meningitis in travelers: differential diagnosis, disease management, prevention, and control. J Travel Med. 2009;16:267-75.
11. Wang QP, Lai DH, Zhu XQ, Chen XG, Lun ZR. Human angiostrongyliasis. Lancet Infect Dis. 2008;8:621-30.
12. Ramirez-Avila L, Slome S, Schuster FL, Gavali S, Schantz PM, Sejvar J, et al. Eosinophilic meningitis due to *Angiostrongylus* and *Gnathostoma* species. Clin Infect Dis. 2009;48:322-7.

Hong Kong J Radiol. 2023;26:53-7 | https://doi.org/10.12809/hkjr2317491

CASE REPORT

Breast-Implant-Related Fibromatosis in a Patient with Free Silicone Injection: a Case Report

YS Chan, C Tsoi, HY Hung, WCW Chu, HL Chau

Department of Imaging and Interventional Radiology, Prince of Wales Hospital, Hong Kong

CASE REPORT

A 36-year-old woman, gravida 4 and parity 1 with three previous miscarriages, with good past health and no family history of malignancy, was referred to our institution. She had been prescribed oral contraceptives for the last 13 years but had stopped taking them prior to presentation. She had a history of bilateral breast augmentation at age 23 years. The material injected was unknown.

At the age of 36, she presented to an outside institution with a 6-month history of self-detected left breast lump, increasing in size and associated with mastalgia. A lesion at left 5 o'clock (L5H) position was detected and subsequent biopsy revealed focal fat necrosis with scarring.

Physical examination at our institution revealed an immobile, hard left breast mass at L5H position with no palpable lymphadenopathy. The overall clinical picture warranted a repeated core biopsy due to suspicion of a malignant disease process.

Review of her previous mammogram showed multiple densities diffusely over both breasts suggestive of free silicone injection (Figure 1). Ultrasound revealed a snowstorm appearance in both breasts, also in keeping with the presence of free silicone (Figure 2a). The presenting lump was not well visualised, likely due to the heavy shadowing of injected silicone. Ultrasound-guided core biopsy was performed assisted by palpation of the mass with an 18-gauge biopsy needle and two cores of tissue obtained (Figure 2b). Histology showed benign breast tissue with fat necrosis and inflammation. She was offered a lumpectomy but was indecisive.

Unfortunately, 4 months later the patient presented again with rapid increase in size and pain that was not relieved by analgesics. She expressed her wish for resection in view of the worsening symptoms. Due to the rapid disease progression, the surgical team requested magnetic resonance imaging (MRI) for further evaluation and a core biopsy was repeated to exclude the possibility of malignancy. An enhancing mass at L5H position was evident with chest wall invasion

Correspondence: *Dr YS Chan, Department of Imaging and Interventional Radiology, Prince of Wales Hospital, Hong Kong*
Email: juliannayschan@cuhk.edu.hk

Submitted: 20 Oct 2021; Accepted: 14 Jan 2022.

Contributors: YSC and CT designed the study. YSC and HLC acquired and analysed the data. YSC drafted the manuscript. YSC, HYH, WCWC and HLC critically revised the manuscript for important intellectual content. All authors had full access to the data, contributed to the study, approved the final version for publication, and take responsibility for its accuracy and integrity.

Conflicts of Interest: As an editor of the journal, WCWC was not involved in the peer review process. Other authors have disclosed no conflicts of interest.

Funding/Support: This study received no specific grant from any funding agency in the public, commercial, or not-for-profit sectors.

Data Availability: All data generated or analysed during the present study are available from the corresponding author on reasonable request.

Ethics Approval: This study was conducted in accordance with the Declaration of Helsinki. The patient provided consent for all tests and procedures.

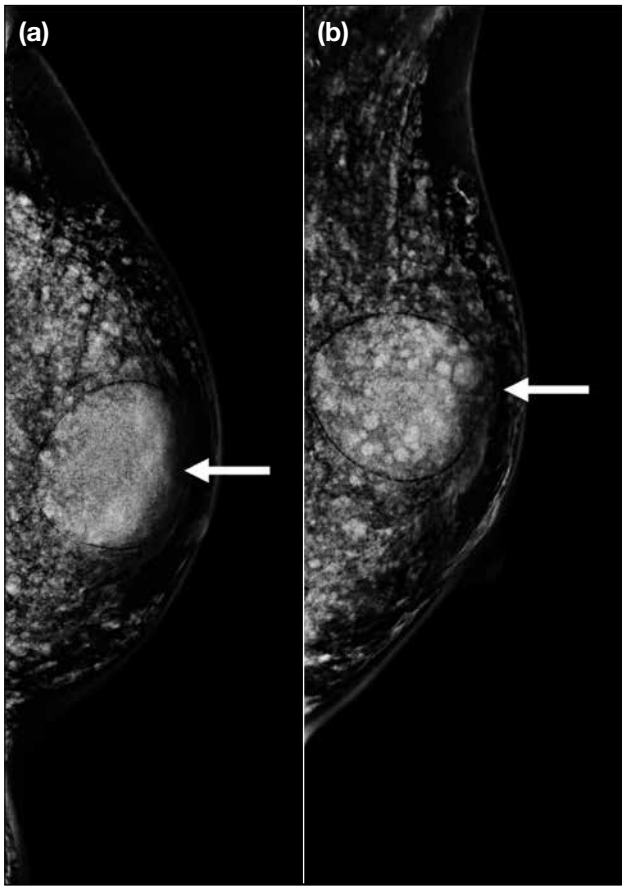

Figure 1. (a) Craniocaudal and (b) mediolateral oblique views of the mammogram showing multiple densities diffusely over both breasts with extension to the bilateral axillary fossa, in keeping with free silicone injection. There is a circumscribed medium density mass at the left upper breast (arrows) corresponding to loculated silicone.

(Figure 3). Dynamic post-contrast images showed a type I kinetic curve. Imaging features remained suspicious of malignancy. Core biopsy was repeated with a 14-gauge biopsy needle under ultrasound guidance and palpation, with three cores of tissue obtained. Histology confirmed fibromatosis. In view of this unusual diagnosis, the case was taken to our multidisciplinary meeting for further discussion of management.

The multidisciplinary meeting consensus was a trial of systemic treatment before consideration of surgery since the chest wall invasion of the fibromatosis would necessitate radical surgery rather than a simple lumpectomy, and the extent of surgical resection may be scaled down if there was a good response to systemic treatment. Due to the significant length of time between the last MRI and the meeting, a repeated MRI was performed to review the progress of the disease and provide a new baseline prior to starting treatment, which showed an increased size of the ill-defined enhancing mass (Figure 4). The lesion invaded the pectoralis muscle and directly abutted the underlying rib. It again showed a type I kinetic curve on dynamic contrast images. The patient was prescribed sulindac and tamoxifen and reported static pain and size of lesion after 3 months. A follow-up MRI has been arranged.

DISCUSSION

Fibromatosis is a rare soft tissue tumour that is considered of 'intermediate nature' due to its local aggressiveness.[1]

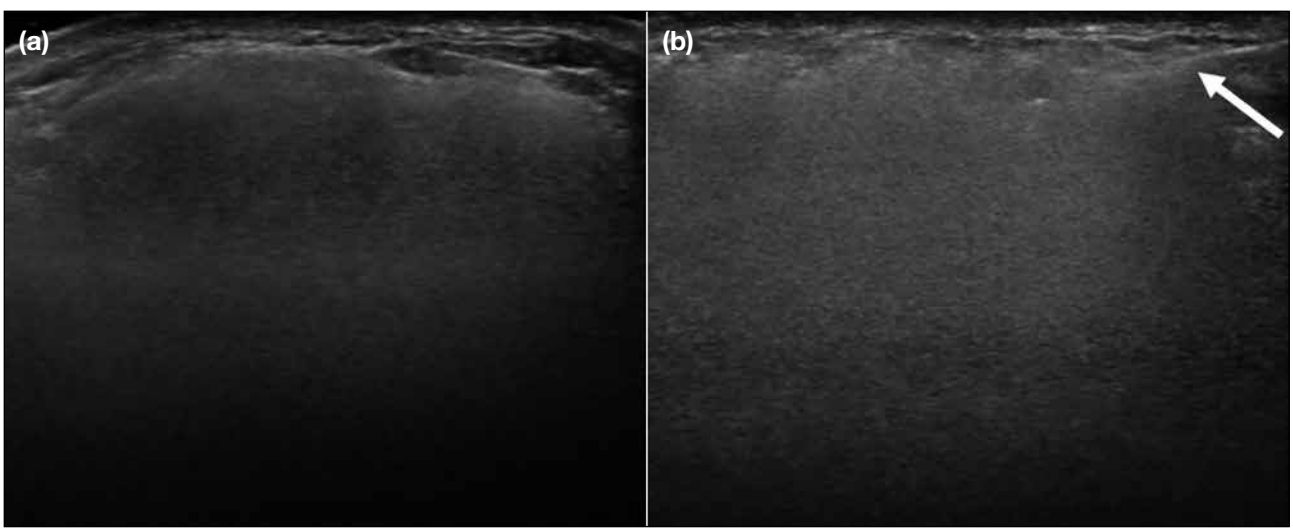

Figure 2. (a) Ultrasound at left 5 o'clock (L5H) position with snowstorm appearance caused by free silicone injection. (b) Ultrasound-guided biopsy at L5H position with limited visualisation of the biopsy needle (arrow).

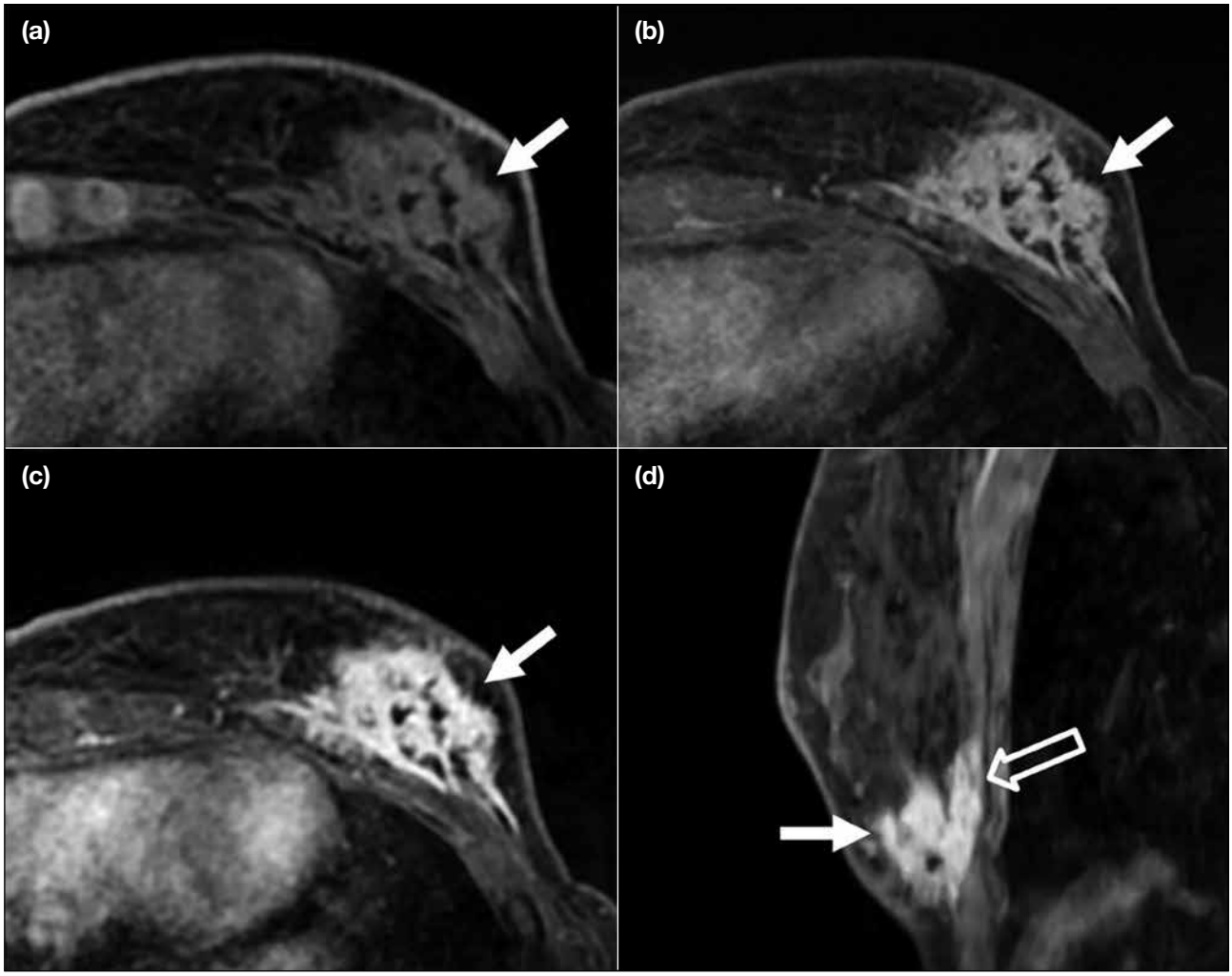

Figure 3. Magnetic resonance images. (a) Axial fat-saturated T1-weighted images showing an isointense lesion (arrow) at left 5 o'clock position, hyperintense on (b) axial fat-saturated water sensitive images (arrow). (c) Axial fat-saturated T1-weighted post-contrast image showing enhancement of the irregular lesion (arrow). (d) Sagittal T1-weighted fat-saturated post-contrast image showing the enhancing lesion (arrow) with underlying pectoralis muscle invasion (open arrow).

It is not metastasising but has a high risk of recurrence.[1-4] It accounts for up to 4% of extra-abdominal fibromatosis cases, and constitutes only 0.2% of breast tumours.[1,4,5] It has been reported to be associated with trauma, prior surgery, pregnancy, increased oestrogen level, implant, and familial adenomatous polyposis (particularly Gardner syndrome).[2,4,6,7]

To date, fewer than 50 cases of implant-related breast fibromatosis have been reported.[2-4,6-13] Reported cases are seen more often with silicone implants than saline implants, possibly due to the higher prevalence of the former.[6] Fibromatoses are usually reported to develop within 2 to 3 years of implant surgery.[2,6] The exact causal relationship between implants and fibromatosis is nonetheless unclear.[6,7,10] The implant material and trauma related to the surgery may both play a role in the development of fibromatoses in patients with breast implants; fibromatoses arising close to or adjacent to the fibrous capsule of a breast implant have been reported.[6,10,13]

Our literature search revealed one case with silicone implant and intracapsular rupture.[7] To the best of our knowledge, there has been no reported case of breast fibromatosis associated with free silicone injection. Free silicone injection as a means of breast augmentation is an outdated practice and uncommon in Asia and South America. It was introduced in the 1940s but has fallen out of favour in view of safety issues and poor cosmetic

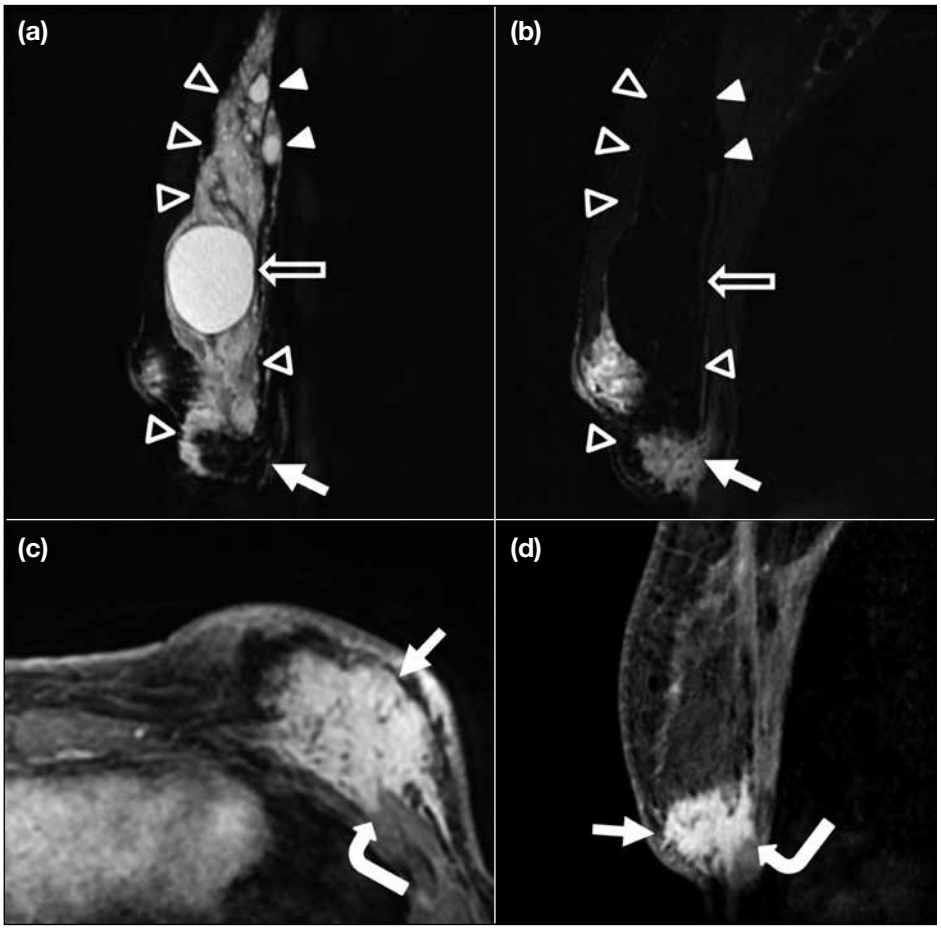

Figure 4. (a) Sagittal silicone-only T2-weighted fat- and water-saturated sequence and (b) sagittal silicone suppressed T2-weighted fat- and water-saturated sequence in the same plane confirm presence of free silicone (open arrowheads), some as tiny locules (arrowheads), and one larger locule (open arrows) corresponding to prior mammogram-detected circumscribed mass at left upper breast. The index mass at left 5 o'clock (arrows) position is also visualised. (c) Axial and (d) sagittal T1-weighted fat-saturated contrast-enhanced images showing the enlarged irregular enhancing mass lesion (arrows) with chest wall invasion through the pectoralis major muscle, abutting the underlying rib (curved arrows).

outcomes although patients with such a clinical history are still occasionally encountered.

Our case is consistent with the literature wherein breast fibromatosis is described as a mimicker of malignancy, both clinically and radiologically.[5]

Clinically, similar to our case, patients with breast fibromatosis are commonly reported to present with a unilateral solitary mass, but bilateral or even multicentric disease has been reported.[6,14] Non-palpable disease has also been detected on screening mammogram.[4] The mass is usually firm or hard and can be mobile or fixed to the chest wall.[6,14] Nipple retraction and skin changes have also been reported, which are features that raise a suspicion of malignancy.[4,6,14] It can be slow or rapidly growing. Since it is not metastasising, lymphadenopathy is not a feature.

On mammogram, breast fibromatosis has a variable appearance ranging from normal (especially for small lesions), architectural distortion, or a circumscribed lesion, to a high-density irregular mass with spiculated margins. Calcifications are rare.[4-6,12,14] On ultrasound, features likewise vary, ranging from a circumscribed parallel mass to a non-parallel hypoechoic mass with obscured, irregular or spiculated borders. More common features include hypoechogenicity, irregular border and posterior acoustic shadowing.[4-6,14] Similar to its clinical presentation, these radiological features show a lot of overlap with breast cancer and commonly point towards malignancy after completion of triple assessment. Unique to our patient, mammogram and ultrasound played a very limited role in assessment of the lesion as the presence of free silicone largely obscured the index lesion, but these modalities clarified the nature of the previously unknown injected material.

MRI is reported to be useful when determining the local extent of the disease since chest wall invasion is

not uncommon. It is also superior to ultrasound and mammogram in the detection and evaluation of a mass in the absence of breast implants or injected materials. On MRI, breast fibromatosis has been reported to be T1-weighted hypo- or iso-intense and T2-weighted–hypointense, but is heterogeneously hyperintense on fat-saturated T2-weighted images.[4-6,14] It shows heterogeneous contrast enhancement and all three types of kinetic curves (types I, II and III) have been reported. The most common pattern is a progressive enhancement curve (type I) that may point away from the usual presumptive diagnosis of breast cancer while not excluding the possibility.[4,5] The MRI findings in our patient were consistent with the literature. We documented additionally the progression of the lesion on serial MRI, which was not reported previously. MRI was also useful in determination of the nature of injected material by silicone- and water-sensitive and suppressed sequences.

Since breast fibromatosis commonly presents as a malignancy mimicker, core biopsy is usually performed for histological diagnosis. These cancer-mimicking features of the lesion also prompted the repeated core biopsies in our patient. The histology findings are beyond the scope of discussion of this text.

The treatment of breast fibromatoses is evolving and remains controversial, but there had been discussion of surgery (most commonly described is wide local excision with clear margins), and systemic therapy with nonsteroidal anti-inflammatory drugs such as sulindac, hormone therapy with tamoxifen, and tyrosine kinase inhibitors have been used.[4-8,10,12,14] Radiotherapy is suggested to also play a role in management.[5-8,12] It should be kept in mind that local recurrence is not uncommon despite treatment, and follow-up is required.[4,5] In view of the complexity of diagnosis and management, these cases should be presented at multidisciplinary meetings to reach a conjoint decision.

In conclusion, radiologists should be aware of the presence of this malignancy-mimicking entity, and the limitations of mammogram and ultrasound in patients with a history of free silicone injection. MRI is the imaging modality of choice for evaluation of extent of involvement of breast fibromatosis, particularly to determine the presence and degree of chest wall invasion. Finally, the complex diagnosis, clinically and radiologically, warrants a multidisciplinary team discussion to facilitate optimal management of the patient.

REFERENCES

1. Sbaraglia M, Bellan E, Dei Tos AP. The 2020 WHO classification of soft tissue tumours: news and perspectives. Pathologica. 2020;113:70-84.
2. Hill E, Merrill A, Korourian S, Bryant-Smith G, Henry-Tillman R, Ochoa D. Silicone breast implant associated fibromatosis. J Surg Case Rep. 2018;2018:rjy249.
3. Balzer BL, Weiss SW. Do biomaterials cause implant-associated mesenchymal tumors of the breast? Analysis of 8 new cases and review of the literature. Hum Pathol. 2009;40:1564-70.
4. Lorenzen J, Cramer M, Buck N, Friedrichs K, Graubner K, Lühr CS, et al. Desmoid type fibromatosis of the breast: ten-year institutional results of imaging, histopathology, and surgery. Breast Care (Basel). 2021;16:77-84.
5. Guirguis MS, Adrada B, Santiago L, Candelaria R, Arribas E. Mimickers of breast malignancy: imaging findings, pathologic concordance and clinical management. Insights Imaging. 2021;12:53.
6. Alanis L, Roth R, Lerman N, Barroeta J, Germaine P. Radiologic images of an aggressive implant-associated fibromatosis of the breast and chest wall: case report and review of the literature. Radiol Case Rep. 2017;12:431-8.
7. Mátrai Z, Tóth L, Gulyás G, Szabó É, Szentirmay Z, Kásler M. A desmoid tumor associated with a ruptured silicone breast implant. Plast Reconstr Surg. 2011;127:1e-4e.
8. Morales RD, Mendoza AG, Luces C, Abreu EB, Romero G, Pérez G, et al. Aggressive breast fibromatosis following augmentation mastoplasty: a series of case reports. Ecancermedicalscience. 2018;12:833.
9. Silva S, Lage P, Cabral F, Alves R, Catarino A, Félix A, et al. Bilateral breast fibromatosis after silicone prosthetics in a patient with classic familial adenomatous polyposis: a case report. Oncol Lett. 2018;16:1449-54.
10. Silva Filho AF, Alves JC, Portugal EH, Fonseca RP, Almeida AC, Pereira NA, et al. Aggressive fibromatosis (desmoid tumor) associated with breast implant: literature review and presentation of three new cases. Revista Brasileira de Cirurgia Plástica. 2017;32:361-71.
11. Park JS, Lee SE, Choi JH. Desmoid-type fibromatosis associated with silicone breast implants. J Korean Soc Radiol. 2019;80:804-9.
12. Podesta C, Sukumar A, Morgan I, Vidya R. Breast implant–related fibromatosis: a rare but important adverse effect. Eur J Plast Surg. 2021;44:275-8.
13. Jewett ST, Mead JH. Extra-abdominal desmoid arising from a capsule around a silicone breast implant. Plast Reconstr Surg. 1979;63:577-9.
14. Ng WL, Teoh SY, See MH, Rahmat K, Jayalakshmi P, Ramli MT, et al. Desmoid type fibromatosis of the breast masquerading as breast carcinoma: value of dynamic magnetic resonance imaging and its correlation. Eur J Breast Health. 2021;17:197-9.

Hong Kong J Radiol. 2023;26:58-65 | https://doi.org/10.12809/hkjr2317476

PICTORIAL ESSAY

Common Artifacts in Magnetic Resonance Imaging: A Pictorial Essay

CH Ho[1], L Xiao[2], KY Kwok[1], S Yang[1], BWH Fung[1], KCH Yu[1], WH Chong[1], TW Yeung[1], A Li[1]

[1]Department of Radiology, Tuen Mun Hospital, Hong Kong
[2]Medical Physics Unit, Department of Oncology, Tuen Mun Hospital, Hong Kong

INTRODUCTION

Magnetic resonance (MR) imaging provides a non-invasive, radiation-free mode of imaging. New MR technologies including MR spectroscopy and functional imaging provide a novel range of diagnostic information. With its complexity, diversity and versatility, MR imaging is one of the most powerful diagnostic tools in a wide variety of clinical situations.

MR artifacts are common in MR imaging. They are defined as any signal or void in the images that does not have an anatomic basis, or that arises as a result of distortion, addition or deletion of information.[1] MR artifacts can be related to patient motion, tissue characteristics, imaging techniques or hardware issues, and may be confused with genuine pathology or reduce image quality. Some MR phenomena, which contribute to MR artifacts, are also exploited for various clinical applications, e.g., out-of-phase imaging and susceptibility-weighted imaging (SWI). This article provides an overview of common MR artifacts. It is important for radiologists and MR technologists to recognise them and be able to minimise their effects.

COMMON MAGNETIC RESONANCE ARTIFACTS

Truncation Artifact

Truncation artifact, also known as Gibbs, ringing, or spectral leakage artifact, refers to alternating bright and dark lines that occur near an abrupt high-contrast boundary. This artifact is caused by an inadequate number of encoding steps for high spatial frequency data,[2] which represent the edge between areas of high contrast. When there is under-sampling, the highest spatial frequency data are cut off, leading to the artifact. It can occur in both frequency- and phase-encoding directions, but is more common in the latter due to fewer phase-encoding steps in most examinations. It can occur in the brain due to sharp signal changes between the brain parenchyma and cerebrospinal fluid (Figure 1). It may also simulate a syrinx in the spinal cord or a meniscal tear in the knee. Common remedies include increasing the size of matrix (more encoding steps) and reducing the field of view (FOV).[2]

Cross-Excitation Artifact

Cross-excitation artifact is caused by imperfect non-

Correspondence: *Dr CH Ho, Department of Radiology, Tuen Mun Hospital, Hong Kong*
Email: hch1931@ha.org.hk

Submitted: 21 Sep 2021; Accepted: 15 Dec 2021.

Contributors: All authors designed the study. CHH and LX acquired and analysed the data. CHH drafted the manuscript. All authors critically revised the manuscript for important intellectual content. All authors had full access to the data, contributed to the study, approved the final version for publication, and take responsibility for its accuracy and integrity.

Conflicts of Interest: All authors have disclosed no conflicts of interest.

Funding/Support: This study received no specific grant from any funding agency in the public, commercial, or not-for-profit sectors.

Data Availability: All data generated or analysed during the present study are available from the corresponding author on reasonable request.

Ethics Approval: This study was approved by New Territories West Cluster Research Ethics Committee of Hospital Authority (Ref No.: NTWC/REC/21064). Informed patient consent was waived by the Committee as this retrospective study involves no additional patient participation and all patient data are anonymised.

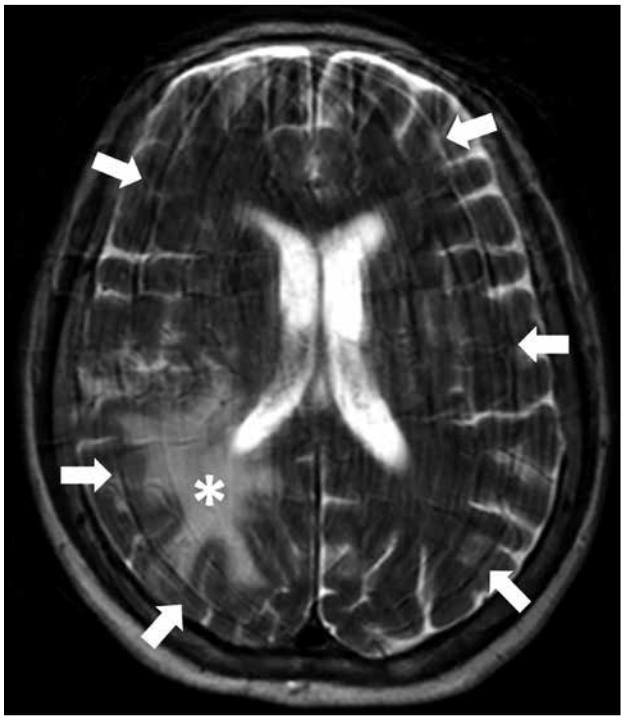

Figure 1. Axial T2-weighted image of the brain showing significant truncation artifact (white arrows) along the high-contrast brain-fluid interface, obscuring the normal anatomy. This patient has significant vasogenic oedema at the right frontal and parietal white matter (white asterisk) due to underlying brain metastasis.

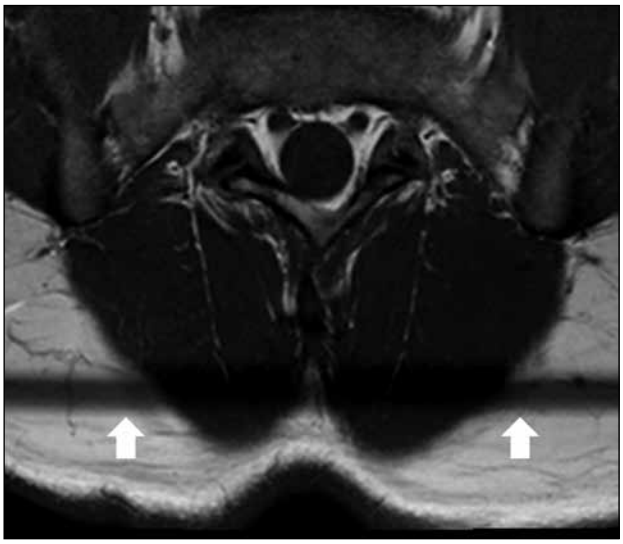

Figure 2. Axial T1-weighted image of the lumbar spine with multi-angle acquisition. Hypointense signal band (white arrows) is observed due to cross-excitation with saturation effect.

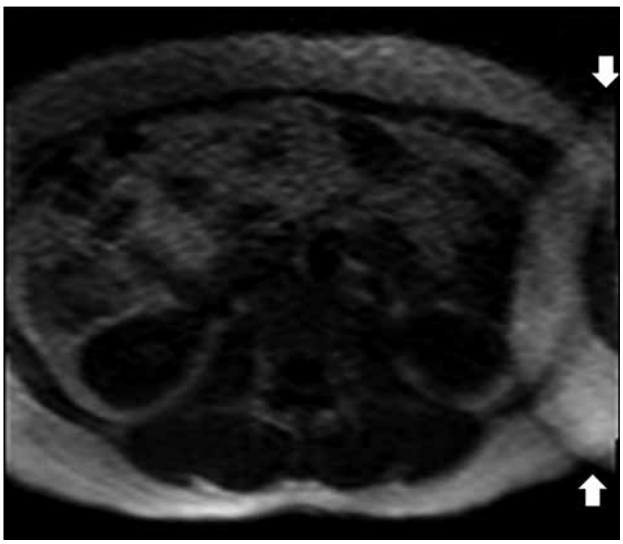

Figure 3. Axial localiser scan of the abdomen demonstrates aliasing artifact (white arrows). The body part outside the field of view is projected to the opposite side of the image and masks the relevant anatomical structure.

rectangular shape of radiofrequency (RF) excitation or multi-angle acquisition. As a result, there is some overlap between adjacent slices during sequential acquisition. Tissue within the overlapping region is excited repeatedly during acquisition, causing saturation effect and decreased signal intensity[3] (Figure 2). Common remedies include increasing slice gap and using interleaved slices for acquisition.

Aliasing

Aliasing occurs when the body part outside the FOV is projected inside and overlaps on the opposite side of the image[1,4] (Figures 3 and 4). It can mask the anatomical structures in the region of clinical interest. It can occur in both frequency- and phase-encoding directions but is generally more severe along the phase-encoding axis.

During image acquisition, structures outside the FOV are also excited and produce signals. If the frequencies of the signals outside the FOV exceed the Nyquist frequency (the highest frequency that can be unambiguously sampled), those signals will be falsely detected as lower frequencies and misregistered, leading to wraparound phenomenon.[4,5] For phase-encoding direction, similar ambiguity and misregistration can result due to its circular nature that repeats every 360°C.[1] In parallel acquisition techniques, aliasing artifacts have different appearances and the location of the artifacts depends on the acceleration factor. Common remedies include increasing FOV (at the expense of resolution), oversampling, reducing the acceleration factor, adding pre-saturation pulses for structures outside the FOV, using surface coils and switching phase- and frequency-encoding directions.[4]

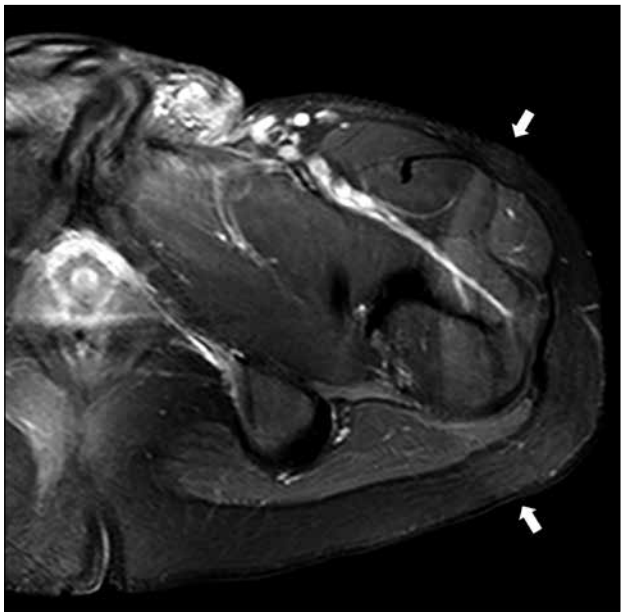

Figure 4. Axial T1-weighted post-contrast image of the left hip showing aliasing artifact at the lateral aspect of left hip, with a rim of signal hyperintensity overlapping the anatomy (white arrows).

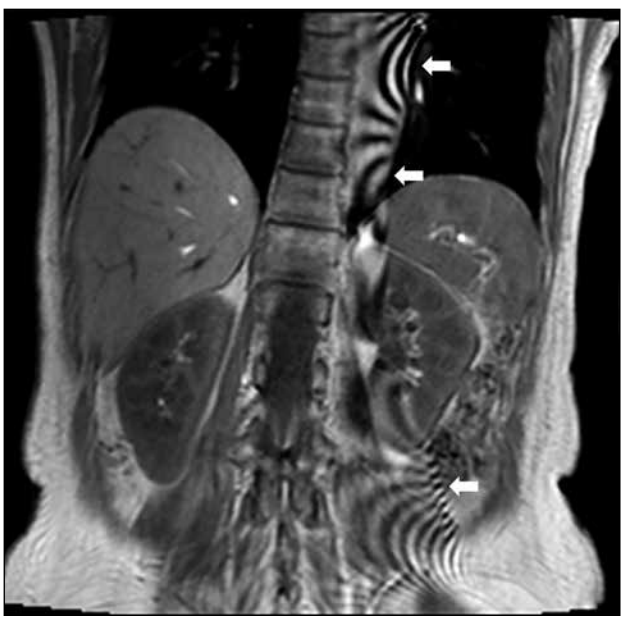

Figure 5. Coronal T1-weighted gradient echo image of the abdomen demonstrates the Moiré fringes or zebra artifacts (white arrows). This artifact is caused by a combination of aliasing and magnetic field inhomogeneity.

Moiré Artifact

The combination of aliasing artifact and magnetic field inhomogeneity can cause Moiré fringes or zebra artifacts.[1] Homogeneity of the magnetic field degrades towards the edges of the field, especially when the FOV is large, causing phase differences between the two edges. When aliasing occurs, the overlapping signals with mismatched phases cause interference patterns and produce Moiré artifact[1,5] (Figure 5). This is more commonly seen in gradient echo imaging with body coil. Common remedies are similar to those for aliasing artifact.

Zipper Artifact

Zipper artifact is most often caused by the interference of extrinsic RF signals to the MR scanner and is picked up by the receiver system. The appearance varies with the frequency and bandwidth of the source. Broadband source will affect the entire image, while narrow-frequency source will create discrete bright and dark broken lines perpendicular to the frequency-encoding direction[6] (Figure 6). The sources of the extrinsic RF include electronic devices (e.g., monitoring equipment), static electricity, opened door and a breach in the RF shield. Common remedies include removing the external RF sources, closing the door completely before scanning, and inspecting thoroughly the scanner room for any breach of RF shield.[1]

Geometric Distortion

Geometric distortion can arise from different sources and can be hardware-related or tissue-related. The main

Figure 6. Sagittal balanced steady-state free precession image of the thorax showing zipper artifact (white arrow) perpendicular to frequency-encoding direction from a narrow-frequency source.

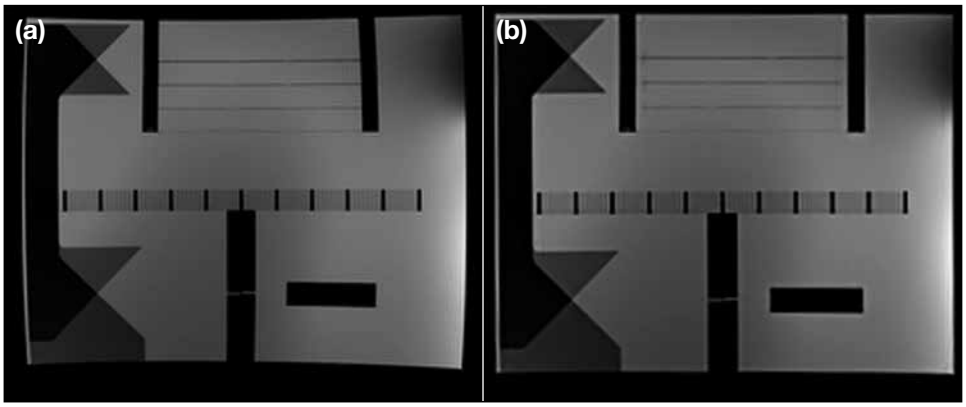

Figure 7. (a) Phantom image showing geometric distortion within the slice plane indicated by the curved outline of the phantom image. (b) After the manufacturer's correction algorithm was applied, the acquisition was repeated and showed significant improvement of the geometric distortion.

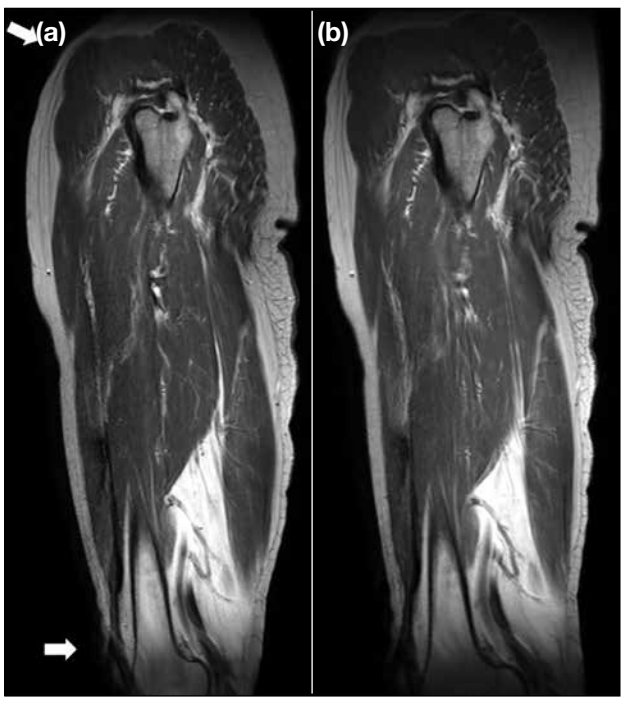

Figure 8. (a) Axial T1-weighted image of the right thigh demonstrates geometric distortion due to gradient field non-linearity (white arrows), more significant at the periphery of the image. (b) After application of the manufacturer's correction algorithm, the acquisition was repeated and the geometric distortion was significantly minimised.

hardware-related source is gradient field non-linearity in contemporary MR systems, in which the gradient strength and slew rate (rate of gradient rise) are much higher[7] (Figures 7 and 8). Distortions are usually minimal at the isocentre and more significant at the periphery. Geometric distortion becomes a clinical concern when a high level of spatial precision is required, e.g., during MR-guided interventions or radiotherapy planning. Different correction algorithms are available from major manufacturers of MR systems to minimise hardware-related geometric distortion.

Susceptibility Artifact

Magnetic susceptibility refers to the tendency of a structure to contribute a magnetic field on its own under an external magnetic field.[4] This will create local magnetic field inhomogeneities, altering the frequency and phase of local spins and also leading to stronger dephasing of the spins.[8] Severe artifacts can occur near ferromagnetic objects, e.g., metallic implants and distort normal anatomy (Figure 9). Such effect can also be found at the boundary of tissues with different susceptibilities, for example a tissue-air interface. Increasing field strength worsens the magnitude of this effect. Common remedies include using spin echo instead of gradient echo sequences, orienting the phase-encoding gradient along the same axis as the susceptibility gradient, reducing echo time, reducing slice thickness, increasing the acquisition matrix, improving the local field homogeneity, and increasing receiver bandwidth.[8]

The differences in tissue susceptibility can be exploited in SWI to help diagnose haemorrhage and calcifications. Both appear hypointense on SWI images. The filtered phase images of SWI sequences can help further differentiate paramagnetic (haemorrhage) and diamagnetic (calcification) products since the latter have different phases.[9]

Chemical Shift Artifact

Chemical shift artifact refers to signal alterations that result from inherent differences in the Larmor frequencies of protons when they are in a different chemical environment, most frequently observed between water and fat.[10] It occurs in both spin echo and gradient echo

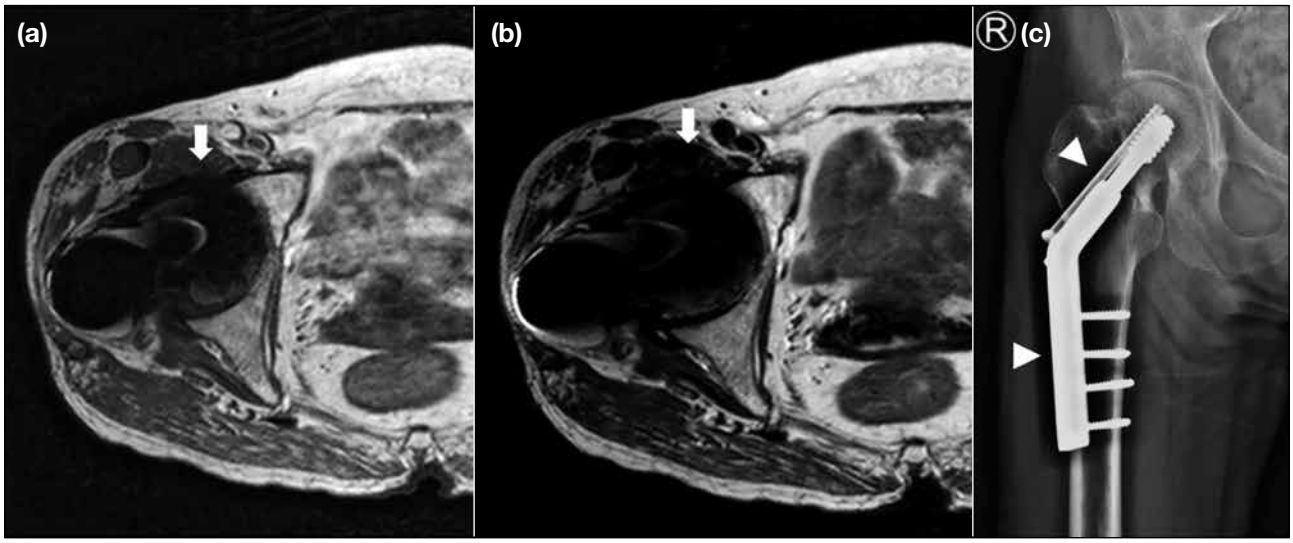

Figure 9. (a and b) Axial T1-weighted and T2-weighted fast spin echo images of the right hip at 1.5T magnetic resonance imaging showing significant susceptibility artifact (white arrows) due to the presence of metallic screw at the proximal right femur. (c) Radiograph of right hip showing the presence of metallic screw at the proximal right femur (white arrowheads).

imaging, and along the frequency-encoding direction. It creates signal void as well as superimposition due to the shifting, and usually manifests as a bright line on one side and a dark line on the opposite side of the fat-water interfaces (Figure 10).

The difference is caused by different chemical structures of fat and water. The hydrogen atoms in fat are contained in a much larger molecule compared with those in water. As a result, there is a much stronger shielding effect from the molecule's electron shell of fat on the static magnetic field, and the Larmor frequency of the hydrogen atoms in fat is lowered.[10] The difference in Larmor frequency is usually expressed as a difference of 3.5 parts per million relative to the Larmor frequency of water.[11] It is directly proportional to the main field strength. Common remedies to chemical shift artifact include using a higher receiver bandwidth, decreasing FOV and using a fat suppression technique.

Figure 10. Coronal T1-weighted image of the upper abdomen demonstrates chemical shift artifact of the first kind around the kidneys. Bright rims are seen around the superior pole of the kidneys (white arrows) and dark rim is seen at the opposite sides (black arrows).

Out-of-Phase Signal Cancellation Artifact

Out-of-phase signal cancellation, or type 2 chemical shift artifact, refers to intravoxel signal cancellation due to phase difference between the spinning protons in fat and water. Since the precession of hydrogen atoms in water and in fat are at different frequencies, they have different phase directions at different time points and therefore at certain time points, they can be in-phase or 180°C out-of-phase. At 1.5T, out-of-phase occurs at 2.2 ms and in-phase occurs at 4.4 ms. By adjusting the echo time, both in-phase and out-of-phase images can be produced.

At out-of-phase imaging, the signals from protons in water and fat within the same pixel are cancelled out, leading to the appearance of a dark band at the fat-water interface. Unlike chemical shift artifact of the first kind that can be seen in both spin echo and gradient echo imaging, this artifact occurs only in gradient echo sequences since the 180°C rephrasing RF pulse in spin echo imaging will compensate this phase shift.[11] Moreover, type 2 chemical shift artifacts can be seen in all pixels along a fat-water interface, unlike chemical

shift artifact of the first kind that is limited to the frequency-encoding direction.

The out-of-phase signal cancellation effect is valuable for diagnostic purposes. A drop in signal intensity at out-of-phase images indicates the presence of fat within the voxel. This is helpful for diagnosing fat-containing lesions e.g., adrenal adenoma or renal angiomyolipoma (Figure 11).

Another added benefit of this dual gradient echo imaging is to assess signal loss related to magnetic susceptibility effect. Magnetic susceptibility causes signal intensity loss with time, therefore more signal loss occurs in in-phase images with longer echo time than out-of-phase images. This is helpful when diagnosing iron deposition, haemorrhage and siderotic hepatic nodules, etc[11] (Figure 12).

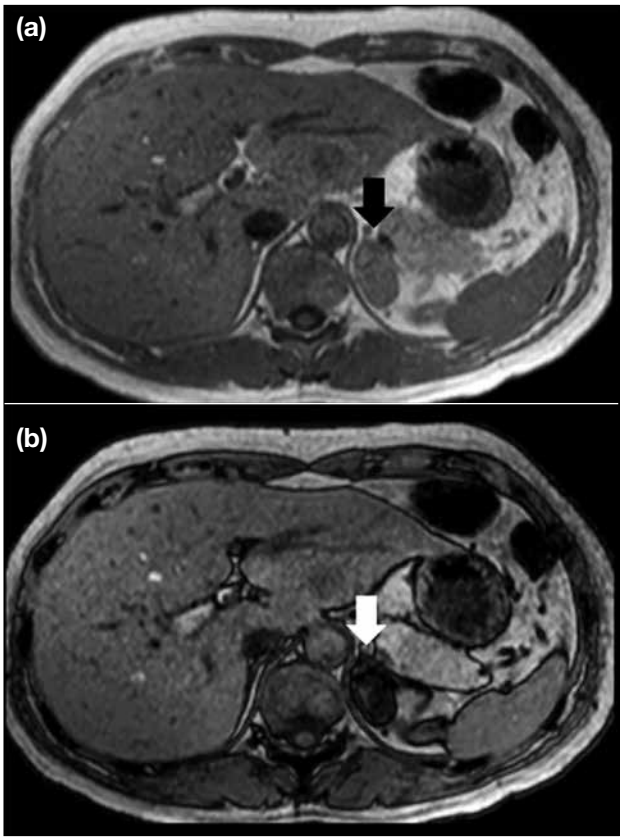

Figure 11. Case of left adrenal adenoma. (a) Axial T1-weighted in-phase gradient echo image of the abdomen showing a left adrenal mass (black arrow). (b) Axial T1-weighted opposed-phase gradient echo image of the abdomen showing signal drop at the left adrenal mass (white arrow), signifying the presence of intravoxel fat which is a feature of adrenal adenoma.

Motion Artifact

Motion artifact is the principal source of artifact in MR imaging, primarily due to the prolonged time required for most MR imaging sequences. It can be briefly classified as periodic (e.g., pulsation of blood vessels) or random (e.g., bowel peristalsis) [Figures 13 and 14]. Random motion generally creates a blurring of images while periodic motion produces ghost images.[1] Motion artifact is usually most apparent in the phase-encoding direction due to the much slower sampling time.

Recent advances have improved the situation in some cases, for example breakthrough in parallel imaging enables faster imaging that decreases the chance of involuntary patient motion. Nonetheless improvement in resolution and signal-to-noise ratio will also increase the sensitivity to motion.[12]

There are different remedies to reduce motion artifacts, including motion reduction (e.g., physical immobilisation or sedation), rapid imaging sequences (e.g., parallel imaging, triggering and gating for periodic movements, such as respiratory or cardiac movements), and motion artifact reduction sequences (e.g., the PROPELLER [periodically rotated overlapping parallel lines with enhanced reconstruction] technique).[12]

Coil-Related Artifact

Signal intensity artifact can result from improper coil or patient positioning and manifests as areas of signal intensity loss (Figure 15). This error is easily corrected and should be recognised before the more complicated investigations. Other signal intensity artifacts related to coils include intensity gradient from local coils, local intensity shift artifact from RF-induced eddy currents, protocol errors, failure of decoupling mechanisms, and improper coil tuning[13] (Figure 16).

Dielectric Effect

Dielectric effect manifests as abnormal bright and dark areas due to the interaction of matter with the electric field. This artifact is mainly found in abdominal and pelvic imaging at 3T or higher field strength. The wavelength of RF pulses decreases as the main magnetic field strength increases. The wavelength at 1.5T is approximately 52 cm in soft tissue, larger than the size of most adults. Nonetheless at 3T, the wavelength becomes approximately 26 cm in soft tissue, similar to the body torso size of adults. This results in standing wave effects that lead to areas of constructive and destructive interference and prevents excitation of the spins at the centre of imaged volume. Another reason for this

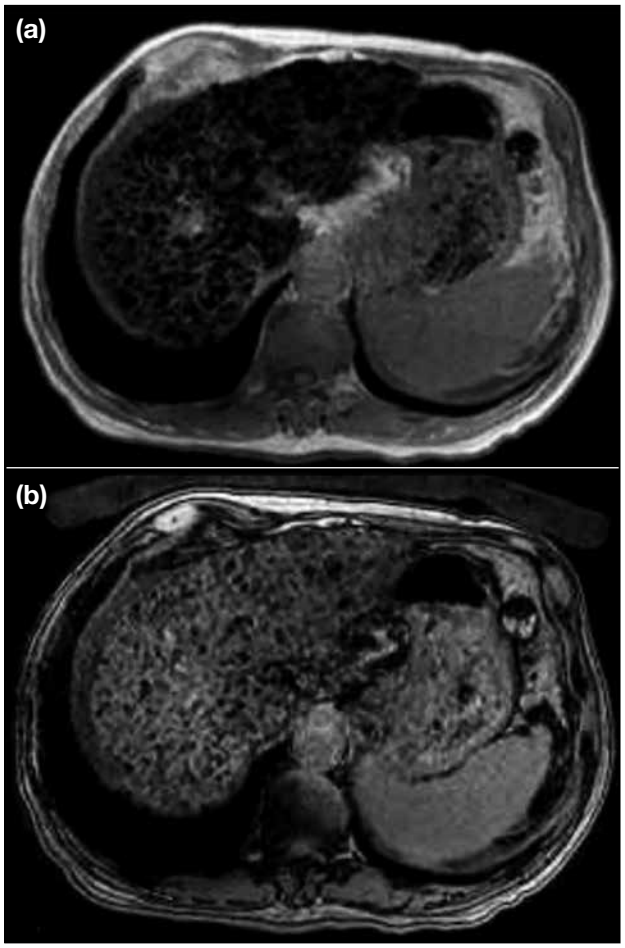

Figure 12. Case of iron overload due to thalassaemia. Axial T1-weighted gradient echo images of the abdomen with in-phase and opposed-phase show signal drop of the liver parenchyma in in-phase image. It is due to susceptibility artifact from iron overload due to thalassaemia. This patient also has liver cirrhosis.

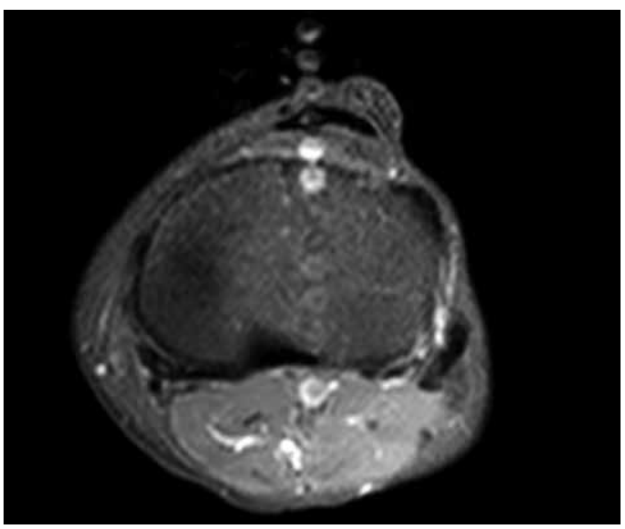

Figure 13. Axial T1-weighted post-contrast image of the knee with fat saturation showing ghosting artifact of the popliteal artery along the phase-encoding direction due to pulsation.

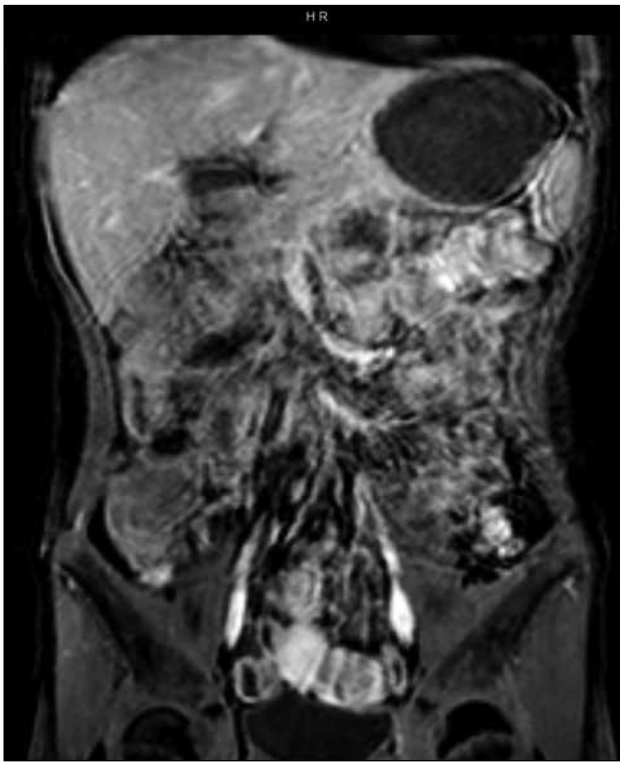

Figure 14. Coronal T1-weighted post-contrast image of the abdomen with fat saturation showing blurring of the image due to the combination of breathing motion, bowel peristalsis and patient's movement.

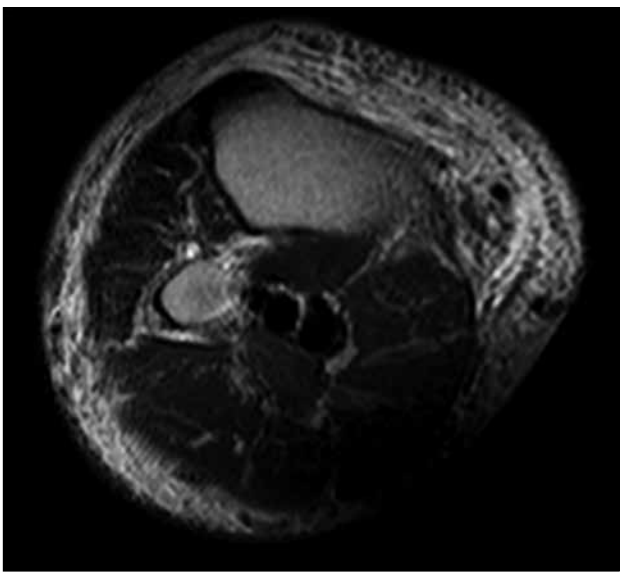

Figure 15. Axial T1-weighted image of the leg showing focal area of signal loss at the posterior compartment of the leg. This is due to suboptimal positioning of the coil.

Figure 16. (a) Sagittal T1-weighted fat-saturated post-contrast image of the lumbar spine. Severe blurring of the image is noted due to coil connector malfunction. (b) After changing the connector, the artifact is no longer observed. This patient has an infective spondylodiscitis at the lumbar spine.

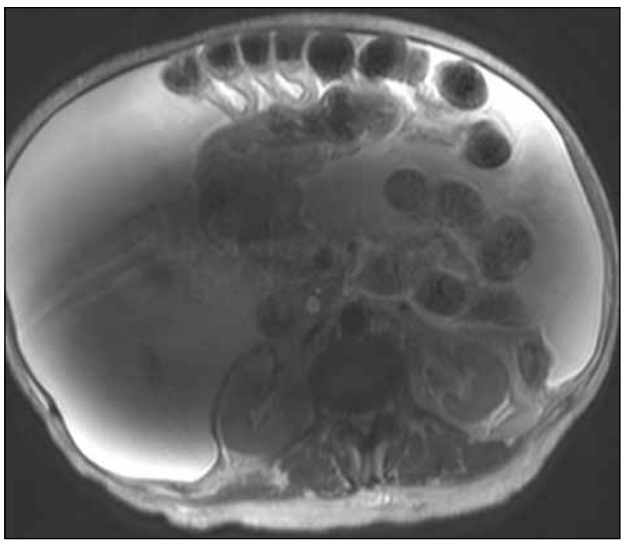

Figure 17. Axial T2-weighted image of the abdomen showing the dielectric effect with signal loss at the centre of the abdomen. Note that this patient has significant ascites that contributes to the dielectric effect.

artifact is the generation of eddy current from RF pulses, which is more pronounced at 3T, causing magnetic field inhomogeneity. The combined effects of standing wave and eddy current cause focal areas of abnormal signals[14] (Figure 17).

This artifact is accentuated when the imaged structures are large, e.g., patients with ascites, obesity or pregnancy. Dielectric effects are variable and difficult to predict, since the shape of the body surface and the conductivity of the tissue determine the conditions.[15] Common remedies include placing a dielectric pad and using a 1.5T scanner instead.

CONCLUSION

MR artifacts are common in clinical MR imaging. This article gives an overview of common MR artifacts encountered in clinical practice. It is important for radiologists and MR technologists to recognise the artifacts and know how to minimise their effects. On the contrary, some of these MR phenomena can have clinical applications and help in making diagnosis.

REFERENCES

1. Stadler A, Schima W, Ba-Ssalamah A, Kettenbach J, Eisenhuber E. Artifacts in body MR imaging: their appearance and how to eliminate them. Eur Radiol. 2007;17:1242-55.
2. Gallagher TA, Nemeth AJ, Hacein-Bey L. An introduction to the Fourier transform: relationship to MRI. AJR Am J Roentgenol. 2008;190:1396-405.
3. Schwaighofer BW, Yu KK, Mattrey RF. Diagnostic significance of interslice gap and imaging volume in body MR imaging. AJR Am J Roentgenol. 1989;153:629-32.
4. Morelli JN, Runge VM, Ai F, Attenberger U, Vu L, Schmeets SH, et al. An image-based approach to understanding the physics of MR artifacts. Radiographics. 2011;31:849-66.
5. Zhuo J, Gullapalli RP. AAPM/RSNA physics tutorial for residents: MR artifacts, safety, and quality control. Radiographics. 2006;26:275-97.
6. Budrys T, Veikutis V, Lukosevicius S, Gleizniene R, Monastyreckiene E, Kulakiene I. Artifacts in magnetic resonance imaging: how it can really affect diagnostic image quality and confuse clinical diagnosis? J Vibroengineering. 2018;20:1202-13.
7. Wang D, Strugnell W, Cowin G, Doddrell DM, Slaughter R. Geometric distortion in clinical MRI systems part I: evaluation using a 3D phantom. Magn Reson Imaging. 2004;22:1211-21.
8. Stradiotti P, Curti A, Castellazzi G, Zerbi A. Metal-related artifacts in instrumented spine. Techniques for reducing artifacts in CT and MRI: state of the art. Eur Spine J. 2009;18 Suppl 1:102-8.
9. Haacke EM, Mittal S, Wu Z, Neelavalli J, Cheng YC. Susceptibility-weighted imaging: technical aspects and clinical applications, part 1. AJNR Am J Neuroradiol. 2009;30:19-30.
10. Hood MN, Ho VB, Smirniotopoulos JG, Szumowski J. Chemical shift: the artifact and clinical tool revisited. Radiographics. 1999;19:357-71.
11. Shetty AS, Sipe AL, Zulfiqar M, Tsai R, Raptis DA, Raptis CA, et al. In-phase and opposed-phase imaging: applications of chemical shift and magnetic susceptibility in the chest and abdomen. Radiographics. 2019;39:115-35.
12. Zaitsev M, Maclaren J, Herbst M. Motion artifacts in MRI: a complex problem with many partial solutions. J Magn Reson Imaging. 2015;42:887-901.
13. Jones RW, Witte RJ. Signal intensity artifacts in clinical MR imaging. Radiographics. 2000;20:893-901.
14. Huang SY, Seethamraju RT, Patel P, Hahn PF, Kirsch JE, Guimaraes AR. Body MR imaging: artifacts, k-space, and solutions. Radiographics. 2015;35:1439-60.
15. Schick F. Whole-body MRI at high field: technical limits and clinical potential. Eur Radiol. 2005;15:946-59.

Hong Kong J Radiol. 2023;26:66-71 | https://doi.org/10.12809/hkjr2317539

PICTORIAL ESSAY

Artificial Ascites and Hydrodissection in Percutaneous Thermal Ablation Cases at a Tertiary Institution: A Pictorial Essay

RK Mak, JB Chiang, HS Fung, WL Poon

Department of Radiology and Imaging, Queen Elizabeth Hospital, Hong Kong

INTRODUCTION

Percutaneous thermal ablation is gaining popularity as a curative form of treatment for many cancers. With increasing demand for such treatment, there are likewise increasing challenges when handling tumours close to vital structures and unintended thermal injury now needs to be considered. This may arise due to an inadequate margin as the operator attempts to avoid a critical structure. Artificial ascites and hydrodissection are effective and economical techniques that can push away critical structures, allowing a safe and complete ablation. This pictorial review demonstrates the various ways in which artificial ascites and hydrodissection can be used in percutaneous ablation, and discusses the different methods and mediums used at our institution as well as the challenges and complications encountered over a 3-year review period.

Cases with hydrodissection performed under ultrasound (US), computed tomography (CT), and magnetic resonance (MR) guidance from January 2018 to September 2021 were retrieved from the Radiology Information System under Hospital Authority of Hong Kong using keywords 'hydrodissection' and 'artificial ascites'. Images from illustrative cases have been selected to showcase different areas in the body where hydrodissection was performed.

Artificial ascites and/or hydrodissection was performed in 128 patients at our centre, Queen Elizabeth Hospital, with the majority involving hepatocellular carcinomas (85.9%, n = 110) or renal cancers (10.2%, n = 13). Miscellaneous target lesions included adrenal nodules, iliac lymph nodes, pelvic collections, and breast nodules. Examples of hydrodissection include the gallbladder fossa, hepatic bare area, duodenum, and abdominal large vessels. Hydrodissection of the renal pelvis and porta hepatis have also been successfully performed.

All our percutaneous thermal ablation patients are referred to us by the surgical department. Patients with liver lesions first undergo a targeted US to ascertain whether the index lesion can be well visualised on US. The targeted US, as well as correlation with previous cross-sectional imaging, also identifies nearby non-target structures and determines whether artificial ascites

Correspondence: *Dr RK Mak, Department of Radiology and Imaging, Queen Elizabeth Hospital, Hong Kong*
Email: mrk575@ha.org.hk

Submitted: 19 Feb 2022; Accepted: 7 Jul 2022.

Contributors: All authors designed the study. RKM acquired the data. RKM and JBC analysed the data. RKM drafted the manuscript. All authors critically revised the manuscript for important intellectual content. All authors had full access to the data, contributed to the study, approved the final version for publication, and take responsibility for its accuracy and integrity.

Conflicts of Interest: All authors have disclosed no conflicts of interest.

Funding/Support: This study received no specific grant from any funding agency in the public, commercial, or not-for-profit sectors.

Data Availability: All data generated or analysed during the present study are available from the corresponding author on reasonable request.

Ethics Approval: This study was approved by the Research Ethics Committee (Kowloon Central/Kowloon East) of the Hospital Authority (Ref No.: KC/KE-21-0228/ER-2). A waiver for written informed consent of patients was granted by the Committee as this manuscript is for pictorial review only and does not involve patient's treatment/procedure.

or hydrodissection is needed. If the index lesion and the hydrodissection pathway are suboptimally seen on US, a CT-guided approach will be chosen.

An MR-guided approach for liver lesions, which is rare, is reserved only for cases in which the lesion is both US and CT occult. On the contrary, all renal tumours are referred for MR-guided cryoablation. This is due to departmental preference. Patients with renal tumours are seen by our interventionists at the interventional radiology clinic, where cross-sectional imaging of patients is reviewed and the procedural details and complications were discussed with the patient. Since most of our MR-guided renal tumour ablations are performed under local anaesthesia and/or conscious sedation, one of the important issues debated during the interventional radiology clinic session is the ability of the patient to lie prone for an extended period of time as this is pivotal to these procedures.

TECHNIQUES AND PROCEDURES

Ultrasound Guidance

Ultrasound-guided (USG) artificial ascites and hydrodissection remain the most common technique, especially for liver lesions, making up to 87.5% (n = 112) of reviewed cases. For artificial ascites, two methods are adopted at our institution. In the first,[1,2] the liver is directly punctured superficially with a 16-gauge angiocatheter needle (Becton Dickinson Infusion Therapy Systems Inc, Mexico) under US guidance. The needle is removed and the patient is instructed to breath in and out making use of the relative movement between the peritoneum and liver to allow the plastic sheath to fall into the peritoneal space. Concomitant gentle advancement of a 0.035-inch guidewire (Terumo Medical Corporation, Japan) is continued until smooth guidewire advancement is felt. CT or fluoroscopy may be used to confirm the intraperitoneal location of the guidewire prior to exchange for a 6-French Neo-hydro catheter (Bioteque Corporation, Taiwan) for fluid infusion. Another method involves a 14- to 18-gauge Portex Tuohy epidural needle (Smiths Medical, Czech Republic) rather than an angiocatheter. This method is not well described in the literature but has been proven effective and less invasive, and is popular among our departmental interventionists. This method utilises the epidural needle's upward-curving tip to displace the liver away and allow insertion into the peritoneal cavity while avoiding puncture of the liver capsule.[3]

In hydrodissection, the target area is punctured under US guidance, usually with a 21-gauge Chiba needle (Cook Medical, Bloomington [IN], U.S.) or a 20-to-22-gauge spinal needle (Becton, Dickinson and Company, U.S.), depending on operator preference. Once the needle is perched at the intended position, 5% dextrose (D5) solution is carefully injected under USG visualisation until the desired effect is achieved.

Computed Tomography Guidance

CT-guided hydrodissection is usually performed for CT-guided percutaneous thermal ablations. In these cases, an angiocatheter or Chiba needle is inserted under CT guidance to the desired region and fluid is injected directly to the expected site. During our review period, 4.7% (n = 6) of hydrodissection procedures were performed under CT guidance, mainly for renal, adrenal and ischial bone lesion biopsies or ablation. For CT-guided ablation cases that require artificial ascites, the ascites is usually created under US guidance using the technique described in the previous section; in these cases, CT serves as an adjunct in confirming guidewire and drain catheter positioning.

Magnetic Resonance Imaging Guidance

MR-guided hydrodissection is performed when the thermal ablation is subsequently performed under MR guidance. Artificial ascites is rarely induced since most of our MR-guided ablation cases involve renal tumours. During our review period, 7.8% (n = 10) of cases received MR-guided hydrodissection.

Our department uses a designated 1.5T MR imaging machine (Siemens) for MR-guided procedures with a DORADOnova laser marking system (LAP, Germany). The procedure begins with patients undergoing a MR scan for planning. T2-weighted BLADE sequence (TR/TE 3000/116 ms, field of view 256 × 256, slice thickness 6 mm) is usually performed since most lesions are visible on this sequence and motion artefacts are reduced. The lesion is identified, and skin entry sites and pathways for hydrodissection and cryoprobe insertion are determined. Their respective coordinates and slice numbers are noted, and the skin entry sites are marked and labelled accordingly on the patient with the aid of laser marking projections. Then, a MR-compatible spinal needle (Innovative Tomography Products GmbH, Germany) is inserted to the desired area under the guidance of MR BEAT-IRTTT sequence (Siemens, Germany; TE/TR 2.2/5.35 ms, flip angle 50°, field of view 400 mm × 400 mm, reconstructed in-plane resolution 1.8 mm × 1.8 mm, slice thickness 4 mm, acquisition time

per slice 1000 ms). After needle insertion, the patient is scanned again (using T2-weighted BLADE sequence) to confirm needle position. The needle is re-adjusted as needed and the patient is re-scanned until the needle tip is at the desired location. D5 solution is then injected carefully. The patient is re-scanned to ensure accurate and adequate hydrodissection.

Cryoablation accounts for more than 90% of our MR-guided ablation cases, with <1% being MR-guided microwave ablation. The choice of ablation method is largely by operator preference, but also rests on the fact that the ice-ball ablation zone in cryoablation is well depicted on MR, which ensures good coverage of the tumour. In contrast, microwave ablation zones are not as clear as on MR.

Anatomical Locations Requiring Hydrodissection

Gallbladder Fossa

Liver lesions situated in segment 5 of the liver often require hydrodissection to dissect away the gallbladder and prevent injury and cholecystitis or rupture. This is done by inserting a Chiba needle under US guidance between the gallbladder and the target lesion (Figure 1). Fluid is then injected into the gallbladder fossa under US visualisation to cushion the gallbladder from thermal injury.[4]

Duodenum

Often, lesions located at the caudate lobe, right inferior segment or left medial segment of the liver may abut the proximal duodenal loop. The duodenum can be dissected away in a similar fashion to the gallbladder (Figure 2).

Colon

Right inferior segment liver lesions and renal lesions are often adjacent to large bowel loops. Hydrodissection can be performed by inserting an angiocatheter at the pericolic space and injecting fluid under US, CT or MR guidance (Figure 3).

Through or Across Stomach

Lesions in deeper parts of the liver are often difficult to

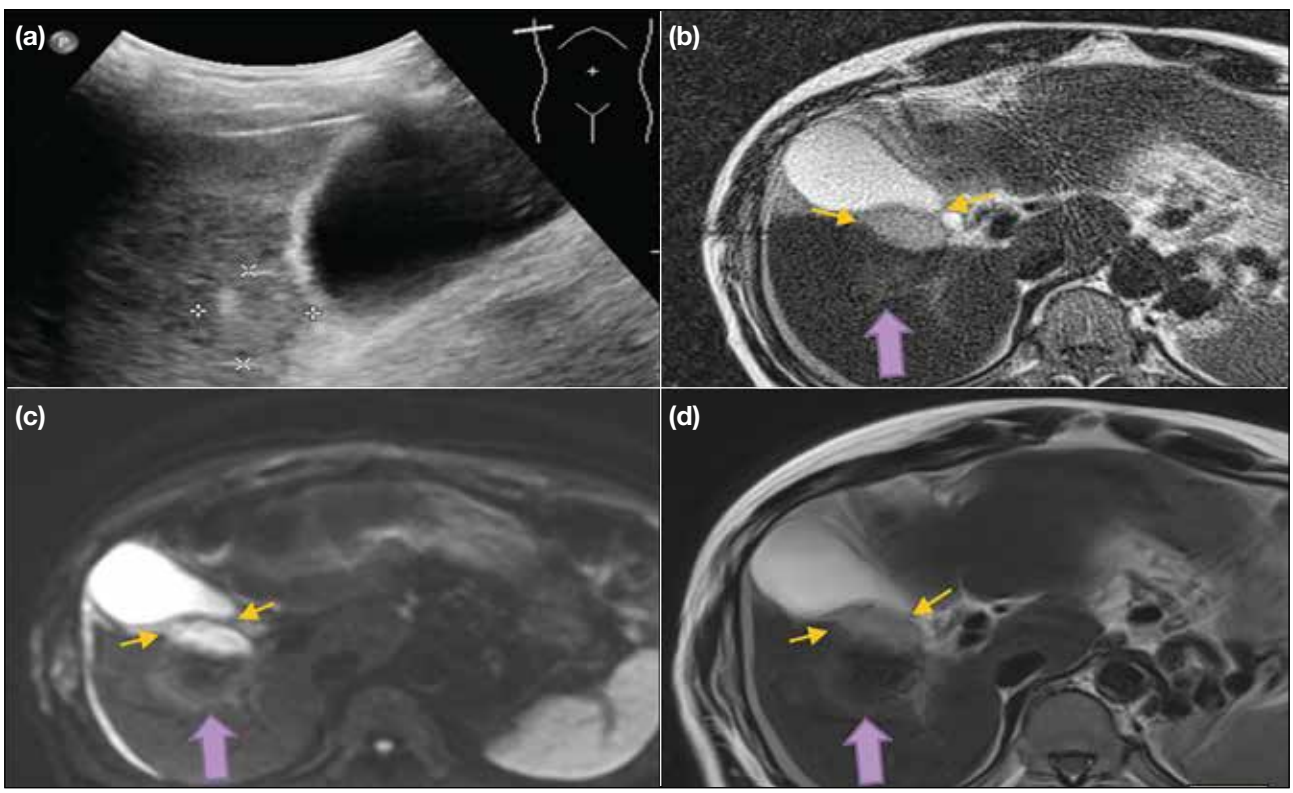

Figure 1. (a) The index lesion is only vaguely seen adjacent to the gallbladder on ultrasound (US). The operator elected to perform magnetic resonance–guided ablation. Under US guidance, the targeted pericholecystic area is punctured with a 16-gauge angiocatheter needle. (b-d) 30-mL 5% dextrose solution is instilled. T2-weighted BLADE, diffusion-weighted and T1-weighted images showing a water cushion (arrows) dissecting the gallbladder away from the target lesion (thick arrows).

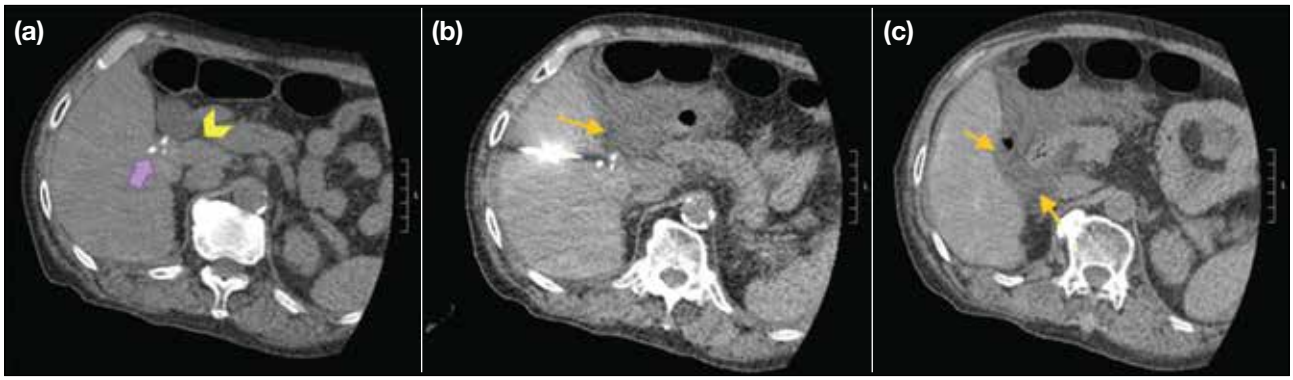

Figure 2. (a) Faint lipiodol uptake in segment 5 of the liver reveals the target lesion (thick arrow), abutting the proximal duodenum (arrowhead). (b) The ablation needle is partially seen (arrow). (c) Hydrodissection is successfully performed, pushing the loop of small bowel away from the target lesion (arrows).

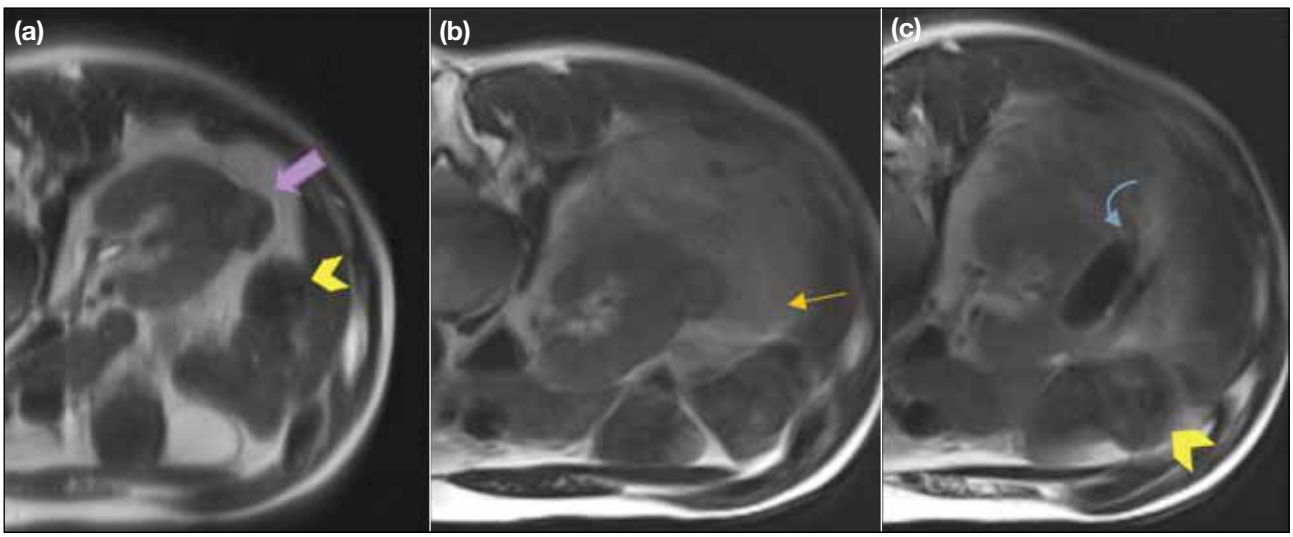

Figure 3. (a) Target lesion is seen in the right kidney (thick arrow), close to a large bowel loop (arrowhead). A 16-gauge angiocatheter is inserted into the right pararenal space and 70-mL 5% dextrose solution is injected. (b and c) Post-hydrodissection images showing fluid (arrow) successfully displacing the large bowel (arrowhead) away from the target lesion. The ice ball (curved arrow) of the cryoprobe is partially seen, successfully ablating the target lesion with no non-target ablation.

access as they are surrounded by various major organs, for example the stomach and the pancreas. In two (1.6%) of our cases during the review period, transgastric hydrodissection was performed for ablation of liver lesions in segment 3, aided by both US and CT. US-guided transgastric insertion of a 21-gauge Chiba needle into the retroperitoneal space is performed and 60- to 70-mL D5 solution is injected (Figure 4). The needle position and hydrodissection effect is confirmed with CT.

Hepatic Bare Area

Lesions can occur in the posterior liver dome and ablating these lesions may mean injuring the diaphragm and the pleura. In these cases, hydrodissection of the hepatic bare area is helpful.[5,6] One case of hydrodissection of hepatic bare area was performed during our study period. The hepatocellular carcinoma appeared as a sizable lipiodol-stained mass in the right liver dome, abutting the right hemidiaphragm. Under US guidance, the hepatic bare area was punctured with a 21-gauge Chiba needle. D5 solution was injected under USG visualisation to directly observe the desired hydrodissection effect. In this case, the hydrodissection effect was minimal despite instillation of 50-mL D5 solution. Interval CT scanning showed that the needle tip was in the correct position but that most of the fluid had flown to the peritoneal cavity. In the end,

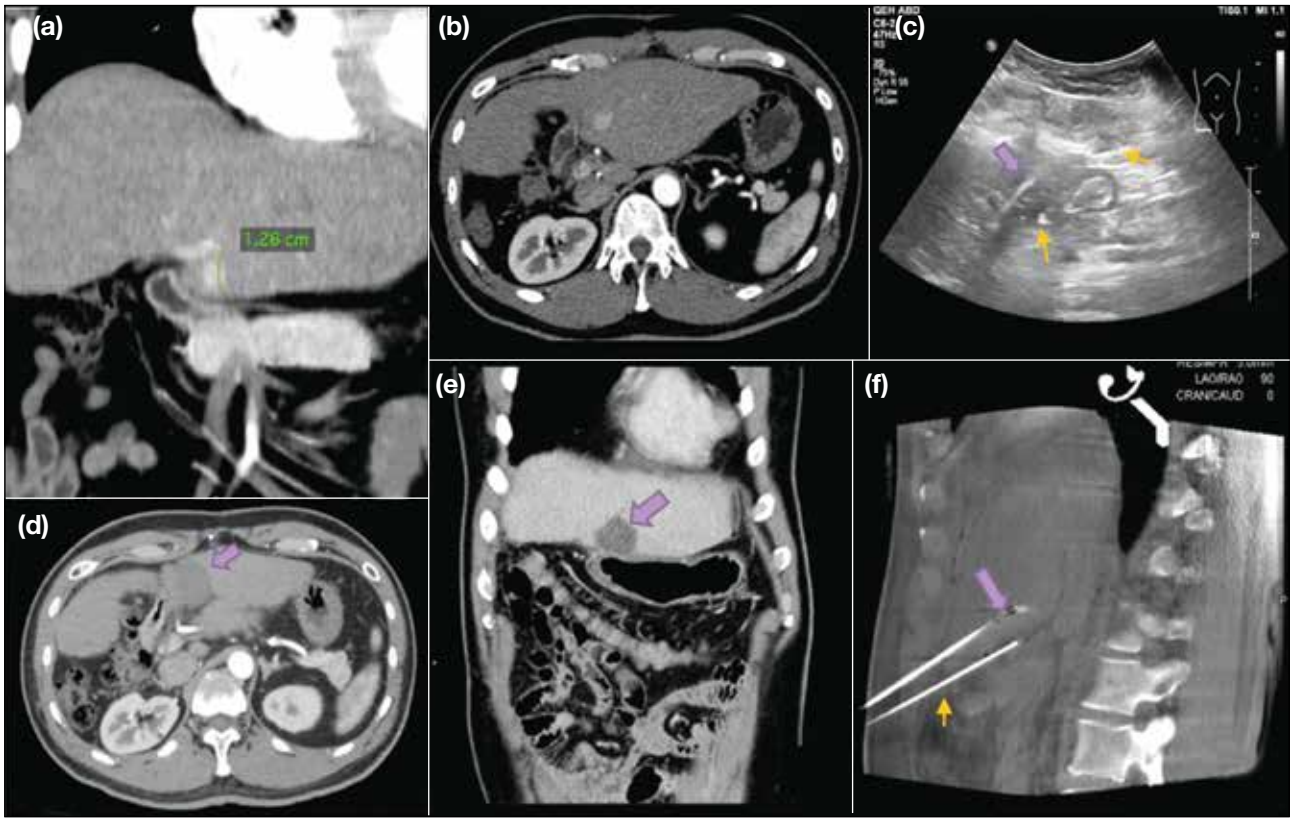

Figure 4. (a and b) Pre-ablation contrast coronal and axial computed tomography (CT) images of the liver showing the segment 3 hepatocellular carcinoma abutting the stomach. (c) Ultrasound image with ablation needle (thick arrow) within the liver lesion, and transgastric insertion of Chiba needle (arrows) into the retroperitoneal space for hydrodissection. (d and e) Post-ablation images 1 month later showing close proximity of the ablation zone (thick arrows) to the stomach and pancreas. (f) DynaCT during the ablation episode showing effective hydrodissection by the inferiorly located Chiba needle (arrow), dissecting away the stomach and pancreas, and successful puncture of target lesion by the microwave antennae (thick arrow).

200-mL D5 solution was injected with a thin layer of fluid retained at the hepatic bare area (Figure 5). The liver dome tumour was successfully ablated. Post-ablation CT showed a small ipsilateral hydropneumothorax that may have been caused by inadvertent Chiba puncture or from ablation-related minor diaphragmatic injury, and for which a 7-French Neo-hydro drain catheter (Bioteque Corporation, Taiwan) was inserted.

Artificial Ascites and Hydrodissection Medium

D5 solution was used as a medium in most of our cases for artificial ascites or hydrodissection. This was due to the high prevalence of radiofrequency ablation cases at our centre that comprised 49.2% (n = 63) of all cases during the review period. In these cases, D5 solution was chosen for its reduced electrical conductivity compared with normal saline. In non-radiofrequency ablation cases, both D5 and normal saline solutions have been used —

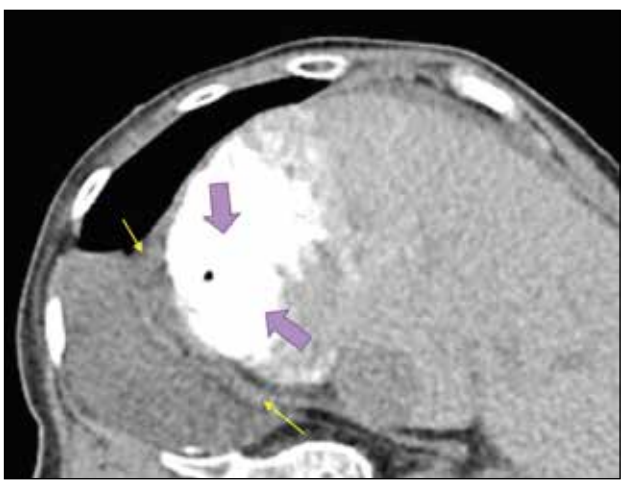

Figure 5. The index tumour in the posterior right liver dome showing avid lipiodol staining (thick arrows). The hepatic bare area is punctured with a 21-gauge Chiba needle under ultrasound guidance and 200-mL 5% dextrose solution was instilled. Only a thin layer of fluid is retained in the hepatic bare area (thin arrows). Small hydropneumothorax is seen after ablation.

these choices are operator dependent or by operator preference. In four cases (3.1%), diluted contrast was used for hydrodissection. Diluted contrast has the added advantage of providing stark contrast to adjacent intra-abdominal organs in unenhanced CT-guided procedures.

Complications

During the review period, there were 12 cases (9.4%) of failed hydrodissection. All were due to iatrogenic adhesions, mostly due to previous surgeries. In one case, ablation was still performed successfully but with possible irritation of the diaphragm causing chest and shoulder pain. There were seven cases (5.5%) of hydrodissection-related complications that included three cases of inadvertent pleural effusion, one case of pneumothorax, one case of gallbladder puncture, one case of hepatic venous injury, and one case of portal venous injury. Pleural-related complications may be due to unintentional puncture or guidewire manipulation and subsequent catheterisation of the pleural cavity, possibly due to puncture near the pleural recess, or due to passage of the guidewire through diaphragmatic fenestrations. In the same inadvertent manner, a hepatic venous branch and a portal venous branch were respectively punctured.

In the case of hepatic venous injury, the left liver lobe was punctured with a 16-gauge angiocatheter needle. Unopposed guidewire manipulation was felt so the catheter-guidewire system was thought to be in the peritoneal cavity, and a 6-French Neo-hydro drain catheter was inserted over the guidewire. Nonetheless active venous bleeding was noted from the drain catheter, and angiogram through the drain catheter under fluoroscopy showed misplacement of the drain within a hepatic vein. A 5-French BRITE TIP sheath (Cordis, Miami [FL], United States) was exchanged and the segmental hepatic vein was cannulated with a 5-French C1 catheter (Terumo Medical Corporation, Japan). This was followed by embolisation with one 12 mm × 40 cm Interlock coil, followed by 50% n-butyl cyanoacrylate glue (mixed with lipiodol) embolisation of the needle tract. No gross intra-abdominal haemorrhage was evident on postoperative US. The ablation procedure was aborted for this case and the patient subsequently referred for transarterial chemo-embolisation.

The cases of portal venous injury and inadvertent gallbladder puncture were self-limiting. Other known complications documented in the literature such as hydro-electrolytic disorders were not encountered in our case series. No cases of non-target ablations occurred during the review period.

CONCLUSION

Adequate artificial ascites and hydrodissection enable the operator to perform ablation in difficult locations by reducing the risk of non-target ablation, hence allowing ablation with an adequate margin. Hydrodissection also has the benefit of aiding access to previously difficult-to-access lesions. Additionally, hydrodissection may improve the patient's comfort during percutaneous intervention, for example reducing pain when the tumour is adjacent to the diaphragm. Further investigation into patient comfort and treatment outcomes would be worthwhile. Comparison of the efficacy of hydrodissection with other thermoprotective methods such as endoluminal cooling, pneumodissection or organ filling would also be helpful.

To conclude, artificial ascites and hydrodissection are easy, effective and economical ways to achieve thermal protection and improve lesion accessibility for ablations.

REFERENCES

1. Kim JW, Shin SS, Heo SH, Hong JH, Lim HS, Seon HJ, et al. Ultrasound-guided percutaneous radiofrequency ablation of liver tumors: how we do it safely and completely. Korean J Radiol. 2015;16:1226-39.
2. Garnon J, Cazzato RL, Caudrelier J, Nouri-Neuville M, Rao P, Boatta E, et al. Adjunctive thermoprotection during percutaneous thermal ablation procedures: review of current techniques. Cardiovasc Intervent Radiol. 2019;42:344-57.
3. Hinshaw JL, Lubner MG, Ziemlewicz TJ, Lee FT Jr, Brace CL. Percutaneous tumor ablation tools: microwave, radiofrequency, or cryoablation — what should you use and why? Radiographics. 2014;34:1344-62.
4. Garnon J, Koch G, Caudrelier J, Ramamurthy N, Auloge P, Cazzato RL, et al. Hydrodissection of the gallbladder bed: a technique for ablations located close to the gallbladder. Cardiovasc Intervent Radiol. 2019;42:1029-35.
5. Garnon J, Cazzato RL, Auloge P, Ramamurthy N, Koch G, Gangi A. Adjunctive hydrodissection of the bare area of liver during percutaneous thermal ablation of sub-cardiac hepatic tumours. Abdom Radiol (NY). 2020;45:3352-60.
6. Rhim H, Lim HK. Radiofrequency ablation for hepatocellular carcinoma abutting the diaphragm: the value of artificial ascites. Abdom Imaging. 2009;34:371-80.

Hong Kong J Radiol. 2023;26:72-7 | https://doi.org/10.12809/hkjr2317425

PICTORIAL ESSAY

Underdiagnosed Wernicke's Encephalopathy in Children: Spectrum of Imaging Findings in Three Local Cases

YS Lee[1], KC Wong[2], EYL Kan[2]

[1]Department of Radiology, Tuen Mun Hospital, Hong Kong
[2]Department of Radiology, Hong Kong Children's Hospital, Hong Kong

INTRODUCTION

Although vitamin B1 deficiency is increasingly being recognised in ill adults, Wernicke's encephalopathy (WE) remains underrecognised in children. We present three local cases of paediatric WE observed over a 2-year period.

Importantly, WE was not considered a primary differential diagnosis at initial presentation. This article aims to raise awareness of paediatric WE since time from recognition to thiamine replacement determines prognosis and mortality. We also illustrate some of its magnetic resonance imaging (MRI) findings to promote early radiological detection of the disease.

CASE REPORTS

Three patients with WE, aged between 12 and 17 years, are described. All three patients were prescribed total parenteral nutrition (TPN) prior to development of WE. All were examined with MRI. In all cases, diagnosis was confirmed by symptom regression, serum transketolase increase, and/or improved MRI findings following thiamine administration. Details of these three cases are illustrated in the Table.

Case 1

A 12-year-old boy was undergoing chemotherapy for osteosarcoma. One week prior to presentation, he was started on TPN due to recurrent severe vomiting. He then developed confusion and athetoid movements. Computed tomography revealed subtle hypodensity in bilateral thalami (Figure 1). MRI revealed symmetrical T2 hyperintensity and restricted diffusion at the dorsomedial thalami (Figure 2). After the possibility of WE was raised, he was given high doses of thiamine (>1000 mg daily) and slowly resumed oral feeding. Clinically, the child regained his usual functional and neurological status with no residual neurological deficits. Follow-up MRI 6 months later showed resolution of the thalamic signal abnormalities (Figure 3).

Case 2

A 17-year-old girl was undergoing chemotherapy for osteosarcoma. She presented insidiously with dullness

Correspondence: *Dr YS Lee, Department of Radiology, Tuen Mun Hospital, Hong Kong*
Email: lys273@ha.org.hk

Submitted: 27 Jun 2021; Accepted: 5 Oct 2021.

Contributors: YSL designed the study. KCW acquired the data. YSL analysed the data and drafted the manuscript. EYLK critically revised the manuscript for important intellectual content. All authors had full access to the data, contributed to the study, approved the final version for publication, and take responsibility for its accuracy and integrity.

Conflicts of interest: All authors have disclosed no conflicts of interest.

Funding/support: This study received no specific grant from any funding agency in the public, commercial, or not-for-profit sectors.

Data Availability: All data generated or analysed during the present study are available from the corresponding author on reasonable request.

Ethics Approval: The study was approved by HKCH Research Ethics Committee (Ref No.: HKCH-REC-2021-021) and conducted in compliance with the Declaration of Helsinki.

Table. Case summary.

	Case 1	Case 2	Case 3
Age, y	12	17	12
Sex	Male	Female	Male
Underlying illness	Osteosarcoma on chemotherapy	Osteosarcoma on chemotherapy	Haemolytic uraemic syndrome
Presentation	Confusion, athetoid movements	Dullness, flaccid tones	Lethargy, unsteady gait, vertical nystagmus
Duration of total parenteral nutrition prior to presentation	1 week	2 months	Episodic with various lengths over 3 years
Magnetic resonance imaging findings	Dorsomedial thalamic T2 hyperintensity and restricted diffusion	T2 hyperintensity and restricted diffusion at mammillary bodies, thalami, and PAG; cerebral cortex involvement; contrast enhancement in mammillary bodies	Cerebral atrophy, especially at PAG
Laboratory findings (post thiamine replacement)	Increased TKS and normal TPP effect	Normal TKS and TPP effect	Increased TKS and decreased TPP effect
Outcome	Complete resolution of symptoms	Improved mental status but limited motor control	Resolved gait and gaze disturbance; underperforming in life

Abbreviations: PAG = periaqueductal grey matter; TKS = transketolase; TPP = thiamine diphosphate.

Figure 1. Plain computed tomography in case 1. Non-enhanced computed tomography shows only subtle hypodensity in bilateral thalami (arrows).

and generalised flaccid tone after being on TPN for 2 months due to poor intake. She was admitted in a decorticate posture, had fixated gaze and generalised areflexia. MRI showed T2 hyperintensity and restricted diffusion at mammillary bodies, dorsomedial thalami, periaqueductal grey matter, and around the third ventricle on fluid-attenuated inversion recovery. The mammillary bodies and colliculi showed subtle contrast enhancement. Notably, signal abnormalities were also detected in parts of bilateral cerebral cortices (Figure 4). Thiamine (1500 mg daily) was given and enteral feeding was resumed. Nonetheless despite improvement in mental status, she regained very minimal voluntary motor control and remained bedbound.

Case 3

A 12-year-old boy was on monoclonal antibody therapy for recurrent atypical haemolytic uraemic syndrome. He had experienced bouts of pancreatitis over the years and was put on bowel rest and TPN episodically. He developed lethargy, unsteady gait and vertical nystagmus 1 week after the current episode of TPN. Compared with MRI images 2 years previously, there was generalised cerebral atrophy, with volume loss most significant at bilateral thalami (evidenced by widening of the third ventricle), mammillary bodies, colliculi, and hippocampi (Figure 5). Features and interval changes were highly suggestive of chronic WE. This suspicion was substantiated by interviews with the carer who reported past episodes of abnormal behaviour in the form of disinhibition and limb twitching. He was prescribed thiamine (1000 mg daily) and resumed enteral feeding. His gait disturbance and eye signs soon subsided but he remained underperforming in academic and social aspects.

DISCUSSION

WE is a potentially fatal acute neuropsychiatric disease

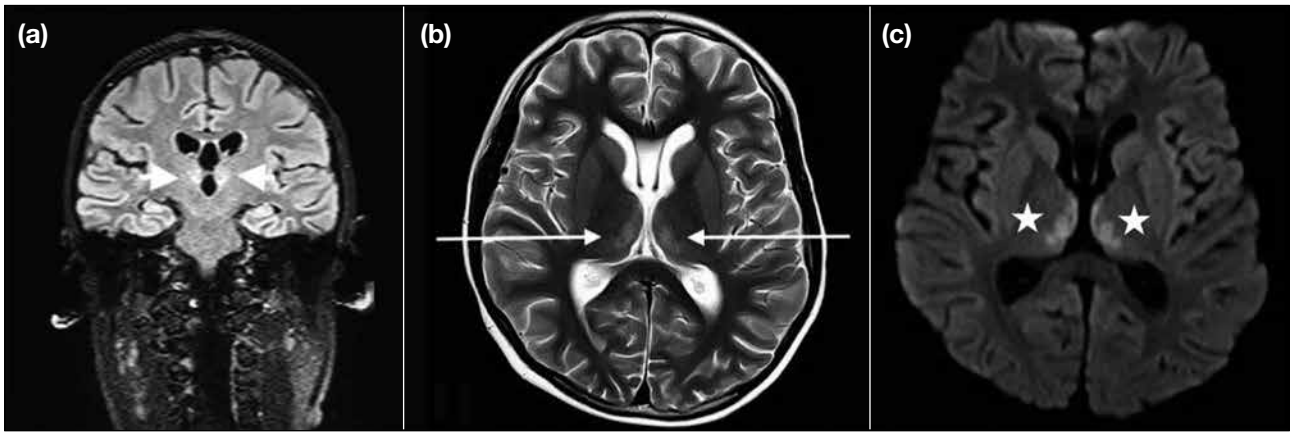

Figure 2. Magnetic resonance imaging in case 1. (a) Fluid-attenuated inversion recovery and (b) T2-weighted sequences showing symmetrical T2 hyperintensity in bilateral thalami (arrows). (c) Diffusion-weighted imaging showing corresponding restricted diffusion (stars).

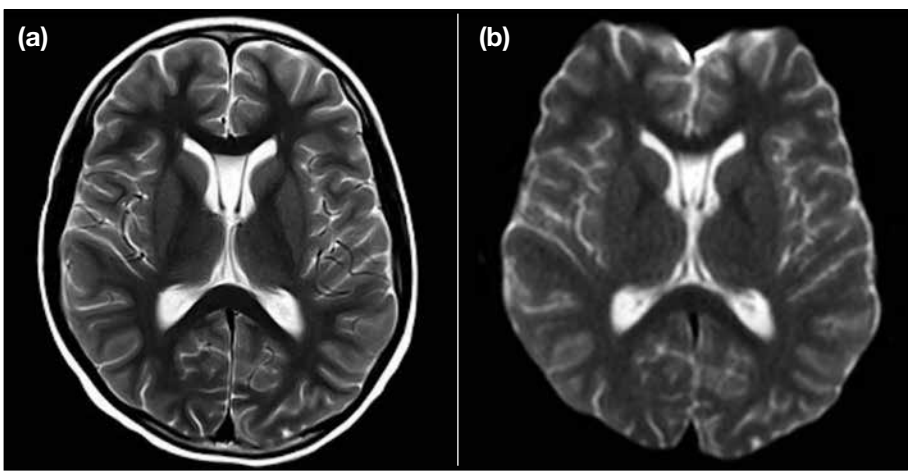

Figure 3. Follow-up magnetic resonance imaging in case 1 after 6 months of presentation. There is resolution of thalamic signal abnormalities on both (a) T2-weighted and (b) diffusion-weighted imaging sequences.

caused by thiamine (vitamin B1) deficiency. Thiamine, in its biologically active form thiamine pyrophosphate, is an essential coenzyme in several biochemical pathways in the brain. The body's reserve of thiamine can be readily depleted over 2 to 3 weeks[1] after which brain lesions develop, usually restricted to selective, vulnerable regions with high thiamine content and turnover.

Epidemiology

Although WE is a relatively well-recognised disease entity in alcoholic adults, it remains underrecognised in children. There has been increasing academic and clinical interest in WE in sick children over the last two to three decades, but as many as 58% of paediatric WE cases have been missed at clinical examination and recognised only on autopsy.[2] This lack of awareness of WE in the paediatric patient group may be due to poor clinical familiarity, non-classic presentation, and atypical imaging features.

Thiamine deficiency in childhood is most often associated with cancer.[2] Other recognised causes are prolonged parenteral nutrition without supplementation of thiamine, gastrointestinal surgery, and other systemic diseases.[3] Seear et al[4] reported that as many as four of six children undergoing chemotherapy, and 10 of 80 children receiving intensive care were deficient in thiamine. Such prevalence is much higher than previously believed; therefore, clinical awareness and a low threshold of suspicion are vital.

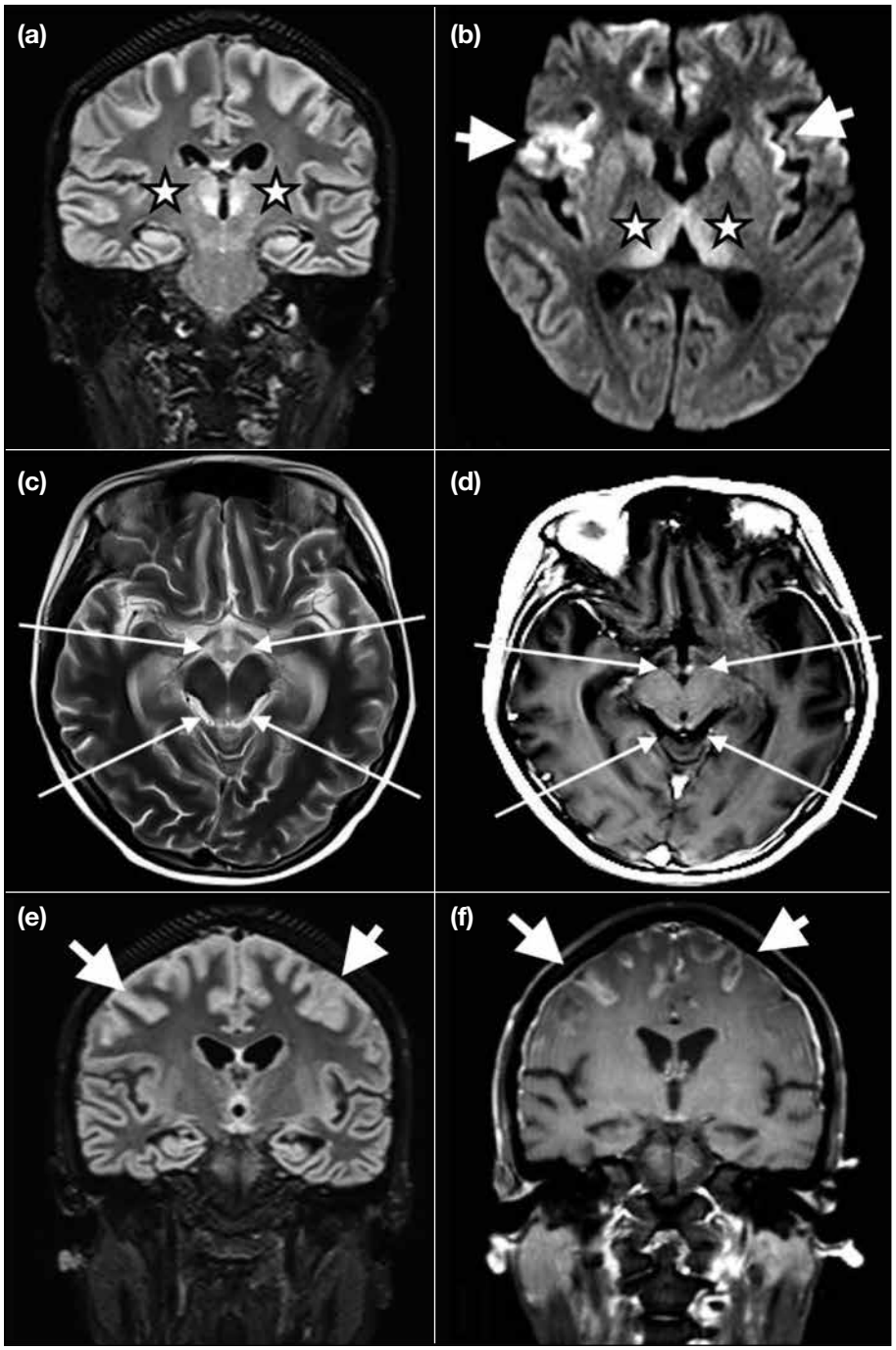

Figure 4. Magnetic resonance imaging of case 2. (a) Fluid-attenuated inversion recovery (FLAIR) shows symmetrical bilateral thalamic hyperintensity and (b) diffusion-weighted imaging (DWI) shows restricted diffusion in corresponding areas (stars), similar to case 1. (c) Mamillary bodies and colliculi show T2 hyperintensity and (d) contrast enhancement (long arrows). Features of cortical involvement (short arrows) imply poorer prognosis; there is (b) restricted diffusion in DWI, (e) gyral oedema in FLAIR, and (f) contrast enhancement.

Clinical Presentation

Early detection of subclinical thiamine deficiency is difficult as symptoms in children can be vague and non-specific such as headache, fatigue, irritability, and decline in growth rate.[1] Textbooks describe a classic triad of confusion, ataxia and ophthalmoplegia in only 16% to 21% of adult patients at presentation, with up to 19% having none of these symptoms.[2,5] More consistently though, 82% of WE patients will experience some degree of altered mental status ranging from confusion, sluggishness and apathy to coma and death.[5] Other less common presentations include stupor, hypotension and tachycardia, hypothermia and seizures, all of which can be related to insults to the hypothalami and thalami.[1]

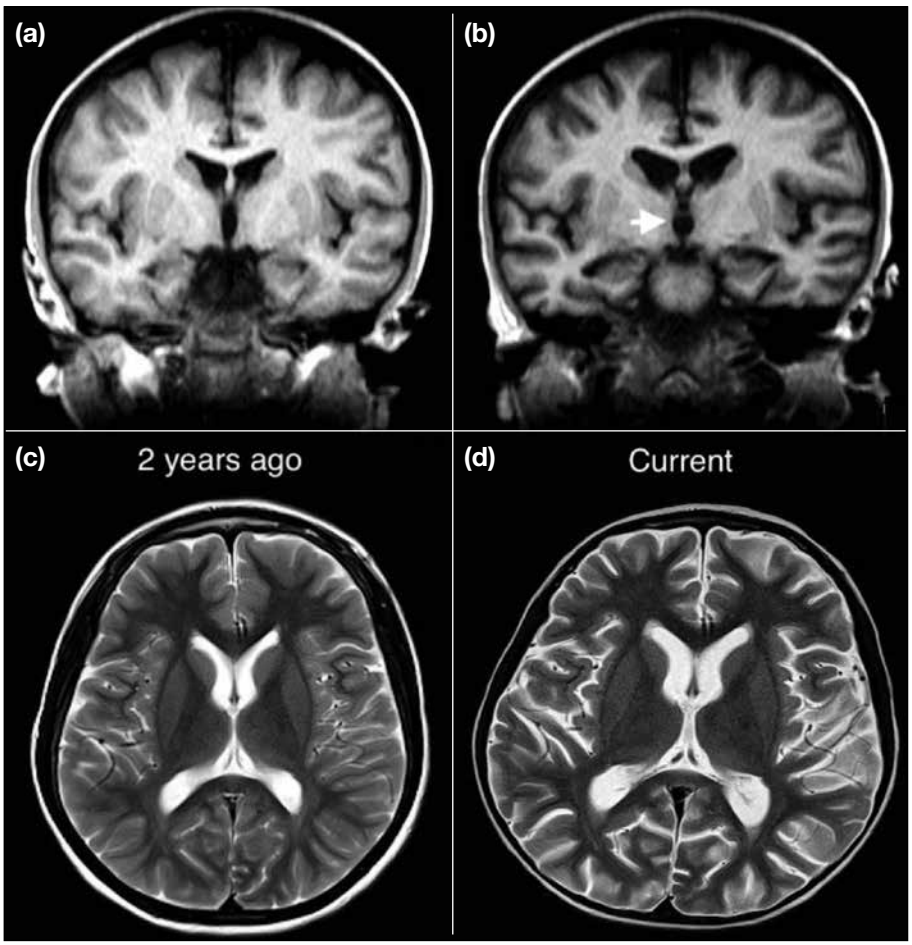

Figure 5. Comparison of magnetic resonance imaging 2 years apart in case 3. Features of chronic Wernicke's encephalopathy evidenced by interval neuronal loss at (b) bilateral thalami (note widening of third ventricle, short arrow) and mammillary bodies (as compared with [a]), as well as (d) generalised cerebral atrophy (note widened sulci and the Sylvian fissure; as compared with [c]).

Imaging Features

Neuroimaging is the most valuable method in diagnosing WE. In all our patients, the radiologist was the first to propose a diagnosis of WE.

A normal computed tomography of the brain cannot exclude WE since changes are subtle or even undetectable. The most useful imaging modality is MRI that has a high specificity of 93% and an acceptable sensitivity of 53%.[6] As demonstrated in our cases, typical MRI findings of acute WE are symmetrical signal intensity alterations (usually in the form of T2 hyperintensity and restricted diffusion as shown in Figure 2) in the dorsomedial thalami, mammillary bodies, tectal plate, and periaqueductal area. Selective involvement of the cerebellum (particularly the vermis), cranial nerve nuclei, red nuclei, cerebellar dentate nuclei, fornix, splenium, and cerebral cortex has been previously described.[7] Interestingly, basal ganglia involvement, which has not been reported in adults, has been observed in up to 55% of paediatric WE patients.[2,3] This finding may be related to the high thiamine-dependent metabolism of nuclear-basal regions in children. Importantly, albeit uncommon, mammillary body contrast enhancement (Figure 4) can be the only sign of WE.[8,9] Cortical involvement in WE (Figure 4) usually implies poorer prognosis, as shown by the inferior outcome in case 2.[10]

In chronic WE, the brain can show necrosis, gliosis, and neuronal loss.[11] As illustrated in case 3 (Figure 5), these changes can be gradual and subtle. Thus, it is salient that a comparison has to be made with prior imaging studies to detect temporal differences. MR spectroscopy, if performed, will reveal the expected lactate doublet and decreased N-acetylaspartate peak at the periaqueductal lesion, reflecting anaerobic metabolism and necrosis.[10]

Blood Tests

Traditionally, blood tests with measurement of serum thiamine, thiamine pyrophosphate effect and

transketolase have been performed to diagnose WE. These tests are now considered inadequate for diagnosis due to their poor sensitivity and specificity.[12] In addition, a normal serum thiamine level does not necessarily exclude the presence of WE.[13] In our cases, serum thiamine was not measured, and transketolase level and thiamine pyrophosphate effect showed varied changes in each case following thiamine replacement (Table).

Imaging Differential Diagnoses

There are other disease entities that can show similar MRI features to WE. These include paramedian thalamic infarction, ventriculoencephalitis, demyelinating disease, Leigh disease, primary cerebral lymphoma, Behçet's disease, variant Creutzfeldt–Jakob disease, other metabolic disturbances, and intoxication. When the clinical history lacks a predisposing factor for thiamine deficiency, or when response to thiamine replacement is unclear, these differential diagnoses should be considered.

Management

Since the timing of thiamine replacement determines outcome, WE is regarded as a medical emergency. In all cases when the disorder is suspected, thiamine therapy should be initiated immediately. There is currently no consensus on thiamine dosage or route of administration for individuals with WE, but high-dose intravenous infusion is common.

A retrospective study by Wrenn et al[14] found no significant allergic reactions in more than 300,000 patients treated with parenteral thiamine. Given its generally safe profile, some institutes advocate administration of prophylactic thiamine supplements to patients with predisposing factors or suggestive neurological symptoms.[15]

CONCLUSION

In this article, we have demonstrated the spectrum of MRI findings of WE. In all three cases, the radiologist was the first to propose WE as a differential diagnosis. We suspect that these cases may just be the tip of the iceberg in terms of the prevalence of malnutrition in children with long-term illnesses, in particular cancers. Further investigations are warranted to reveal the true prevalence of paediatric malnutrition, which is currently presumed rare, in this world city.

In the case of WE, since the time to thiamine replacement determines prognosis, we recommend radiologists maintain a high level of suspicion when imaging children with abnormal behaviour, especially if there is a recent history of parenteral nutrition without thiamine replacement. Awareness of this entity and its findings can facilitate early diagnosis and timely management to improve disease outcome.

REFERENCES

1. Sechi G, Serra A. Wernicke's encephalopathy: new clinical settings and recent advances in diagnosis and management. Lancet Neurol. 2007;6:442-55.
2. Vasconcelos MM, Silva KP, Vidal G, Silva AF, Domingues RC, Berditchevsky CR. Early diagnosis of pediatric Wernicke's encephalopathy. Pediatr Neurol. 1999;20:289-94.
3. Zuccoli G, Siddiqui N, Bailey A, Bartoletti SC. Neuroimaging findings in pediatric Wernicke encephalopathy: a review. Neuroradiology. 2010;52:523-9.
4. Seear M, Lockitch G, Jacobson B, Quigley G, MacNab A. Thiamine, riboflavin, and pyridoxine deficiencies in a population of critically ill children. J Pediatr. 1992;121:533-8.
5. Harper CG, Giles M, Finlay-Jones R. Clinical signs in the Wernicke-Korsakoff complex: a retrospective analysis of 131 cases diagnosed at necropsy. J Neurol Neurosurg Psychiatry. 1986;49:341-5.
6. Antunez E, Estruch R, Cardenal C, Nicolas JM, Fernandez-Sola J, Urbano-Marquez A. Usefulness of CT and MR imaging in the diagnosis of acute Wernicke's encephalopathy. AJR Am J Roentgenol. 1998;171:1131-7.
7. Zuccoli G, Pipitone N. Neuroimaging findings in acute Wernicke's encephalopathy: review of the literature. AJR Am J Roentgenol. 2009;192:501-8.
8. Zuccoli G, Gallucci M, Capellades J, Regnicolo L, Tumiati B, Giadás TC, et al. Wernicke encephalopathy: MR findings at clinical presentation in twenty-six alcoholic and nonalcoholic patients. AJNR Am J Neuroradiol. 2007;28:1328-31.
9. Shogry ME, Curnes JT. Mamillary body enhancement on MR as the only sign of acute Wernicke encephalopathy. AJNR Am J Neuroradiol. 1994;15:172-4.
10. Kornreich L, Bron-Harlev E, Hoffmann C, Schwarz M, Konen O, Schoenfeld T, et al. Thiamine deficiency in infants: MR findings in the brain. AJNR Am J Neuroradiol. 2005;26:1668-74.
11. Kril JJ. Neuropathology of thiamine deficiency disorders. Metab Brain Dis. 1996;11:9-17.
12. Talwar D, Davidson H, Cooney J, St JO'Reilly D. Vitamin B(1) status assessed by direct measurement of thiamin pyrophosphate in erythrocytes or whole blood by HPLC: comparison with erythrocyte transketolase activation assay. Clin Chem. 2000;46:704-10.
13. Galvin R, Bråthen G, Ivashynka A, Hillbom M, Tanasescu R, Leone MA, et al. EFNS guidelines for diagnosis, therapy and prevention of Wernicke encephalopathy. Eur J Neurol. 2010;17:1408-18.
14. Wrenn KD, Slovis CM. Is intravenous thiamine safe? Am J Emerg Med. 1992;10:165.
15. Thomson AD, Cook CC, Touquet R, Henry JA; Royal College of Physicians, London. The Royal College of Physicians report on alcohol: guidelines for managing Wernicke's encephalopathy in the Accident and Emergency Department. Alcohol Alcohol. 2002;37:513-21.

CATEGORIES OF PAPERS

Hong Kong Journal of Radiology publishes various categories of articles. Each category serves a distinct purpose and is judged by different criteria.

EDITORIAL

Commissioned article presenting the author's opinion on a topical subject or an article published in the current issue. Unsolicited Editorials are not accepted.

Format: An abstract is not required. The text is limited to 1000 words, with a maximum of 1 table or figure, and up to 10 references.

REVIEW ARTICLE

Systematic reviews or meta-analyses of recent developments in a specific topic. Scoping reviews of the literature that identify area(s) for future research will also be considered. No new information is described, and no subjective opinion or personal experiences are expressed.

Format: A structured abstract of ≤ 250 words; headings should include: Objective(s), Methods, Results, Conclusion. The text is limited to 5000 words, with a maximum of 20 tables and figures (total), and up to 60 references.

ORIGINAL ARTICLE

Provides new information based on original research. Includes prospective studies with in-depth statistical analysis, unique retrospective observations of a disease or disorder, and studies of novel applications of an interventional procedure or treatment method.

Format: A structured abstract of ≤ 250 words; headings should include: Objective(s), Methods, Results, Conclusion. The text is limited to 3500 words, with a maximum of 20 tables and figures (total), and up to 50 references.

PERSPECTIVE

Narrative review articles discussing recent developments in a specific topic. No new information is described; may include subjective opinion or personal experiences.

Format: An unstructured abstract of ≤ 250 words. The text is limited to 2500 words, with a maximum of 20 tables and figures (total), and up to 60 references.

PICTORIAL ESSAY

Teaching exercise with message in the figures and legends. Emphasis is on quality of the illustrations and clinical relevance of the message.

Format: An abstract is not required. The text is limited to 2500 words, with a maximum of 20 tables and figures (total), and up to 15 references.

CASE REPORT

Brief discussion of a case with unique features not previously described. Additional cases (case series) may be added to augment the discussion. The discussion should be succinct and focus on a specific message.

Format: An abstract is not required. The text is limited to 1500 words, with a maximum of 8 tables and figures (total), and up to 15 references.

BRIEF COMMUNICATION

This includes post-meeting commentary, update on new imaging or therapeutic advances, brief description of a specific technique or procedure or new equipment. Teaching exercise aimed at describing a certain radiological or radiotherapeutic technique for trainees and practising radiologists is also welcome.

Format: An abstract is not required. The text is limited to 1500 words, with a maximum of 8 tables and figures (total), and up to 15 references.

LETTER TO THE EDITOR

Short letter on any matter of interest to journal readers, including comments on an article that has previously appeared in the journal. The authors of the article commented on would be invited to reply.

Format: An abstract is not required. The text is limited to 500 words, with up to 5 references. Figures and tables are permitted only exceptionally.

INFORMATION FOR AUTHORS

Aims and Scope

Hong Kong Journal of Radiology is the official peer-reviewed academic journal of the Hong Kong College of Radiologists. It is a multidisciplinary journal covering research work pertaining to the science and practice of the component specialties of the College. The journal publishes various categories of papers, including Reviews, Original Articles, Perspectives, Pictorial Essays, Case Reports, Brief Communications, and Letters to the Editor. Manuscripts will be subject to rigorous peer review. *HKJR* adheres to the Recommendations for the Conduct, Reporting, Editing, and Publication of Scholarly Work in Medical Journals of the International Committee of Medical Journal Editors (ICMJE; www.icmje.org), and the Core Practices of the Committee on Publication Ethics (COPE; publicationethics.org/).

Journal Policies

Reporting Guidelines: *HKJR* recommends the use of reporting guidelines in the preparation of manuscripts, such as those advocated by the EQUATOR Network (eg, CONSORT for randomised trials).

Funding: Any sponsor(s) of the research involved, along with grant number(s) should be provided.

Conflicts of interest: All authors must provide a statement reporting any conflicts of interest. Where none exist, please state 'The authors have no conflicts of interest to declare.'

Ethics: All studies must be conducted in accordance with the Declaration of Helsinki. For studies involving humans, a statement must be included in the manuscript that provides the name of the review board and approval number (or waiver). A statement on patient/guardian consent must also be included. For studies involving animals, appropriate ethics approval is required, and this should be stated in the manuscript.

Submission: Manuscripts should be submitted online via HKAMedTrack (www.hkamedtrack.org/hkjr). Manuscripts must be unpublished works that are not under consideration by another publication.

Copyright: On acceptance of an article by the journal, the corresponding author will be asked to transfer copyright of the article to the College.

Editing: Accepted manuscripts will be copyedited according to journal style. Authors are responsible for all statements made in their work, including changes made by the copy editor.

Proofs and Reprints: The corresponding author will receive page proofs, which should be proofread and returned promptly. Corrections are limited to printer's errors — no substantial author's changes will be made without charge. Quotes for extra copies of reprints are available at the Editorial Office.

Manuscript Preparation

In general, manuscripts should be prepared following the 'IMRaD' structure as recommended by the ICMJE. Please provide a **blinded** manuscript and separate title page in Word format (.doc or .docx). Manuscripts must be written in English. For accepted manuscripts, an abstract in Traditional Chinese will also be required.

Authors: Provide the full name, qualifications (maximum of two), and affiliation (where the study was conducted) for all authors. The authors' names in Chinese characters, if available, should also be provided. **The corresponding author**, on behalf of the authors, is responsible for all contact with the journal. Provide the full name, postal address, telephone and fax numbers, and email address of the corresponding author.

Title: Concisely convey the main topic of the study. Avoid obvious terms such as "a study of" or "novel". If appropriate, please include the study design in the title (eg, 'randomised controlled trial', 'systematic review', 'case report'). An abbreviated title of <45 characters is also required.

Abstract: For article types requiring an abstract, this should provide a complete summary of the article, including the aims/purpose, main methods, key results, and conclusions. Abbreviations and clinical or technical jargon should be avoided. Please refer to the Categories of Papers for details.

Key Words: Five relevant index terms should be provided, selected from the Medical Subject Headings (MeSH; www.ncbi.nlm.nih.gov/mesh).

Tables: Submit tables on separate pages in as simple a format as possible. They should be numbered and concisely titled. Abbreviations should be defined in footnotes.

Figures: Restricted to the minimum necessary to support the textual material. Illustrations should be submitted as separate files (.jpg format, ≥350-dpi resolution). All figures should be numbered with a legend to indicate the anatomical area and pathological condition shown. All symbols and abbreviations should be defined in the legend. Please ensure that legends and illustrations correspond.

References: Should be numbered in the order in which they are first cited in the text. Each reference citation should be in superscript Arabic numerals after full-stops and commas. In the reference list, include the complete title, and names and initials of all authors.

Acknowledgement(s): Any individuals who contributed substantially to the study but does not qualify for inclusion as an author should be acknowledged. Written permission from acknowledged individuals is required.

Please refer to the *HKJR* website for further guidance:
http://www.hkjr.org/page/information-authors

The Hong Kong Society of Diagnostic Radiologists Trust Fund

Hong Kong Society of Diagnostic Radiologists Research Grant

The Hong Kong Society of Diagnostic Radiologists (HKSDR) was founded in 1977 to promote interflow of professional knowledge in diagnostic radiology and to foster close contact among doctors working in the field of diagnostic radiology. The HKSDR Trust Fund was established in 1985.

Taking into account the rapid progress in imaging technology and thus the need to promote research to advance our knowledge and to serve our patients better, the Trust Fund offers three awards of up to HK$17,000 each and is open to application.

The application should be made by the principal investigator of the research project related to the scientific or clinical aspects of diagnostic radiology to be conducted in Hong Kong. The principal investigator should be a trainee/specialist in the field of diagnostic radiology. He/she has to be a registered medical practitioner in Hong Kong.

Application and enquiry can be directed to:

Dr. Lam Chiu Ying Flora, Hon Secretary of Trust Fund Working Group
c/o Ms. HY Ng, Department of Diagnostic & Interventional Radiology
Kwong Wah Hospital
25 Waterloo Road, Yaumatei, Kowloon, Hong Kong.
Tel: (852) 3517 5189

AOSPR 2023

21st Annual Scientific Meeting of
Asian and Oceanic Society for
Paediatric Radiology

2nd-3rd SEPTEMBER

HONG KONG 香港

@ Hong Kong Academy of Medicine
Jockey Club Building

www.aospr2023.org

Organised by

Supported by